Investigation of a Multi-Channel UWB RADAR System for Short Range Target Positioning Applications

Alexandre Rodrigues

A project report submitted to the Department of Electrical Engineering,
University of Cape Town, in partial fulfilment of the requirements
for the degree of Bachelor of Science in Engineering.

Cape Town, October 2005

Declaration

I declare that this project report is my own, unaided work. It is being submitted for the degree of Bachelor of Science in Engineering at the University of Cape Town. It has not been submitted before for any degree or examination in any other university.

Signature of Author . . . . . .

Cape Town

October 2005

Abstract

Ultra-wideband (UWB) impulse technology for radar involves transmitting short (sub-nanosecond) pulses at baseband and measuring the reflected echoes from targets. Using a receive antenna array and an appropriate multi-channel sampling receiver, the capture of multiple downrange profiles of a scene/target is theoretically possible.

The purpose of this thesis is to:

- provide a brief investigation into radar, antenna and ultra-wideband (UWB) theory
- perform software simulations of the expected beam patterns for an antenna array; a multi-channel, bi-static UWB radar system and to develop a beam focusing algorithm
- analyse the operation of an existing UWB radar system
- design and implement a multi-channel, bi-static UWB radar system using predominantly surface mount components
- test and see whether the system can be used to obtain downrange profiles for multiple receiver channels

The software written successfully performed the desired simulations, as well as implemented the beam focusing algorithm used for electronic beam steering. The hardware built managed to capture downrange profiles for single and multiple (three) channels. The performance of the multi-channel system was however not optimal. This was chiefly due to the on-board RF amplifiers, and the lack of UWB antennas. However, the concept has been successfully demonstrated, thus achieving the purpose of this thesis. Future research could include integrating the design of the multiple channel system with the beam focusing algorithm developed, to achieve 2D images of target position.

Acknowledgements

I would like to sincerely thank my supervisor Dr Andrew Wilkinson for all the invaluable guidance, support and expert knowledge offered to me by him. I am also indebted to him for the generous financial assistance received for this project as well as the office space and equipment used, without which this thesis would not have been possible.

Thanks must also go to Mr Samuel Ginsberg, whose advice and assistance in the creation of printed circuit boards (PCB's) was essential.

A final thanks must go to Alvin Chang for his assistance in modifying the radar software interface to incorporate multiple channels.

Contents

Declaration i

Abstract ii

Acknowledgements iii

Nomenclature xi

1 Introduction 1

1.1 Objectives . . . 2
1.2 Sources of Information . . . 2
1.3 Limitations of Research . . . 2
1.4 Plan of Development . . . 2

2 Background Information 4

2.1 General Radar Theory . . . 4
2.1.1 A Simple Radar Model . . . 4
2.1.2 Range Ambiguity . . . 5
2.1.3 Radar Bandwidth . . . 6
2.1.4 Range Resolution . . . 6
2.1.5 The Radar Equation . . . 6
2.1.6 Signal to Noise Ratio . . . 7
2.2 General Antenna Theory . . . 7
2.2.1 Antenna Dimensions . . . 8
2.2.2 Antenna Radiation Patterns . . . 8
2.2.3 Far-Field Distance . . . 9
2.2.4 Antenna Polarization . . . 9
2.2.5 Linear Antenna Arrays . . . 10
2.3 Ultra-Wideband (UWB) Technology . . . 10
2.3.1 Definition of Ultra-Wideband (UWB) . . . 10

2.3.2 Advantages of UWB Technology for Radar 11
2.3.3 Advantages of UWB Technology for Communications 11
2.3.4 Advantages of UWB Hardware Implementation 12
2.3.5 Other Applications of UWB Technology 12

3 Software Simulations 13
3.1 Antenna Beam Patterns 13
3.2 Multi-Channel UWB Radar Simulation 18
3.3 Beam Focusing Algorithm 25

4 Analysis of a Single Channel Radar System 30
4.1 The Antennas 32
4.2 The NI-DAQ Card 32
4.3 The Pulse Generator 34
4.4 The Transmitter 34
4.5 The Receiver 36
4.5.1 The RF Amplifier 37
4.5.2 The Delay-line 38
4.5.3 Fast Sampler/Averager 39
4.5.4 The Differential Amplifier 40
4.6 Software Interface 41

5 Design and Implementation of an UWB Multi-Channel Radar System 43
5.1 Design Criteria 44
5.1.1 Array Length 44
5.1.2 PCB Layout 45
5.1.3 On-board Oscillator 46
5.1.4 RF Amplifiers 47
5.1.5 Power Supplies and Decoupling 51
5.1.6 Impedance Matching 51
5.1.7 Ground Vias for Possible Shielding 51
5.1.8 Placement of Probe Pins 52
5.2 Hardware Implementation 52
5.2.1 Procurement and Choice of Components 52
5.2.2 Manufacture of PCB 52
5.2.3 Soldering of Board 52

6 Test and Results **54**

6.1 Testing 54

6.1.1 Oscillator Testing 54

6.1.2 Transmitter Testing 55

6.1.3 RF Amplifier Testing 60

6.1.4 Delay-line Testing 64

6.1.5 Receiver Testing 64

6.2 Results 67

6.2.1 Results for Single Channel Operation 67

6.2.2 Results for Multiple Channel Operation 73

7 Conclusions and Recommendations **83**

7.1 Conclusions 83

7.2 Recommendations 84

A Software Source Code **85**

A.1 Antenna Beam Pattern Simulation Code 85

A.2 Multi-Channel UWB Radar Simulation Code 86

A.3 Beam Focusing Algorithm 88

Bibliography **90**

List of Figures

2.1 Diagram of a simple radar model (taken from [21]) 4
2.2 Antenna radiation pattern showing 3dB beamwidth 8
2.3 Typical Elliptically Polarized EM field [5] 10

3.1 Receiver array and incident plane wave 14
3.2 Receiver beam pattern showing the 3dB beamwidth for $N = 40$ 15
3.3 Polar plot of beam pattern versus angle of incidence, $N = 40$ 16
3.4 Polar plot of beam pattern versus angle of incidence, $N = 6$ 17
3.7 Polar plot of beam pattern versus angle of incidence, $N = 1$ 17
3.5 Polar plot of beam pattern versus angle of incidence, $N = 5$ 18
3.6 Polar plot of beam pattern versus angle of incidence, $N = 4$ 19
3.8 Transmitted signal 20
3.9 Receiver/target configuration 21
3.10 Magnitude of received signal vs time for E_1 22
3.11 Magnitude of received signal vs range for E_1 23
3.12 Image plot of the Fourier response of the received signal for E_1 24
3.13 Downrange profiles for the five receiver elements 25
3.14 Example of a phasor diagram showing vectors V1 to V5 26
3.15 Phasor diagram showing maximum resultant due to phase shifting 26
3.16 Focused targets in the 30X120 point grid 27
3.17 3D plot of two focused targets in the 30X120 point grid 28
3.18 Focused targets in the 30X120 point grid after the application of a Hanning window 28
3.19 3D plot of two focused targets in the 30X120 point grid after the application of a Hanning window 29

4.1 Block diagram of UWB single channel radar system, based on [6] 31
4.2 Photograph of the UWB single channel radar system described in [6] . . . 31
4.3 Agilent Infinium 54833A Digital Oscilloscope 32
4.4 Graph of bow-tie antenna gain versus frequency [6] 33

4.5 Photograph of the twin bow-tie antennas designed in [15] 33
4.6 A typical NI-DAQ card 34
4.8 Transmitter circuit 34
4.7 Agilent 3320A 20MHZ Arbitrary Waveform Generator 35
4.9 Pulses triggering transistor 36
4.10 Transmitted signal 37
4.11 Receiver circuit 37
4.12 Photograph of the plug-in RF amplifier module 38
4.13 Voltage-controlled, nanosecond variable delay-line 38
4.14 Graph of reverse voltage versus resultant time delay 39
4.15 Fast sampler/averager 40
4.16 Differential amplifier configuration 41
4.17 Screen-shot of the GUI *myRadar* 42

5.1 Block Diagram of Proposed Multi-Channel System 44
5.2 CD4047 oscillator 47
5.3 Receiver chain 49
5.4 Typical biasing configuration for the ERA series amplifiers 50
5.5 Soldered multi-channel UWB PCB 53

6.1 2MHz clock waveform 55
6.2 Transmitted pulse 56
6.3 Transmitted signal after the addition of one capacitor 57
6.4 Transmitted signal after the addition of two capacitors 58
6.5 Fast Fourier Transform (FFT) of transmitted signal 59
6.6 Waveform showing instantaneous transmitted power 59
6.7 Transmitted signal attenuated by 10dB 61
6.8 Transmitted signal first attenuated and then amplified by on-board ERA amplifiers 62
6.9 Transmitted signal first attenuated and then amplified by plug-in amplifier 63
6.10 Ellies TV grid antenna 66
6.11 Twin bow-tie antenna configuration for single channel testing 68
6.12 Metal pole used as reflector/target 68
6.13 Metal grid used as target/reflector 69
6.14 Pyramidal corner reflector used as target/reflector 69
6.15 Background snapshot 70
6.16 Target at 1m 71

6.17 Target at 1m (match filtered) 71
6.18 Target (corner reflector) at 1.5m 72
6.19 Target at 2m 72
6.20 Target at 2.5m 73
6.21 Target at 3m 73
6.22 Ellies grid antenna configuration for the three channel setup 74
6.23 Background snapshot for two channels 75
6.24 Target in front of first (blue) receive antenna 75
6.25 Target directly in front of transmitter 76
6.26 Target in front of second (green) receive antenna 76
6.27 Filter snapshot for two channels 77
6.28 Target in front of first (blue) receive antenna, match filtered 77
6.29 Target in front of transmitter 78
6.30 Target in front of second (green) receive antenna, match filtered 78
6.31 Background snapshot for three channels 79
6.32 Target in front of first (blue) receive antenna, difference mode 79
6.33 Target in front of second (green) antenna, difference mode 80
6.34 Target in front of third (red) antenna, difference mode 80
6.35 Filter snapshot for three channels 81
6.36 Target in front of first (blue) receive antenna, match filtered 81
6.37 Target in middle of scene, match filtered 82
6.38 Target in front of third (red) receive antenna, match filtered 82

List of Tables

5.1 ERA medium power amplifier characteristics (typical) 48

6.1 Bench equipment used for testing 54

Nomenclature

3db Beamwidth—The width of the antenna beam pattern in degrees/radians at which the power of the received/transmitted signal drops by 3dB

AC—Alternating current

ADC—Analogue-to-digital converter

Anechoic chamber—An enclusure designed to act as a perfect absorber of EM waves

Azimuth—Angle in the horizontal plane

Bandwidth—The width of a signal's frequency spectrum

Beamwidth—The angular width of a slice through the mainlobe of the radiation pattern of an antenna in the horizontal, vertical or other plane

Bi-static—A radar system configuration employing separate transmit and receive antennas

BNC—Bayonet Neill-Concelman, a type of cable connector commonly used for television

DAC—Digital-to-analogue converter

DC—Direct current

Dipole—Two element antenna, usually of length $l = \frac{\lambda}{2}$

Downrange Profile—A plot of the return echo of a radar target versus range

EM—Electro-magnetic

GPR—Ground penetrating radar

Heterodyning—Process of mixing a signal up or down in frequency

IC—Integrated circuit

LHP—Left-hand plate of a capacitor

LPI/D—Low probability of detection/interception

Monopole—Single element antenna, usually of length $l = \frac{\lambda}{4}$

Mono-static—A radar system configuration employing a single transceiver antenna

NI-DAQ—National Instruments data acquisition card

Omnidirectional—An antenna that radiates equally in all directions

PCB—Printed circuit board

PRF—Pulse repetition frequency

PSD—Power spectral density

PRF Dithering—A process whereby the PRF of a pulse is varied in order to lower the power spectral density of a signal

Radar—Radio detection and ranging

Range—The radial distance from a radar to a target

RCS—Radar target cross section

RF—Radio frequency

RHP–Right-hand plate of a capacitor

RMS—Root-mean-square

SM—Surface mount

SNR—Signal to noise ratio

UCT—University of Cape Town (South Africa)

UWB—Ultra-wideband

WGN—White, Gaussian noise

Chapter 1

Introduction

This project report describes the simulation, design and implementation of a multi-channel ultra-wideband (UWB) radar system (using multiple receivers and an antenna array) for use in short range target positioning applications. Since UWB impulse technology consists of transmitting pulses of extremely short duration (nanoseconds and shorter), a system bandwidth in the gigahertz range is attainable. This in turn translates into a very high radar range resolution, meaning closely spaced targets can be accurately resolved, which is vital for precise target positioning applications.

UWB pulses are also characterised by short duty cycles, and this fact, combined with a high bandwidth means that these pulses typically possess low average power spectral densities (PSD's) which can be further reduced through techniques such as pulse repetition frequency (PRF) dithering. This results in a low probability of detection/interception (LPI/D) RF signature for UWB pulses, making this technology ideal for covert military operations, and useful for communication purposes.

UWB radar systems designed to operate below 1 and possibly 2GHz can also be used as ground penetrating radars (GPR's) useful for, among other things, geographical subterranean surveying applications. There is also much research being conducted into using UWB radar to perform through wall sensing. What this means is that the positions of targets hidden behind walls can be obtained through non-invasive methods. One such product (labelled *Radarvision*) has already been reputed to have been produced by a company called Time Domain, see [4]. Time Domain's through wall sensing system claims to be able to produce 2D images of the positions of moving objects through concrete and other non-metallic walls. Applications of a system like this could include:

- Providing tactical information (such as the positions of occupants in a room/hiding place) to aid the police and law enforcement teams
- Allowing covert detection of enemy locations without being detected (through UWB technology's inherent LPI/D) to aid the military
- Aiding rescue teams in the search for victims buried under rubble

1.1 Objectives

The objectives of this project are to:

- provide a brief investigation into radar, antenna and UWB theory with the aim of providing a basic understanding of these topics
- perform a software simulation of a far-field generated sinusoidal plane wave incident on an antenna array to obtain magnitude versus incident angle plots (beam pattern plots), and to provide an understanding on antenna arrays
- perform a software simulation of a multi-channel, bi-static UWB radar system in order to obtain idealized downrange profiles to aid in the understanding of an UWB impulse radar system
- develop a software focusing algorithm to perform beam focusing on a grid of points representing a typical radar scene, to obtain 2D profiles of target position
- analyse and describe the operation of the University of Cape Town's (UCT's) single channel UWB radar system in [6]
- design the printed circuit board (PCB) layout for a multi-channel, bi-static UWB radar system in miniature circuit form and have it fabricated
- populate and test to see if the PCB can operate as a multi-channel receiver
- draw conclusions and make recommendations on how the system can be improved/extended

1.2 Sources of Information

The chief sources of information on which this thesis was based upon include knowledge handed down by Dr A.J Wilkinson, gained from reading relevant books and articles, as well as from searching on the Internet.

1.3 Limitations of Research

The limitations of this research project include time delays in the procurement of components and manufacture of the PCB, as well as the limited availability of UWB antennas.

1.4 Plan of Development

The rest of the document is arranged as follows:

Chapter 2: Background Information

This chapter provides a brief informative summary on some of the concepts regarding radar, antenna and ultra-wideband (UWB) theory, pertinent to this thesis.

Chapter 3: Software Simulations

This chapter describes the simulation of expected beam patterns for an antenna array as well as the idealized downrange profiles for a multi-channel UWB impulse radar system. It then proceeds with the derivation and implementation of a beam focusing algorithm used to obtain the positions of targets in 2D.

Chapter 4: Analysis of a Single Channel System

This chapter deals with the analysis of an existing UWB single channel radar system, with the purpose of aiding in the understanding and design of a multi-channel version.

Chapter 5: Design and Implementation of an UWB Multi-Channel Radar System

This chapter provides details and calculations of the design criteria and steps implemented in order to create an UWB multi-channel radar system.

Chapter 6: Tests and Results

This chapter describes the testing performed on the hardware, the technical difficulties encountered, as well as the results that were achieved.

Chapter 7: Conclusions and Recommendations

The final chapter presents the conclusions drawn, based on the outcomes of the findings. It also makes recommendations on how the radar system can be improved, and highlights possible future work.

Chapter 2

Background Information

The purpose of this section is to take a brief look into radar, antenna and UWB theory. It is not intended to delve too deeply into this theory, as most of the important ideas and concepts are better brought out through the investigations performed, whether they be simulation or implementation.

2.1 General Radar Theory

The term *radar* is a contraction of the words *radio detection* and *ranging.* It is ultimately an electronic device used to determine the range and/or position of objects [16]. It achieves this function by transmitting electromagnetic (EM) waves and measuring the attributes (time delay, attenuation, phase etc) of the echo signals. What follows is a bit of information on basic radar theory with the aim of aiding in the understanding of the concepts involved with this technology.

2.1.1 A Simple Radar Model

Consider the simple radar model of Figure 2.1.

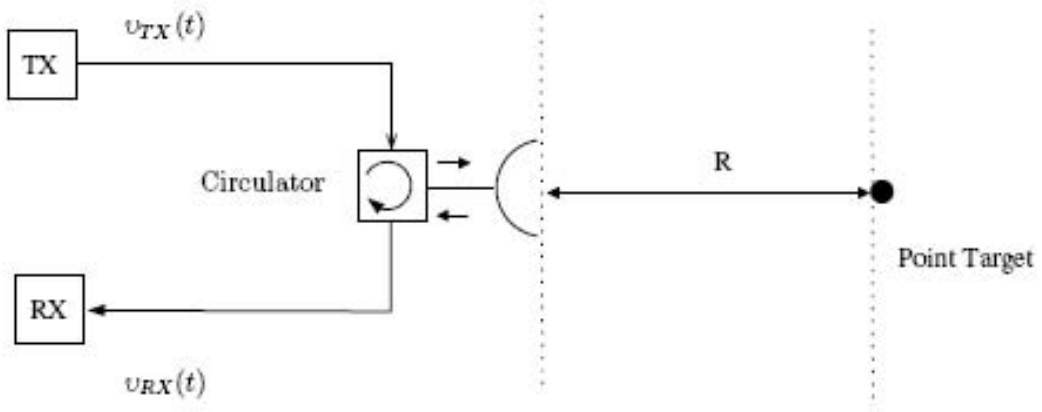

Figure 2.1: Diagram of a simple radar model (taken from [21])

It consists of a transmitter, receiver, circulator (to multiplex the signals from the monostatic antenna), antenna and single point target at range R from the antenna. The radar operates by transmitting an RF signal given by $v_{tx}(t)$. If the signal bandwidth is less than the receive antenna, the return response from a single point target can be modelled as a delayed, scaled version of the transmitted signal given by:

$$v_{rx}(t) = \zeta v_{tx}(t - \tau) \tag{2.1}$$

where $\tau = \frac{2R}{c}$ is the time delay of the echo,

and ζ is a scaling factor accounting for system and propagation effects [21].

For narrowband systems, ζ is related to the radar equation (see Section 2.1.5), as can be illustrated by the following proportionality:

$$\zeta \propto \sqrt{\frac{G^2\sigma\lambda^2}{4\pi^3 R^4}} \tag{2.2}$$

where G is the gain of the antenna,

σ is the radar cross section (RCS) of the target

and λ is the wavelength of the signal [21].

For wideband radar systems, however, ζ may vary considerably over a large enough frequency range, and so it is necessary to compute ζ as a function of frequency (and hence time) using the integral relationship given by:

$$v_{rx}(t) = \int_{-\infty}^{+\infty} \zeta(\tau) v_{tx}(t - \tau) d\tau = \zeta(t) \otimes v_{tx}(t) \Rightarrow V_{rx}(f) = \zeta(f) V_{tx}(f) \tag{2.3}$$

where $\zeta(t)$ is the impulse response of the scene or target.

This interpretation is quite insightful, as it shows us that the radar's received signal is effectively just a windowed version of the scene's impulse response, where $V_{tx}(f)$ is the windowing function [21]. The larger the bandwidth of the transmitted signal, the more detailed the target's/scene's impulse response is. This has possible implications for radars being able to detect what type of object is being interrogated (rather than just its position), by characterising the target's RF signature.

2.1.2 Range Ambiguity

Consider a radar waveform being transmitted at a frequency (also known as the pulse repetition frequency, or PRF) given by $fr = \frac{1}{T}$, where T is the period of the pulse. If a target is at too large a distance away from the radar, the echo from the first transmitted pulse could possibly arrive just after the transmission of the second pulse, making the target seem much closer than it really is [16]. This maximum target distance is known as the radar's unambiguous range, and is given by:

$$R_{unam} = \frac{c}{2f_r} \tag{2.4}$$

The target must thus lie within this unambiguous range in order to avoid range discrepancies.

2.1.3 Radar Bandwidth

The radar system bandwidth of the detector is commonly chosen as the bandwidth needed to obtain the largest possible peak signal from the target and the minimum amount of white noise. This is also known as the matched filter bandwidth and, for a rectangular pulse, is given by:

$$B = \frac{1}{\tau} \tag{2.5}$$

where τ is the pulse width.

Another interpretation is that all realisable filters (any linear, time invariant system can be modelled by a filter) have a finite impulse response which can be represented by a *sinc* function, where B corresponds to the width between the nulls [10].

2.1.4 Range Resolution

This is defined as the minimum range separation needed between two targets in order to be able to distinguish or resolve their return echoes. Consider a radar pulse of width τ, and two objects separated in range by a distance $\Delta R = \frac{c\tau}{2}$. At some time $t_1 = t_0 + \frac{\tau}{2}$, pulse 1 arrives at target 1 and is about to be reflected. At some later time, $t_2 = t_1 + \frac{\tau}{2}$, a second pulse arrives at target 2, and is about to be reflected, while pulse 1 has travelled a distance back towards the transmitter proportional to $\frac{\tau}{2}$, and lies at $t_1 - \frac{\tau}{2} = t_0$. Thus, at time t_2, the trailing edge of pulse 1 is at t_0, while the leading edge of pulse 2 is at $t_2 - \tau = (t_0 + \frac{\tau}{2} + \frac{\tau}{2} - \tau) = t_0$. Thus, if two objects are spaced closer than a distance,

$$\Delta R = \frac{c\tau}{2} = \frac{c}{2B} \tag{2.6}$$

the returns from the two pulse will overlap each other, and the detector will not be able to resolve the two objects separately. This minimum target separation is known as the radar range resolution [10].

2.1.5 The Radar Equation

The radar equation relates the peak power received in a radar system, to the peak transmitted power. It is given by the following expression:

$$P_r = \frac{P_t GtGr\lambda^2\sigma}{(4\pi)^3 R^4} \tag{2.7}$$

where P_r = received power (in W),

P_t = transmitted power (in W),

G_t = gain of transmit antenna,

G_r = gain of receive antenna,

λ = wavelength (in m),

σ = the radar cross section (RCS) of the target (in m^2),

R = range to the target (in m).

What is important to notice is how rapidly the received power decreases with range due to the inverse power of four relationship [10]. The radar equation applies mainly to narrowband systems however, as alluded to in Section 2.1.1.

2.1.6 Signal to Noise Ratio

The amount of received noise in a system is given by [20]

$$N_r = kT_eB \tag{2.8}$$

where k = Boltzmann's constant = $1.38 \times 10^{-23} J/K$

T_e = the equivalent noise temperature of the receiver in degrees Kelvin (K),

B = the bandwidth of the receiver in Hertz (Hz).

The signal to noise ratio (at the input to the receiver) is thus given by:

$$SNR = \frac{P_r}{Nr} \tag{2.9}$$

where P_r= received power (in W),

N_r= received noise power (in W).

2.2 General Antenna Theory

Antennas are basic components in radar systems whose function it is to radiate or receive electromagnetic (EM) waves, using free space as the primary medium of propagation. They are thus resonating elements, and are designed in order to achieve various objectives, some of which can include (but are not restricted to) the ability to radiate efficiently, to provide a desired gain, directionality, compactness (for mobile technology) etc. A few aspects of antenna theory were researched in order to gain a better understanding of some of the concepts involved when using antennas for radar.

2.2.1 Antenna Dimensions

Antenna dimensions can vary from fractions of a wavelength to several wavelengths. The wavelength (in m) is calculated from the simple formula:

$$\lambda = \frac{c}{f} \tag{2.10}$$

where c is the speed of light in the propagating medium (usually air, in which case the *in vacuo* value of $3 \times 10^8 m/s$ is used),

and f is the operating frequency (in Hz) of the antenna.

Common (but by far the only) wire antenna dimensions used to achieve effective radiation are typically lengths $l = \frac{\lambda}{2}$ and $l = \frac{\lambda}{4}$ for dipoles and monopoles respectively [17].

2.2.2 Antenna Radiation Patterns

The radiation pattern of an antenna is a plot of the magnitude of the far-field strength (or sometimes power) versus angular position around the antenna. A typical antenna beam pattern is shown in Figure 2.2.

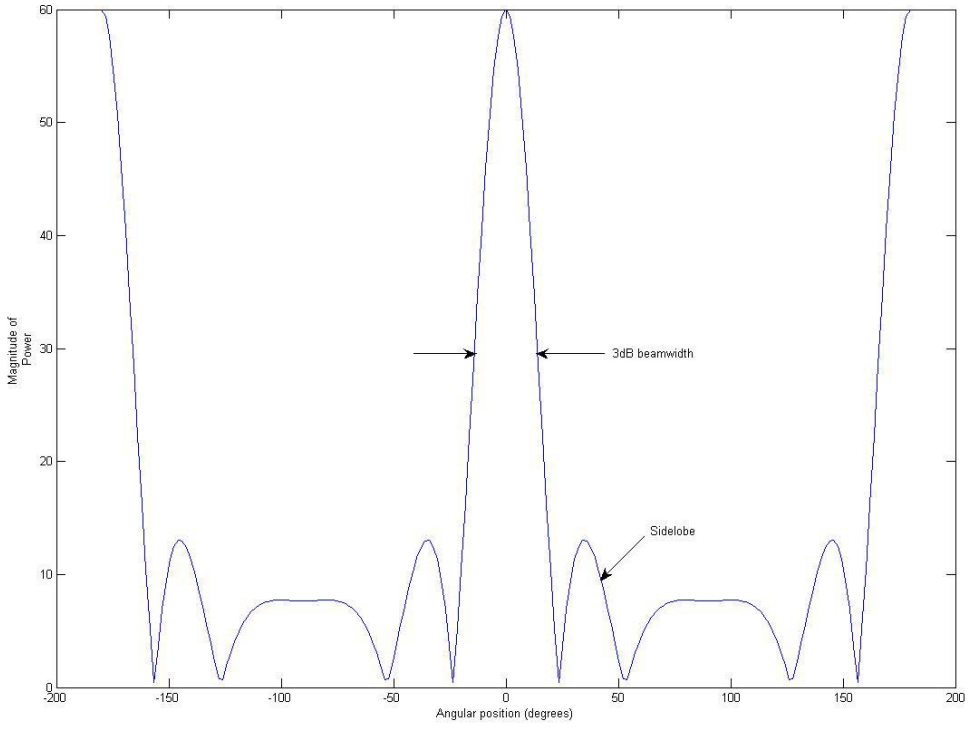

Figure 2.2: Antenna radiation pattern showing 3dB beamwidth

The lobe with the maximum value is usually referred to as the main beam, while additional, lower level lobes are called sidelobes [12]. The $3dB$ beamwidth of an antenna is defined as the angular width of the main beam at which the power level has been halved

(dropped by $3dB$ from its maximum value). The $3dB$ beamwidth (in radians) of an antenna can be approximated by the formula:

$$\theta_{3dB} = \frac{\lambda}{d} \tag{2.11}$$

where λ = the wavelength of the radiated/received signal in metres (m),

d = the antenna aperture dimension (usually azimuthal length, in m).

Antennas thus have the ability to focus power in a certain direction. The larger the length of the aperture, the more narrow or focused the beam is, and *vice versa*.

An antenna radiating power equally in all directions in the azimuthal (horizontal) plane is referred to as omni-directional or isotropic, while a directional antenna has a main beam over an angular region less than 360^o.

2.2.3 Far-Field Distance

The far-field distance of an antenna refers to the distance at which the spherical wavefront of a radiated/received wave can be approximated by that of an ideal plane wave [12]. This distance (in m), also known as the Rayleigh criterion, is given by:

$$R_{ff} = \frac{2d^2}{\lambda} \tag{2.12}$$

where λ is the wavelength of the radiated signal (in m),

d = antenna aperture dimension (in m)

2.2.4 Antenna Polarization

The polarization of an electromagnetic (EM) wave is usually defined with regards to the orientation of its electric field vector, E. This vector is orthogonal to both the magnetic field vector as well as the direction of propagation of the wave, forming a $3D$ plane (see Figure 2.3).

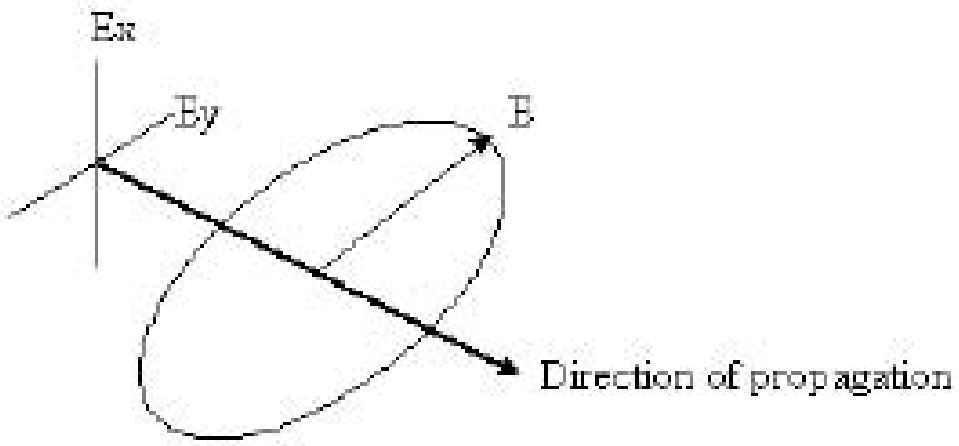

Figure 2.3: Typical Elliptically Polarized EM field [5]

In the figure, E_x refers to the x-component, and E_y refers to the y-component of the electric field vector, E (the vector sum of $E_x$and E_y). In the most general case, the electric field is elliptically polarized as shown[5].

The *IEEE* defines the polarization of an antenna as the polarization of the radiated (electric) field when the antenna is operating as a transmitter [12].

2.2.5 Linear Antenna Arrays

A linear antenna array usually consists of a number of identical individual elements, equally spaced in a line. Because an array is a sampled aperture (not continuous as in a horn antenna, for example), there are limitations on the spacings between the array elements. If these spacing requirements are violated, a phenomenon known as grating lobes occurs, in which repeated main lobes appear in the array radiation pattern at positions other than the array boresite. Without going into the detailed maths involved to derive the spacing criterion (which can be found in [17]), in order to avoid grating lobes, the spacing, d between each element must be such that $d < \lambda$.

With an antenna array, beam steering can be performed (often digitally with software), by phase shifting the received signals from each element relative to some reference phase, and adding the signals together to focus the beam for a specific point in space. In Section 3.3, a beam focusing algorithm is described, developed and implemented in software.

2.3 Ultra-Wideband (UWB) Technology

2.3.1 Definition of Ultra-Wideband (UWB)

The term ultra-wideband (UWB) refers to signals that have a fractional bandwidth greater than 0.25 with respect to their centre frequency. A signal's fractional bandwidth is given

by [**?**]:

$$B_f = \frac{2(f_h - f_l)}{(f_h + f_l)} \tag{2.13}$$

where f_h = the upper frequency limit of the signal,

and f_l = the lower frequency limit of the signal (in Hz).

Since ultra-wideband (UWB) can refer to any system that meets the requirements of the definition given above, it is necessary to specify what type of UWB system is being investigated in this thesis. This thesis deals specifically with UWB *impulse* technology (commonly used as the umbrella term, UWB), where basebanded pulses are generated directly. Ultra-wideband (UWB) impulse technology typically involves the transmission and reception of extremely short (usually sub-nanosecond) pulses with relatively low percentage duty-cycles (often less than 1%), and high fractional bandwidths (in the GHz range). Whereas most narrow-band systems modulate the baseband information on a carrier, due to the extremely broad bandwidths associated with UWB, it is often impossible to determine an RF centre frequency, hence these types of transmission techniques are often termed "carrier-free". The average transmitted energy of an UWB pulse is also very low, due to the pulse's short duty-cycle [1].

2.3.2 Advantages of UWB Technology for Radar

In radar, short pulse durations (*viz*. high bandwidths) translate into very high radar range resolution, meaning the positions of closely spaced targets can be accurately resolved [1].

It is even postulated that the high signal bandwidths and detailed frequency content carried by the UWB return echo could provide more information than just the presence of a target, as was suggested in Section 2.1.1. The content of UWB return waveforms has been shown to change depending on the target's morphology and composition, using a radar technique known as the Singularity Expansion Method (SEM) [**?**].

Due to UWB pulses possessing large bandwidths and low duty cycles, these signals are characterised by having a low average power spectral density (PSD) which can be further reduced through techniques such as pulse repetition frequency (PRF) dithering. This results in a low probability of detection/interception (LPI/D) RF signature for UWB pulses, making UWB radar technology ideal for covert military operations.

UWB (or impulse) radars operating in frequency ranges below 1 and possibly 2GHz can also serve as ground penetrating radars (GPR's) in applications such as geographical land surveying, underground object detection etc.

2.3.3 Advantages of UWB Technology for Communications

Since ultra-wideband (UWB) pulses have extremely large bandwidths and short duty-cycles, their use in communication allows for high speed data transmission ideal for

packet-burst traffic and time-division multiple access (TDMA) sharing of resources. In addition, due to the pulses' short widths, multi-path rejection for wireless communications is improved since direct path and multi-path components are easily discriminated in time, resulting in less destructive interference.

Due to UWB signals possessing a low probability of detection (LPD) RF signature (as was described in Section 2.3.2), the probability of interception by unauthorised receivers is minimised [1]. This implies that UWB radio communication possesses a certain level of inherent security, and is especially useful in military applications where stealth is important. An LPD also reduces interference with proximity and legacy systems while also minimizing RF health hazards, which are key aspects for both military and commercial applications [2].

2.3.4 Advantages of UWB Hardware Implementation

Fewer RF components are needed in an UWB radar system configuration than in traditional narrowband systems employing carriers. Since UWB baseband pulses can be generated directly, no heterodyning is performed thus obviating the need for transmit filters, mixers, phase locked loops and other traditional RF components. As a result, UWB systems can be less complex and expensive. UWB systems also operate at very low pulse repetition frequencies, meaning their signals possess low average power, thus requiring less prime power and allowing for smaller transceiver antennas and battery operation [**?**].

2.3.5 Other Applications of UWB Technology

These include:

- Through-wall Radar Imaging for Military and Law Enforcement Applications
- Altimeter/Obstacle Avoidance
- RF ID or Radar Tags (Facility and Personnel Security, Intelligent Transportation Systems, Electronic Signs, Smart Appliances)
- Intrusion Detection Radars
- Precision Geolocation Systems
- High Speed ($20Mb/s$++) Local Area Networks/Wide Area Networks (LAN/WANs)
- Collision Avoidance Sensors
- Industrial RF Monitoring Systems [2],[**?**].

Chapter 3

Software Simulations

This chapter outlines the software simulations performed in order to gain valuable insight into antenna array beam patterns and idealized ultra-wideband impulse radar downrange profiles. It also explains the beam focusing algorithm developed in this thesis, as well as demonstrates its implementation on the data generated by the simulation in Section 3.2.

All software was written in MATLAB v7, Release 14 running on Windows XP, and can be found in Appendix A, as well as on the CD supplied with this thesis (see the inside back cover).

3.1 Antenna Beam Patterns

The aim of this simulation is to observe the effect on the magnitude of a received plane wave versus the angle of incidence (θ, from $-\pi$ to π radians) for varying values of antenna aperture resolution (*viz.* the spacing between the receiver elements in the array).

Consider a sinusoidal pulse of the form $v_{tx}(t) = \cos(\omega_o t)$, possessing an angular frequency (in rad/s) of $\omega_o = 2\pi \times 1.5 \times 10^9$, unity amplitude and zero initial phase shift. This signal can be expressed in analytical form as, $v_{tx}(t) = \exp^{(j\omega_o t)}$, [21].

Now consider an N element linear receiver antenna array of length D. Since the receive antenna is in the far-field of the transmitted beam, the elements can be approximated as point targets, with a separation $d = \frac{D}{N-1}$ between each element. From the extended target radar model [21], the received signal is just a sum of scaled and delayed versions of the transmitted signal. Hence, it can be expressed as:

$$v_{rx}(t) = \sum_{n=1}^{N} A_n \exp^{(j\omega_o[t-t_n])} = A \exp^{(j\omega_o t)} \sum_{n=1}^{N} \exp^{(-j\omega_o t_n)} \tag{3.1}$$

where A_n is the attenuation factor to the n^{th} receiver element, and t_n is the time delay to the n^{th} element. In the equation, A_n has been factored out as the constant A, since the scaling factor A_n for each element is approximately the same (the attenuation due to the extra distance the received waveform has to travel to adjacent receiver elements is

negligible with regards to the attenuation due to the distance from the transmitter). The term $A\exp^{(j\omega_o t)}$ is thus just a revolving phasor with magnitude A.

If we assume A is unity, then the magnitude of the received signal v_{rx} can be simplified to:

$$|v_{rx}| = \left| \sum_{n=1}^{N} \exp^{(-j\omega_o t_n)} \right| \tag{3.2}$$

i.e. the combined received signal from all the receiver elements is just a sum of complex exponentials, each with a phase shift relative to some reference element. Let the N elements each be labelled E_n, where $1 \leq n \leq N$. Let the reference element be the first element, i.e. E_1, with t_1 as the time delay from the transmitter to E_1. All other elements will thus be phase shifted from E_1 by an amount $\Delta t = t_n - t_1$. From geometry, Δt can be calculated as follows:

Since the transmitted *sine* wave was generated in the receiver's far-field, it can be approximated as a plane wave at the receiver. Assume that the plane wave arrives at E_1 such that a line perpendicular to its wavefront creates an arbitrary angle of incidence θ with the horizontal (dotted line), see Figure 3.1.

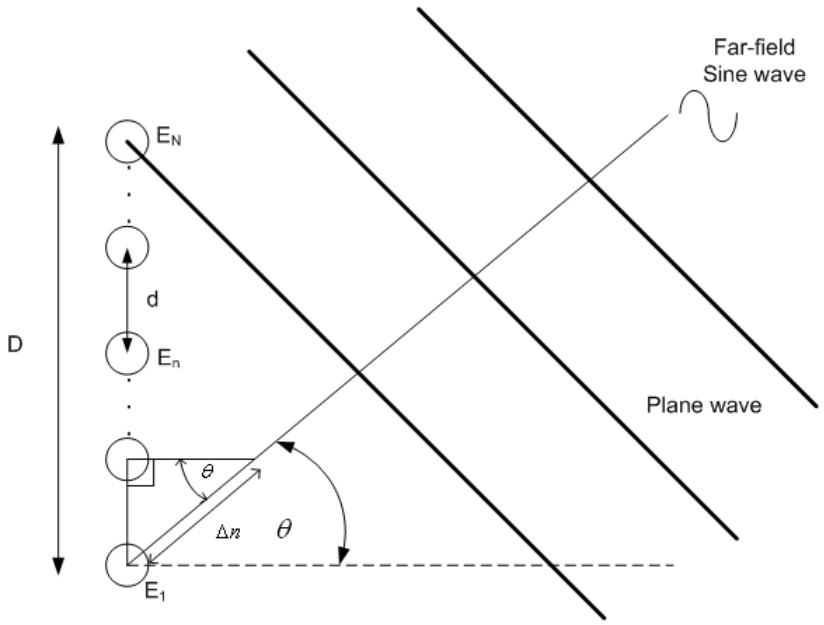

Figure 3.1: Receiver array and incident plane wave

The wave must have travelled the longest distance to E_1, and the smallest distance to the last element, E_N. Thus, the extra distance the wave has to travel from the n^{th} element E_n to E_1 can be given by $\Delta n = (n-1)dsin(\theta)$. This, in turn, can be converted into a time delay,

$$\Delta t = t_n - t_1 = -\frac{\Delta n}{c} \tag{3.3}$$

The programme *sin_array_sim.m* thus calculates the magnitude of the received waveform as θ varies between $-\pi$ and π radians, and plots the results in both polar and Cartesian

form.

For the simulations, the array length, $D = 1$. This corresponds to an aperture $3dB$ beamwidth of $\theta_D = \frac{\lambda}{D} = 0.2rad = 12^o$ (see Figure 3.2 for a plot of the receiver beam pattern, showing the 3dB beamwidth for $N = 40$).

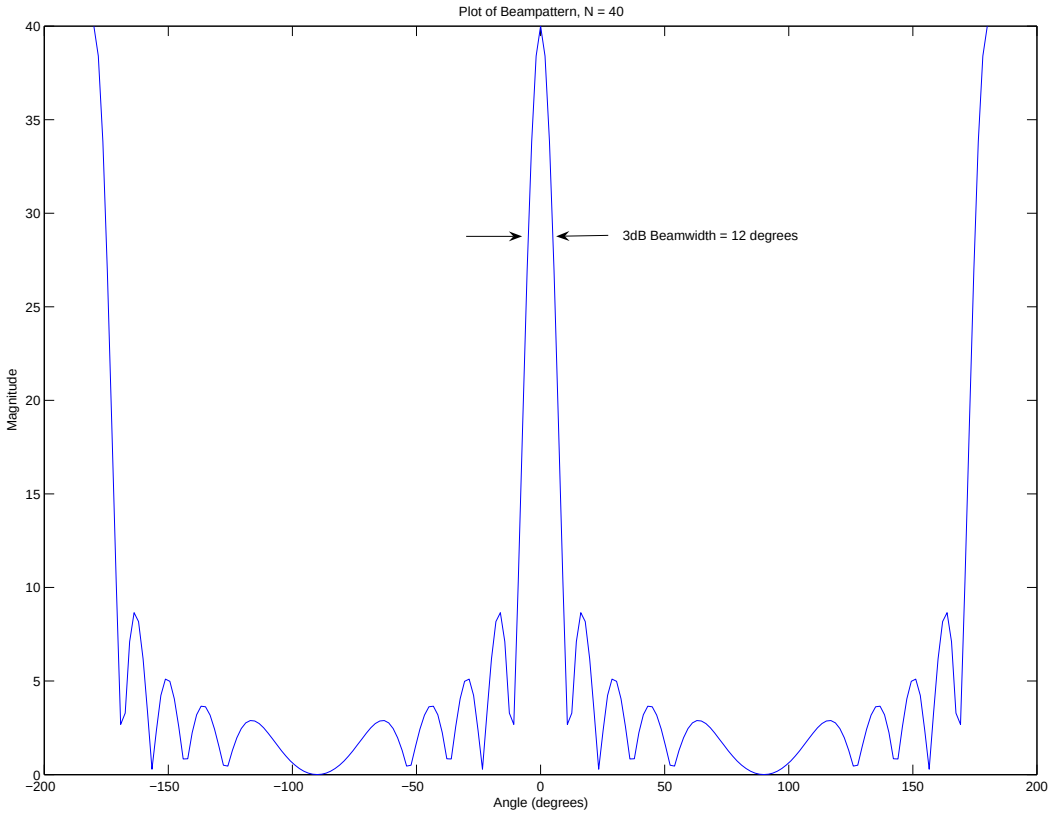

Figure 3.2: Receiver beam pattern showing the 3dB beamwidth for $N = 40$

Furthermore, different values of N were chosen to observe the effect of an under-sampled aperture. If N is not chosen large enough, then the distance (d) between the receiver elements approaches the wavelength of the received waveform and we observe a phenomenon called grating lobes (see Figure 3.5), thus concurring with the theory in Section 2.2.5.

This result is analogous to violating Nyquist's sampling criterion, (e.g. by under-sampling a waveform in digital signal processing), except in this case we are dealing with a "sampled" antenna aperture.

Grating lobes are side-lobes that take on unacceptably large magnitudes, and can eventually manifest themselves as duplicates of the main-lobe, off the antenna boresite.

In this example, the frequency of the sine wave is $f_o = 1.5GHz$ and the wavelength is $\lambda = 0.2m$. To avoid grating lobes, we must have a receiver array with spatial resolution finer than the wavelength of the received wave. Thus, if $d \geq \lambda = 0.2$, grating lobes are formed. This would be true for $N \leq 5$ in the simulation.

Below are a series of polar plots of the receiver beam pattern versus θ (angle of incidence), for various values of N (number of receiver elements).

In Figure 3.3, we see a normal antenna beam pattern, for $N = 40$.

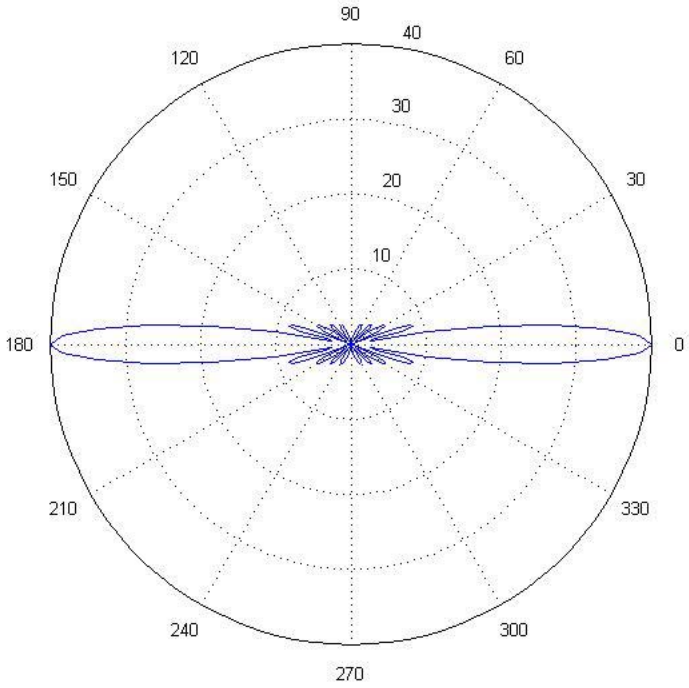

Figure 3.3: Polar plot of beam pattern versus angle of incidence, $N = 40$

In Figure 3.4, one can see the side-lobes starting to increase.

In Figure 3.5, grating lobes are clearly seen at $\theta = \pm 90^o$.

Additional grating lobes are seen in Figure 3.6, as the aperture is further under-sampled.

Finally, as $N = 1$, the receiver is no longer an array and instead models a point or mono-pole, with omni-directional beam pattern, as can be seen from Figure 3.7.

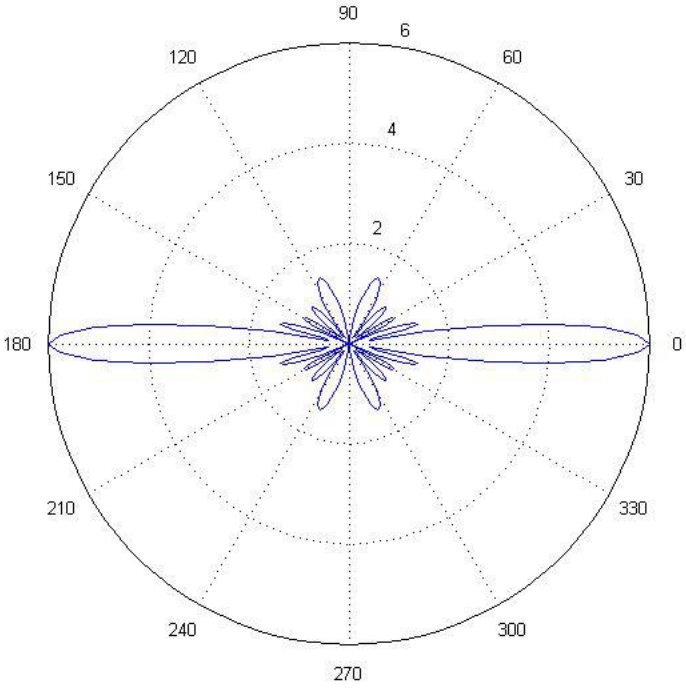

Figure 3.4: Polar plot of beam pattern versus angle of incidence, $N = 6$

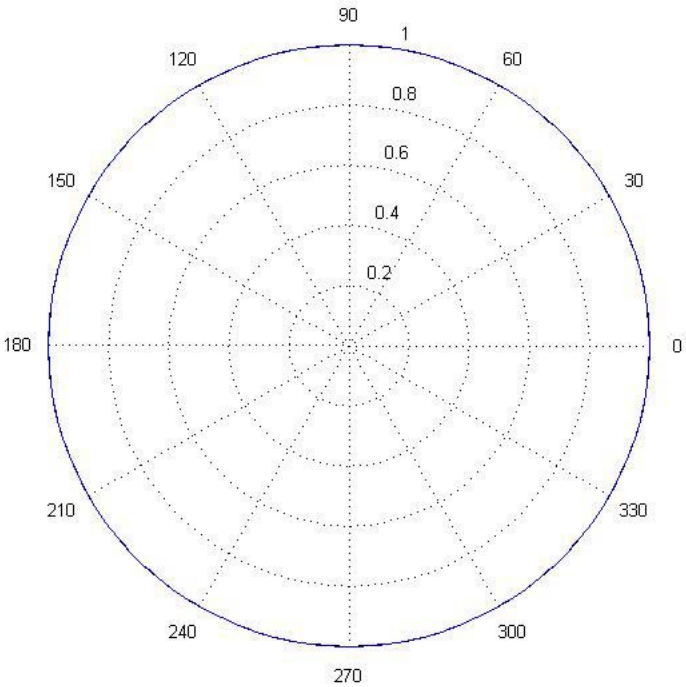

Figure 3.7: Polar plot of beam pattern versus angle of incidence, $N = 1$

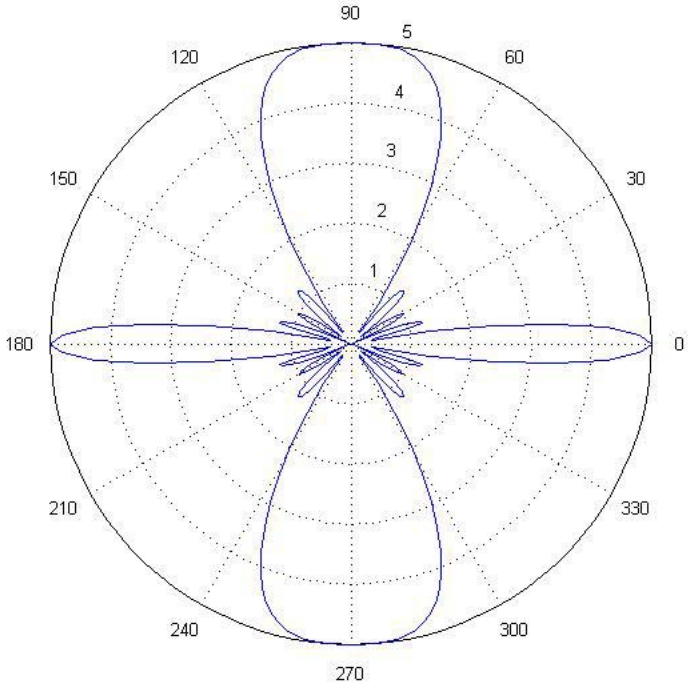

Figure 3.5: Polar plot of beam pattern versus angle of incidence, $N = 5$

3.2 Multi-Channel UWB Radar Simulation

The aim of this simulation is to generate downrange profiles from UWB return echoes as well as sample data to use in the beam focusing algorithm in Section 3.3. It must be emphasised that these downrange profiles are idealized representations, and do not take into account the finite impulse response of receive filters, antenna bandpass filtering as well as antenna ringing.

As was mentioned in Section 2.2.5, an antenna array increases the receive aperture dimension, narrowing the $3dB$ beamwidth of the receiver. The added advantage of having an array (such as a linear antenna array), is that electronic steering of the beam can be achieved by processing the difference in time delay to each element (i.e. its relative phase variation), see Section 3.3.

In the programme *UWB_radar_sim.m*, N receiver antennas are spaced equally apart on the x-axis at positions $[\frac{(n-1)}{N-1}, 0]$, where n represents the n^{th} receive antenna element, and $1 \leq n \leq N$. The aperture dimension, D has been chosen to be $1m$ long (as before).

The default value for $N = 5$, thus the receive antennas (elements one to five, or E_1 to E_5) are placed at [0,0], [0.25,0], [0.5,0], [0.75,0] and [1,0] respectively (where the co-ordinates given are Cartesian co-ordinates, [x,y]).

The individual antennas are placed next to one another in a straight line, thus the aperture beamwidth of each antenna is $\theta_{ant} = N\theta_D$, i.e. in the default case, $\theta_{ant} = 60^o$(five times

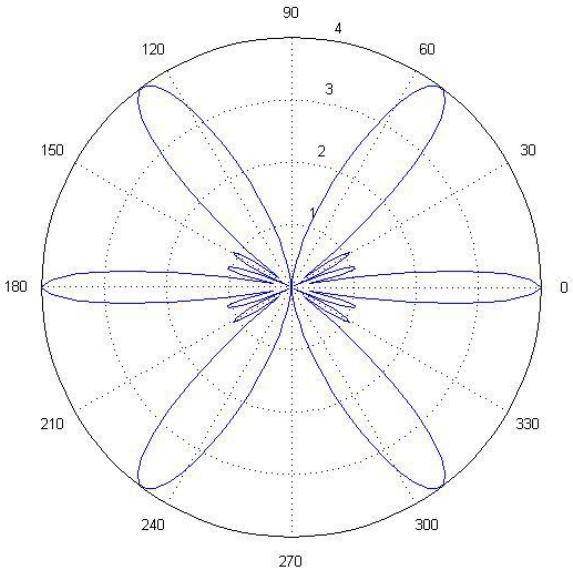

Figure 3.6: Polar plot of beam pattern versus angle of incidence, $N = 4$

broader than the $3dB$ beamwidth $\theta_{array} = 12^o$ of the array as a whole). The aperture dimension of each antenna, $d_{ant} = \frac{D}{N} = \frac{1}{5} = 0.2m$.

A transmit antenna can be placed at any position, with the default position being [0.5,0], i.e. the third (middle) element or antenna functions as a transceiver (transmits and receives).

The transmit antenna transmits a short, UWB pulse which can be expressed in analytical form as:

$$v_{tx} = \exp^{(j2\pi f_o t)} \, rect\left(\frac{t - t_d}{\tau}\right) \tag{3.4}$$

where $f_o = 1.5GHz$ (the antenna operating frequency),

$t_d = 0.5ns$ (time shift to position start of *rect* pulse at time $t = 0$),

and $\tau = 1ns$ (the pulse width).

The signal is thus $1ns$ wide, extending from 0 to $1ns$, with an arbitrarily chosen magnitude of unity. The pulse repetition frequency (PRF) of the transmit antenna is set at $2MHz$. Figure 4.10 shows the transmitted pulse.

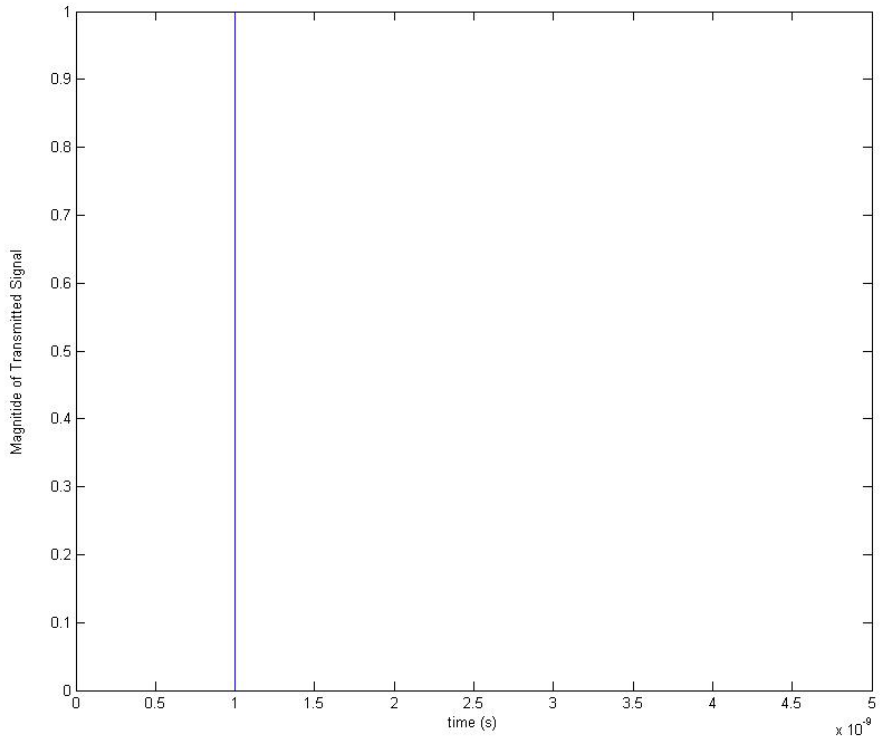

Figure 3.8: Transmitted signal

The unambiguous range of the radar system is given by $R_{unam} = \frac{c}{2fr} = \frac{3\times10^8}{4\times10^6} = 75m$. The range resolution $\Delta R = \frac{c\tau}{2} = \frac{\left(3\times10^8\right)\times1\times10^{-9}}{2} = 0.15m$.

In order to make the assumption that the wave front incident on the receiver is a plane wave, the targets should be in the far-field of the receiver. The far-field range of each antenna is $R_{ff} = \frac{2d_{ant}^2}{\lambda} = \frac{2\times(0.2)^2}{0.2} = 0.4m$.

Any number of point targets can be placed anywhere in front of the antennas to form a scene. Let each point target be represented by a number m, where $1 \leq m \leq M$, and M is the total number of targets. The default setting for the total number of targets, $M = 2$, and these two targets are placed at positions [0.1,4] and [0.8,8] respectively. With these co-ordinates, the targets are well within the unambiguous range, lie in the antenna's far field and are spaced far apart enough so that they can be resolved separately.

To place an upper bounds on the length of the time vector, the maximum target range has been chosen arbitrarily to be $R_{max} = 15m$. This corresponds to a maximum time delay of $T_{max} = \frac{2R_{max}}{c}$.

Since the duration of the transmitted pulse is 1ns, this corresponds to a bandwidth of roughly 1 GHz. If the received signal was basebanded, its maximum frequency component would be 0.5GHz. Thus, in order to satisfy Nyquist's Criterion, we would have to sample the received signal at 1GHz. Since with UWB technology it is difficult to make out the centre frequency of the transmitted pulse and the band-limiting nature of the antennas has not been taken into account, we shall choose to sample the signal at a high enough

rate to avoid any discrepancies. The sampling frequency, f_s has arbitrarily been chosen to be 100GHz, thus certainly satisfying Nyquist's Criterion. The time between samples, $d_t = \frac{1}{f_s} = 10ps$. The time vector thus extends from 0 to T_{max} in steps d_t, resulting in a vector of length 10001. The Figure 3.9 is a graphical representation of the receiver/target configuration.

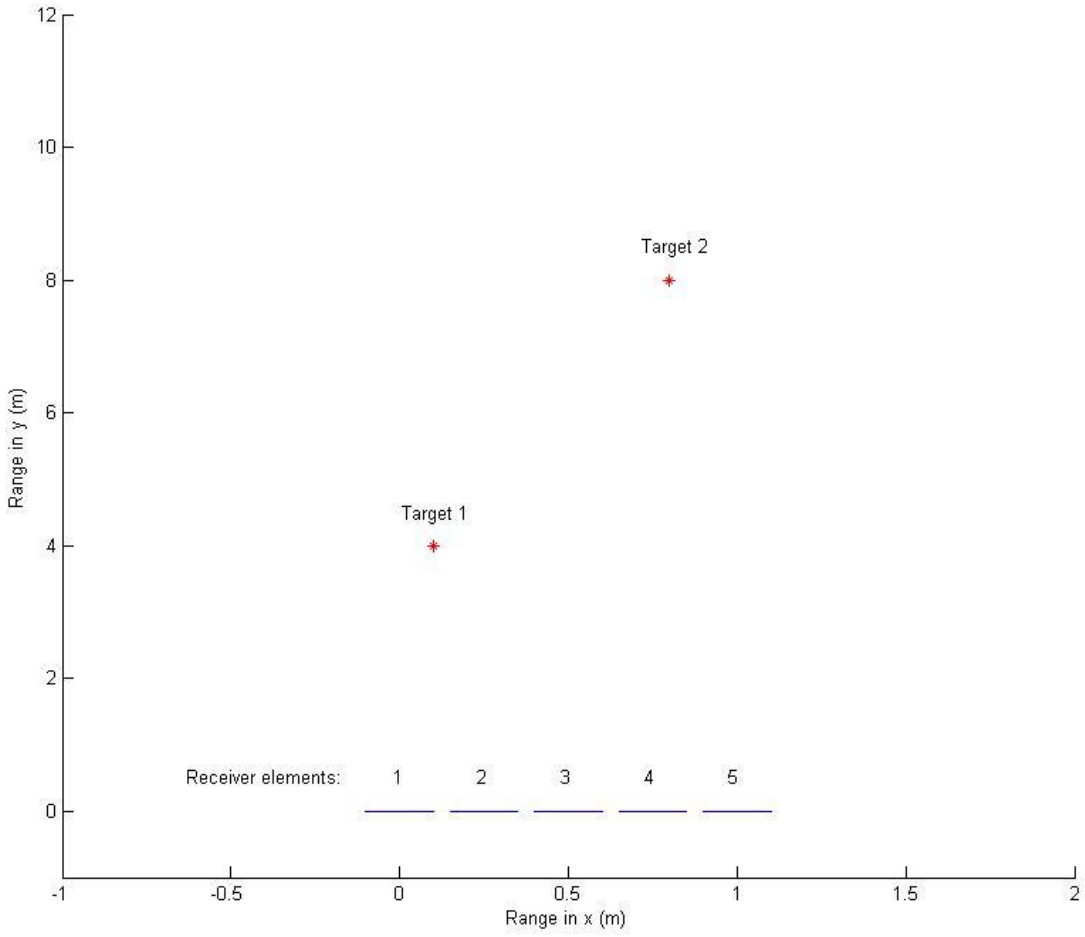

Figure 3.9: Receiver/target configuration

Since the transmit and receive antennas are matched, we can assume that the signal bandwidth and received bandwidth are roughly equal and hence it can be assumed that the received responses are just phase shifted (time delayed), scaled versions of the transmitted pulse (as described in Section 3.1). The programme thus simulates the radar responses as follows:

For each receiver element, the programme calculates the two way range (from transmitter to target, and back from target to receiver element) to every target (simple distance formula). It then converts the two-way range to each target to an equivalent time delay, $T_m = \frac{R_{2way}}{c}$, where m represents the m^{th} target. Since we are dealing with a simulation (and hence are excluding external system propagation and antenna effects), the attenuation factor, ζ_m (for the m^{th} target) as applied to narrowband systems (see Section 2.1.1) is

used to scale the transmitted pulse. Since G (the gain of the transmit and receive antenna, assuming they are equal) and σ (the radar target cross section) are not known, the value for ζ_m has been simplified to $\zeta_m = \frac{1}{R^2}$, where R is the distance to each target, m. The received signal for a particular receiver element, n is just the sum of the returns from all the targets, and can be expressed (in its basebanded form) as:

$$v_{rx_n} = \sum_{m=1}^{M} \zeta_m \exp^{(-j2\pi f_o T_m)} rect\left(\frac{t - T_m - t_d}{\tau}\right) \tag{3.5}$$

where $1 \leq n \leq N$.

Figure 3.10 and Figure 3.11 show the total received signal (i.e. from both targets) versus time and range respectively, for E_1. In radar circles, these plots are commonly referred to as downrange profiles.

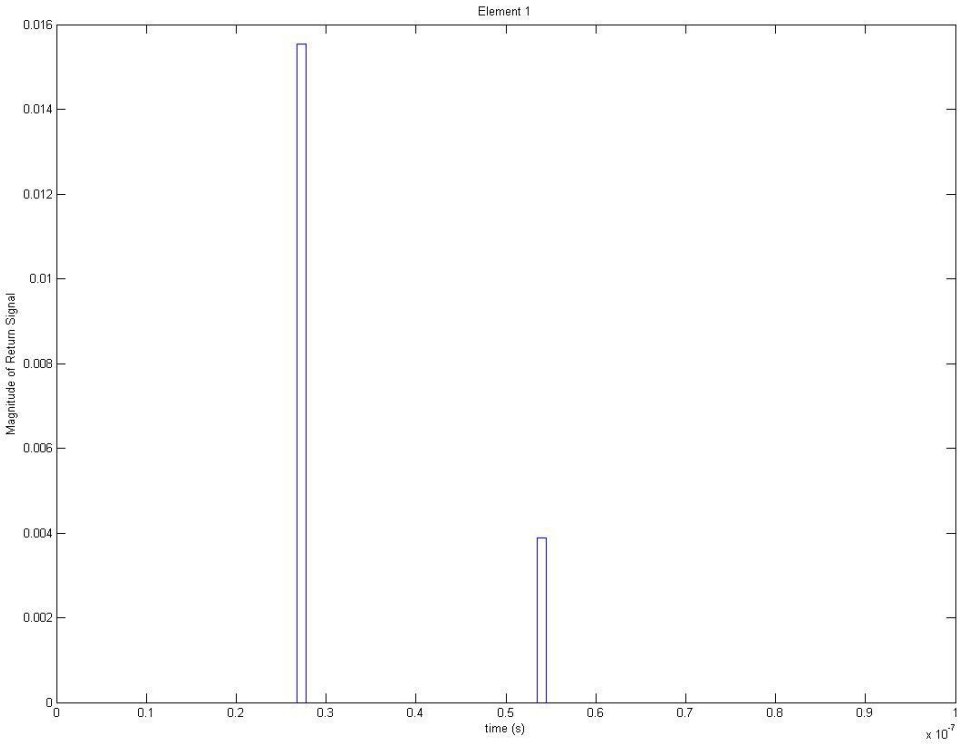

Figure 3.10: Magnitude of received signal vs time for E_1

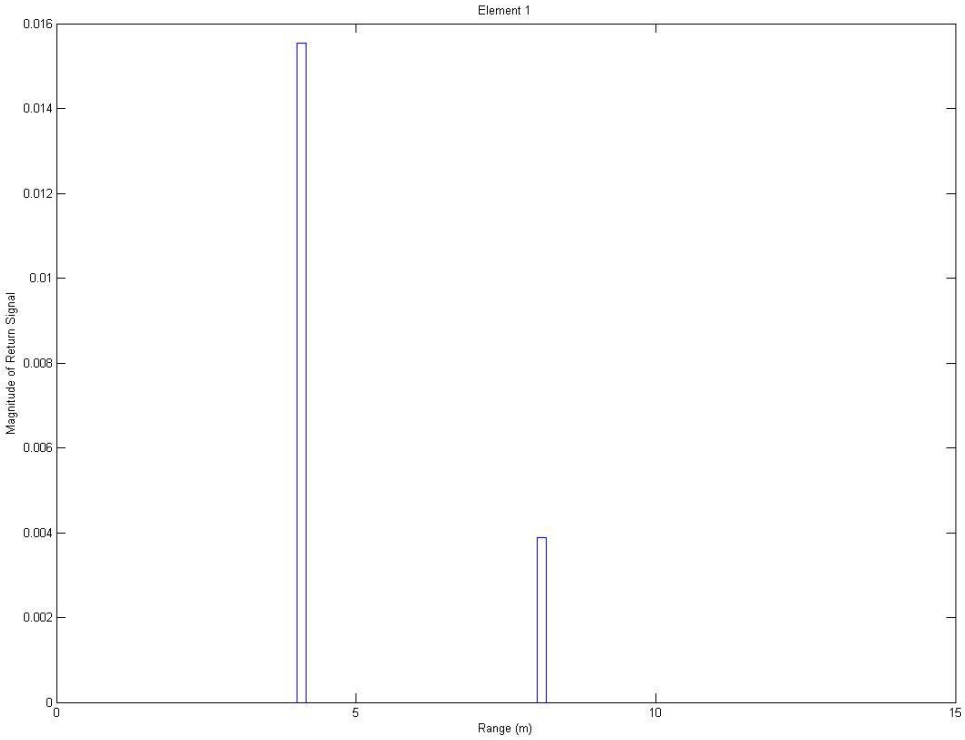

Figure 3.11: Magnitude of received signal vs range for E_1

Figure 3.12 was plotted using the *'imagesc'* command, and represents the magnitude of the Fourier transform of the received signal (due to the two targets) versus sample number for E_1. Note how the closer target (the one that occurs at the lower sample number, also in red) has a larger magnitude than the target further away (in blue).

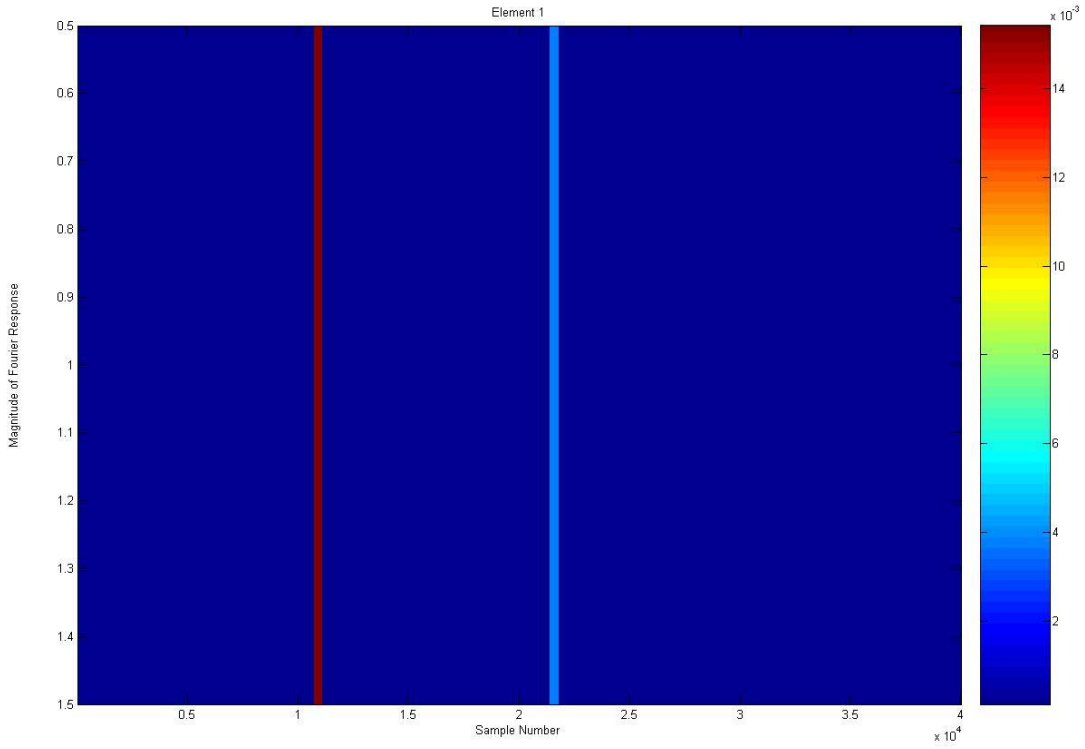

Figure 3.12: Image plot of the Fourier response of the received signal for E_1

Figure 3.13 shows the downrange profiles for each of the five elements plotted on the same figure. Although the magnitudes and phase look the same, they are actually slightly varying, as the micro attenuation and time delay due to the extra distance the received waveform has to travel to adjacent receiver elements is small in comparison with the macro attenuation and time delay due to the distance from the transmitter.

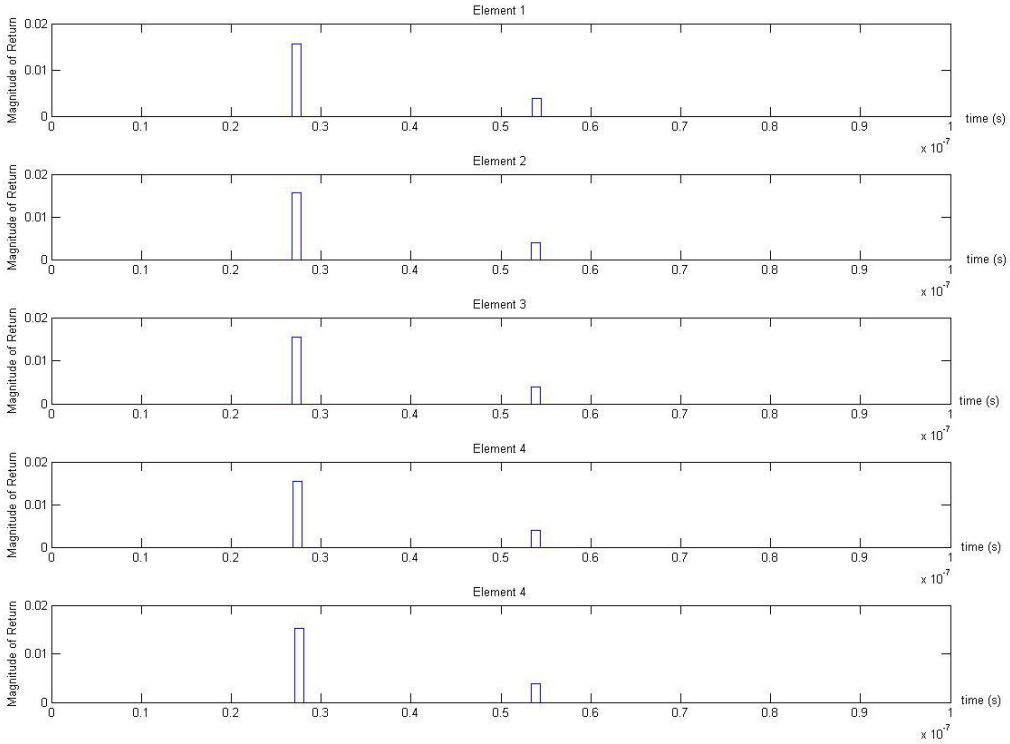

Figure 3.13: Downrange profiles for the five receiver elements

3.3 Beam Focusing Algorithm

The purpose of the beam focussing algorithm is to combine (in time) the signals (generated by the programme *UWB_radar_sim.m* described in Section 3.2) received from each element for every point in a grid of points. In so doing, it is possible to achieve electronic beam steering of the receive beam, and thus determine the position of one or more targets. (Note that the positions of targets within 0.15m of each other will not be accurately resolved due to the finite radar resolution).

The programme *focus_alg.m* begins by defining a rectangular grid, extending in the x-direction from -1 to 2 in steps $d_x = 0.1$, and extending in the y-direction from 3 to 9, in steps d_y = 0.05. This creates a $30X120$ point grid, containing the "unknown" target positions. The programme then scans the grid in both the x and y directions, and, for each receiver element, calculates the two-way range to each point, $[x, y]$ (similar to the procedure in Section 3.2) and hence the time delay. This delay, $T_{x,y}$ is then converted to a sample number, N_{sa} by dividing $T_{x,y}$ by the time step size, i.e. $N_{sa} = \frac{T_{x,y}}{d_t}$, rounded down. This sample number is then used to extract the value of the received signal from a particular receiver element at that grid point.

In order to combine all the received signals (from each receiver element) for a particular point, each signal needs to be phase-shifted or aligned in time. This is because the received signals are vectors (or phasors), each with a specific magnitude and phase. See

Figure 3.14 for an example phasor diagram.

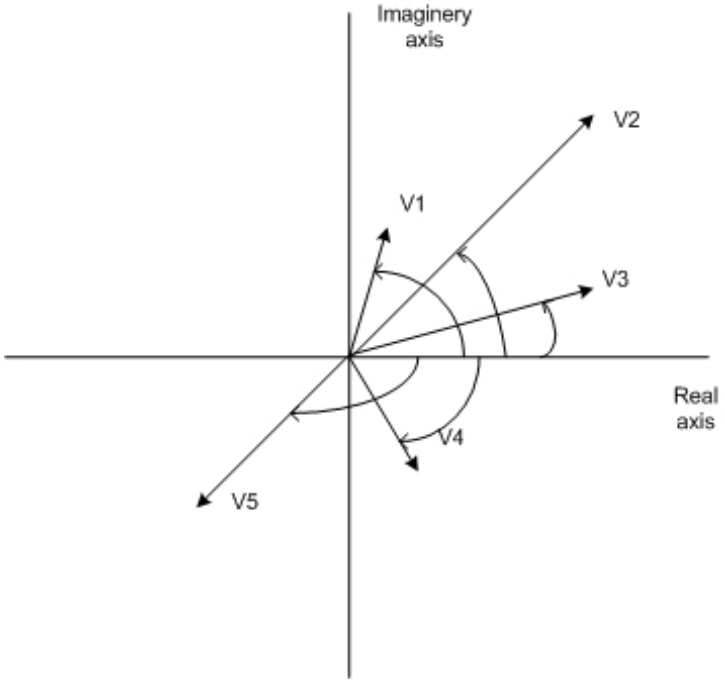

Figure 3.14: Example of a phasor diagram showing vectors V1 to V5

The signals received at each element are thus phase shifted with respect to one another, and hence cannot simply be added together, as cancellations may occur. Their magnitudes may also not simply be added, since they are vectors (not scalars) and require vector addition. Thus, the whole crux behind the beam focussing algorithm is to phase shift the signal received by each element so that they are aligned in time, and then perform vector addition, which means we get maximum signal (or maximum resultant vector, see Figure 3.15) as the addition is completely constructive.

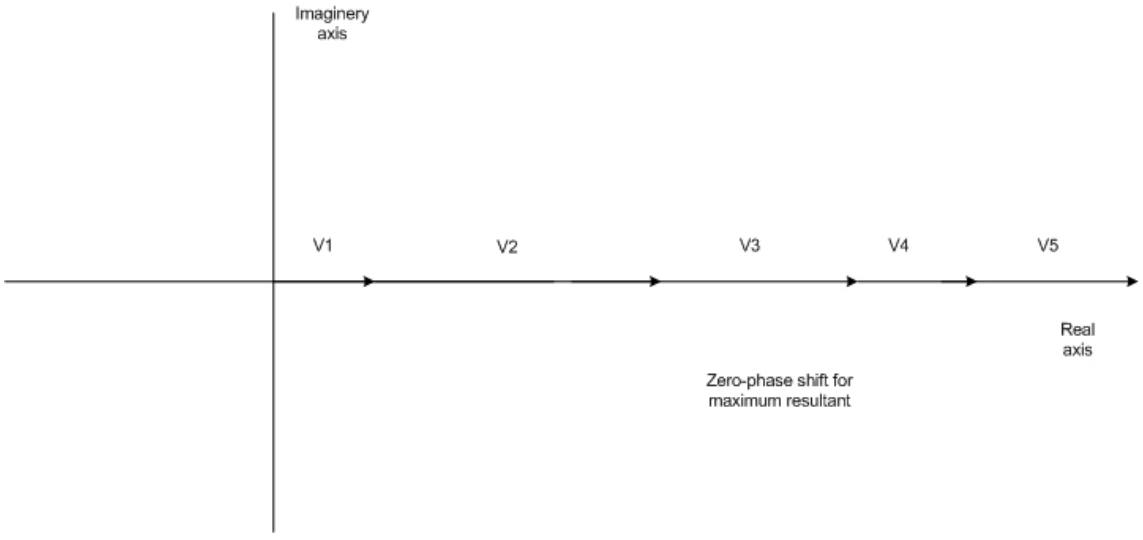

Figure 3.15: Phasor diagram showing maximum resultant due to phase shifting

Thus, for each element, the received signal from a point (and a possible target) in the grid is phase shifted by an amount equal to the delay $T_{n(x,y)}$ to that point, where n is the

number of the receiver element, and $[x, y]$ are the coordinates of the grid point. This is equivalent to multiplying the received signal for each element by $\exp^{j2\pi f_o T_{n(x,y)}}$.

Range compensation gain has also been added to this algorithm by multiplying the received signals by $A = \frac{1}{\zeta}$. By performing the above operations, we are thus able to electronically steer the beam so that it focuses the received signal for each point in a grid, and obtain image plots showing the positions of targets.

Figure 3.16 shows an image of the two focused targets in a 30X120 point grid.

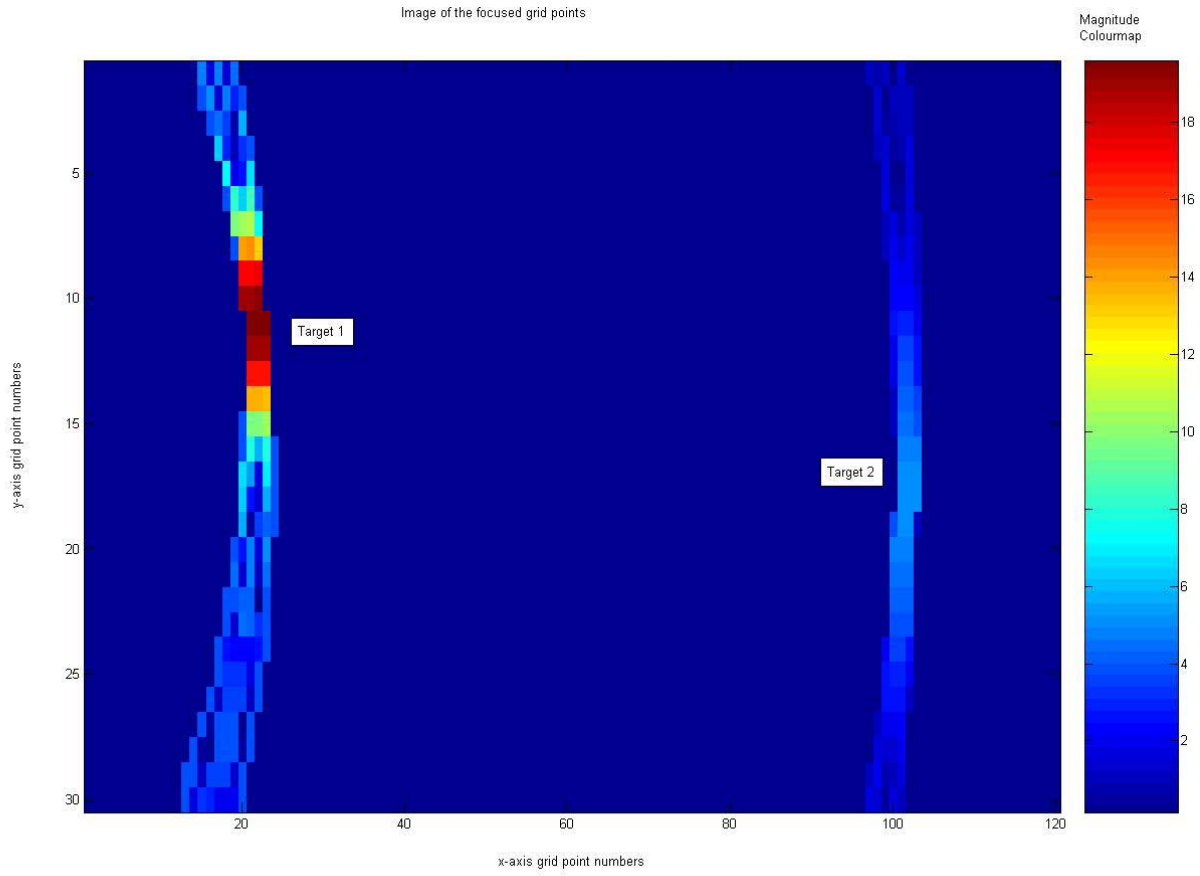

Figure 3.16: Focused targets in the 30X120 point grid

Figure 3.17 was created using the *meshgrid* command, and is a 3D plot of the two focused targets.

In order to reduce the magnitude of the sidelobes somewhat, a windowing function can be applied to the receiver elements in space. Figure 3.18 and Figure 3.19 show the effects of applying a spatial Hanning window to the receiver aperture array.

Notice in Figure 3.19 how the sidelobes have effectively been halved, e.g for target 1, their magnitude has been reduced from 4 to 2, at the expense of main-lobe broadening and flattening (magnitude dropped from 12 to 6.5).

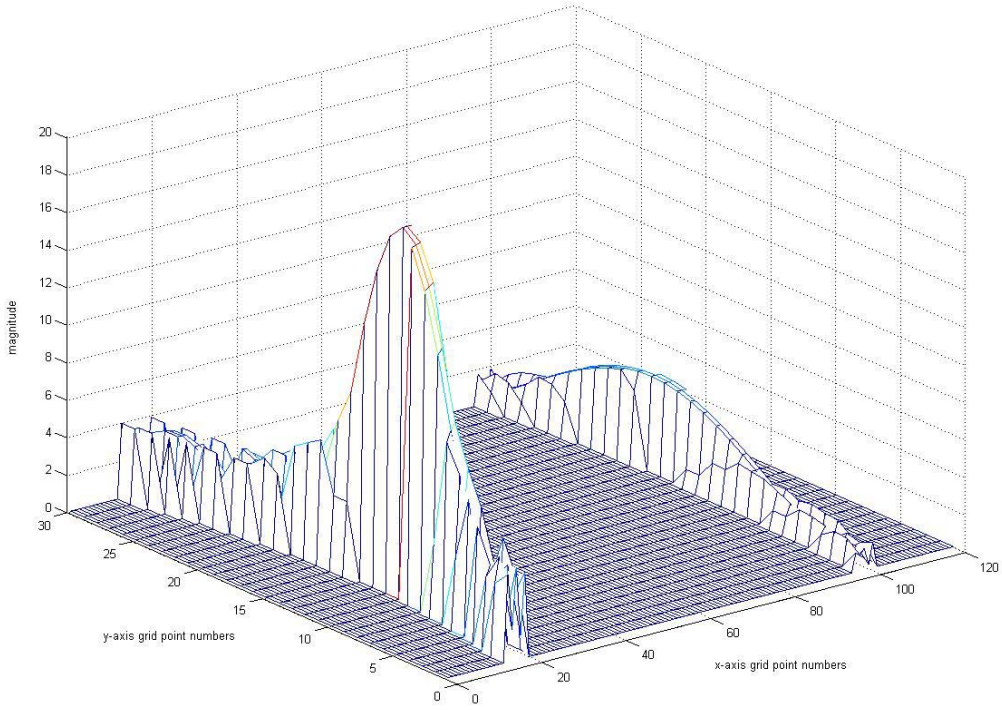

Figure 3.17: 3D plot of two focused targets in the 30X120 point grid

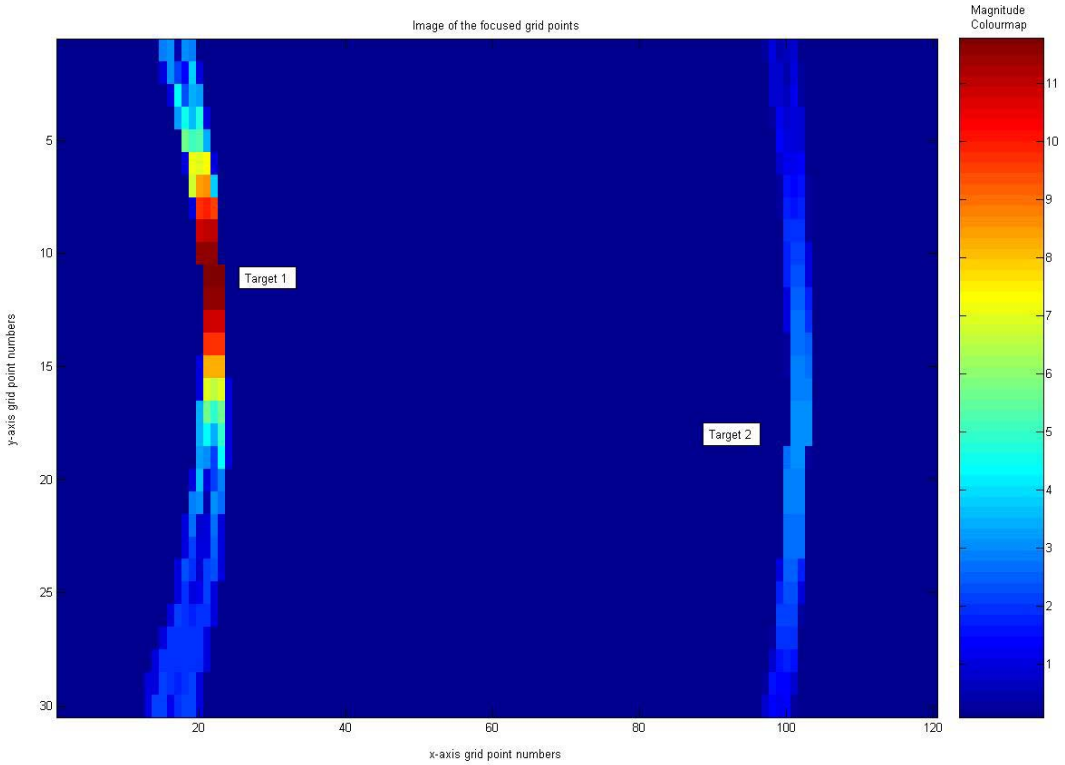

Figure 3.18: Focused targets in the 30X120 point grid after the application of a Hanning window

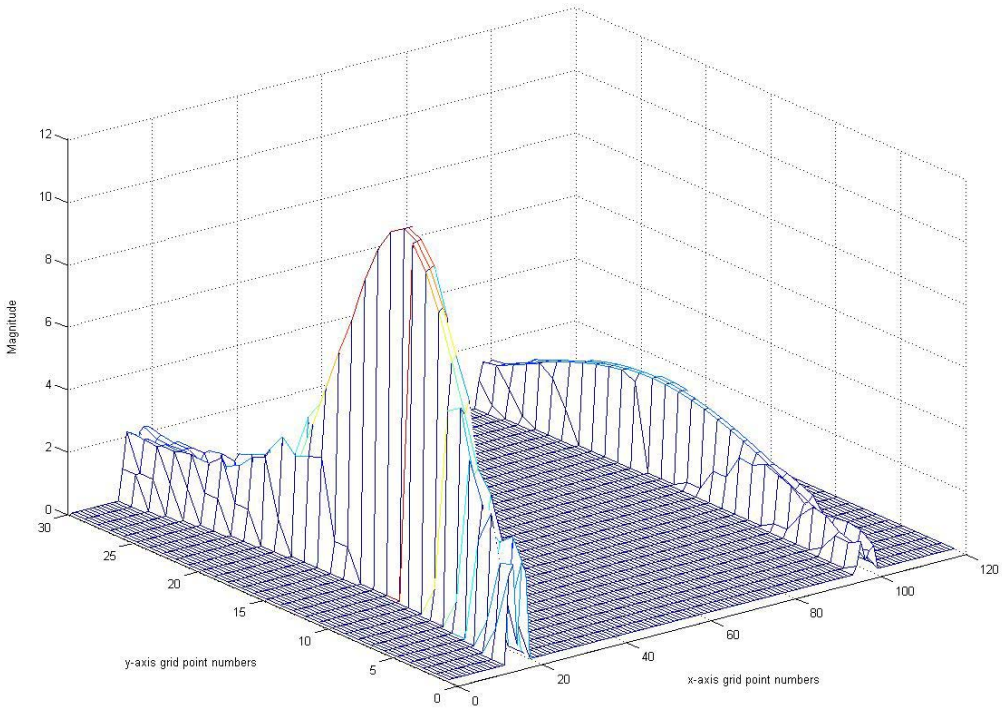

Figure 3.19: 3D plot of two focused targets in the 30X120 point grid after the application of a Hanning window

Chapter 4

Analysis of a Single Channel Radar System

The design of the multi-channel ultra-wideband (UWB) radar system is based on the single channel system described in [6]. In order to proceed to build a multi-channel version of this system, the existing system's operation needed to be analysed and fully understood to facilitate this process. Figure 4.1 shows a block diagram of this system. This UWB radar system functions by transmitting short pulses which reflect off objects and are then received. The received signal is amplified, sampled and sent to a computer where a programme converts the signals into down-range profiles which are displayed real-time. The actual circuit was built on a ground plane, with a separate plug-in RF amplifier in the receiver front-end (see Figure 4.2 for a photograph of the setup).

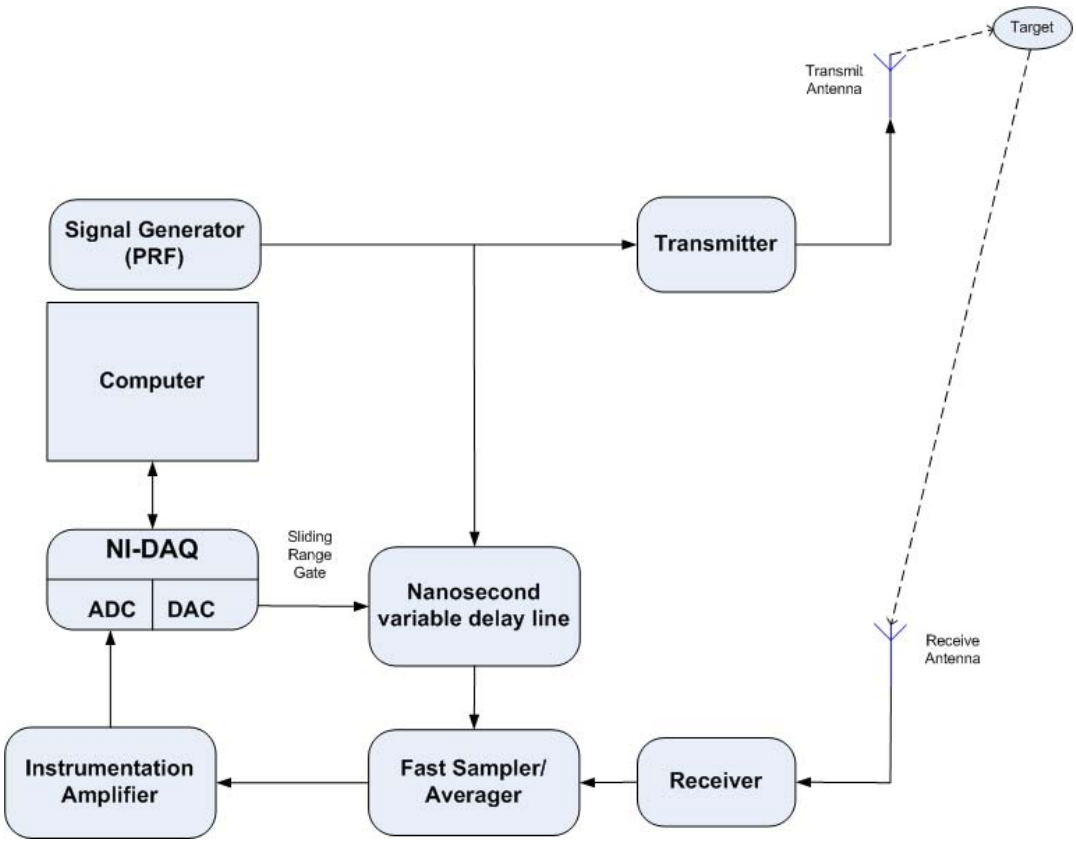

Figure 4.1: Block diagram of UWB single channel radar system, based on [6]

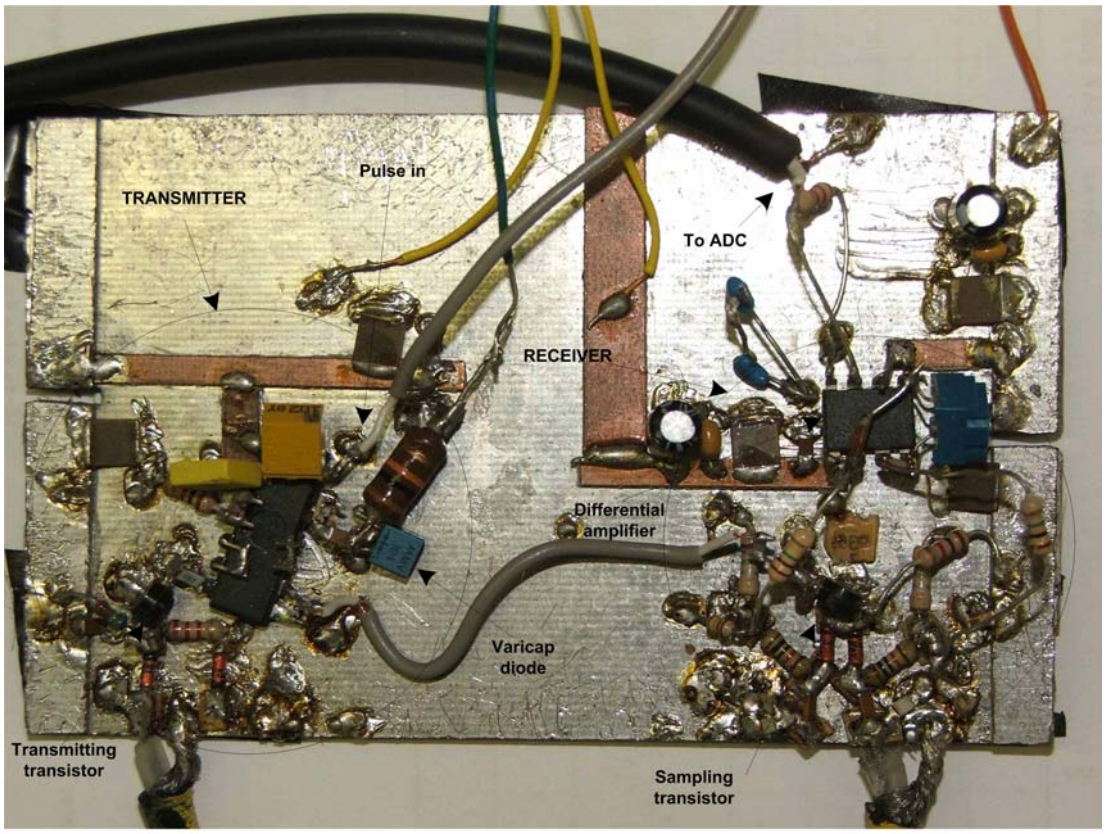

Figure 4.2: Photograph of the UWB single channel radar system described in [6]

In order to be able to analyse the extremely narrow pulses involved in this UWB sys-

tem (roughly 1ns in length), it was necessary to use an Agilent Infinium 54833A digital oscilloscope, which has a 1GHz bandwidth and is capable of delivering 4Gsa/s. See Figure 4.3.

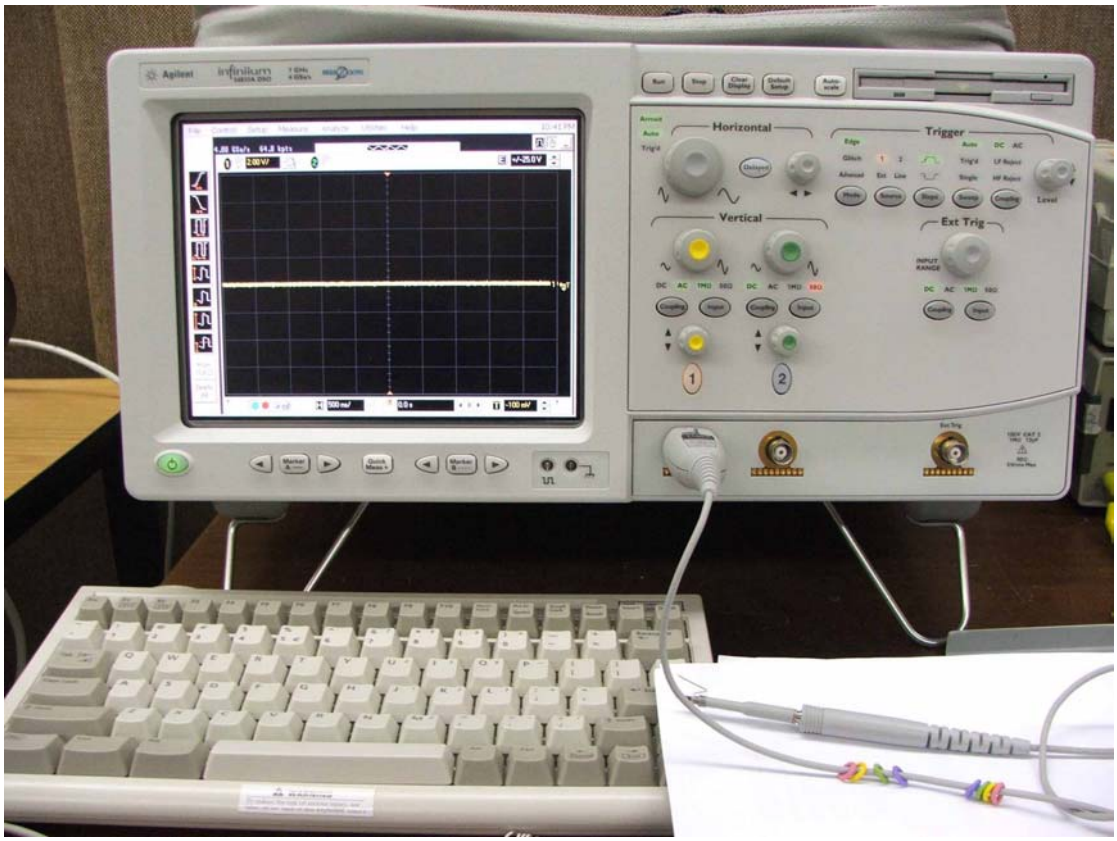

Figure 4.3: Agilent Infinium 54833A Digital Oscilloscope

4.1 The Antennas

A pair of twin bow-tie antennas made by [15] are used for transmitting and receiving power. They have an aperture dimension of approximately $d = 0.2m$. They are fed via BNC connectors and RG58 (50ohm) coaxial cabling. The antennas are mounted on metal plates, to minimize back reflections. The graph of their gain versus frequency is shown in Figure 4.4. One can see that they have a useful gain over a roughly 1GHz bandwidth between 1-2GHz (beyond these points the gain rolls off). This bandwidth corresponds to a range resolution of $\Delta R = \frac{c}{2B} = 0.15m = 15cm$. Figure 4.5 shows a photograph of the twin bow-tie antenna pair.

4.2 The NI-DAQ Card

In order to interface between the computer and the circuitry, a National Instruments Data Acquisition Card (NI-DAQ PCI-M160E) is used. This card has both analog inputs and outputs which work in conjunction with on-board ADC's and DAC's respectively. Its

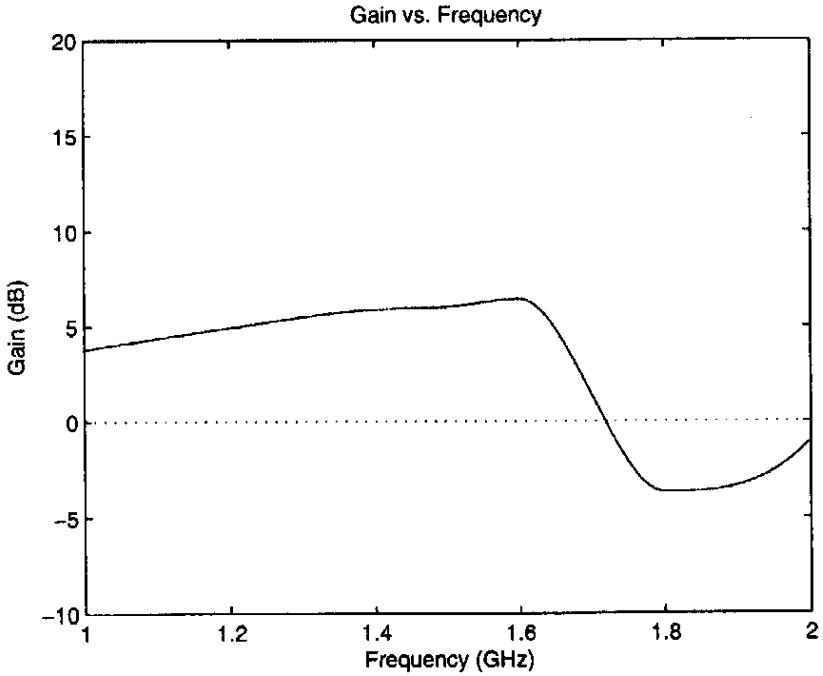

Figure 4.4: Graph of bow-tie antenna gain versus frequency [6]

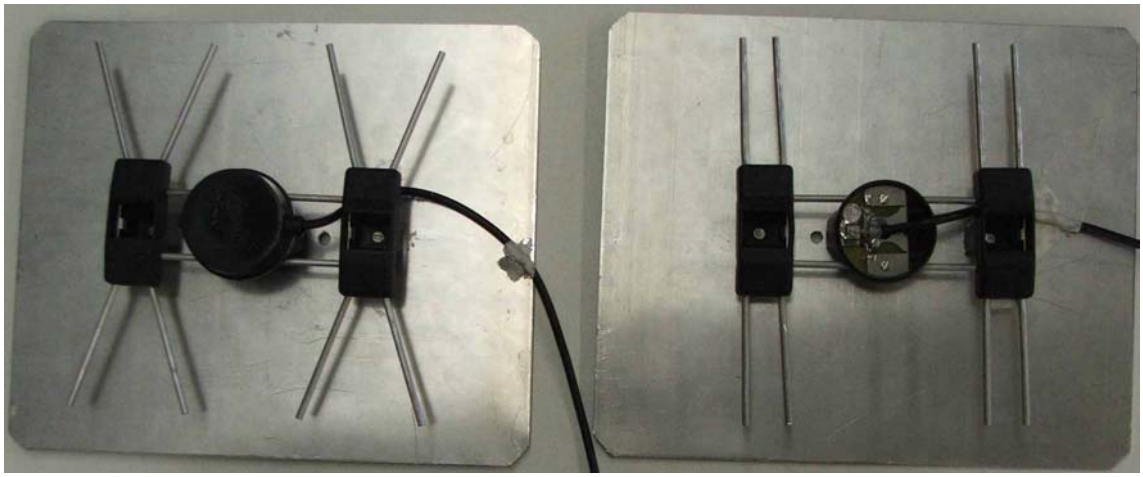

Figure 4.5: Photograph of the twin bow-tie antennas designed in [15]

function is to output the controlling voltage used to generate the variable delay mentioned in Section 4.5.2, as well as to sample the output of the differential amplifier (AD620) in the receiver (see Section 4.5.4).

The current system is designed to sweep (sample the echoes from targets) over a range, $R = 10m$ in 0.5s. Thus, in order to satisfy Nyquist's Criterion spatially, the minimum number of samples (sa) required (to sweep over a 10m range) is $N_{sa} = \frac{R}{\Delta R} = \frac{10}{0.15} = 66.66sa$, which corresponds to a sample rate $fs = 133.33sa/s$ in order to sample the full range in 0.5s. To ensure that Nyquist's is not violated, the system was designed to sample at a slightly higher rate than that, and so a sample rate of $200sa/s$ is the default (the Ni-DAQ card can sample up to $1.25Msa/s$) [6]. Figure 4.6 a photograph of a typical NI-DAQ card.

Figure 4.6: A typical NI-DAQ card

4.3 The Pulse Generator

In the original ultra-wideband (UWB) radar system design described in [**?**], the pulse generator produced a 2MHz square wave with random jitter due to the signal being noise modulated (spreading the power of the signal over a broad frequency range). Since the UWB system being analysed here is used primarily for imaging the position of objects/people rather than for communication, aviation or naval purposes, the addition of a stealth modulation scheme was considered superfluous. Thus, the current system derives the 2MHz, 50% duty cycle clock signal from an Agilent 33220A signal generator. See Figure 4.7 for a photograph of the signal generator.

4.4 The Transmitter

Figure 4.8 shows a diagram of the transmitter chain in [6].

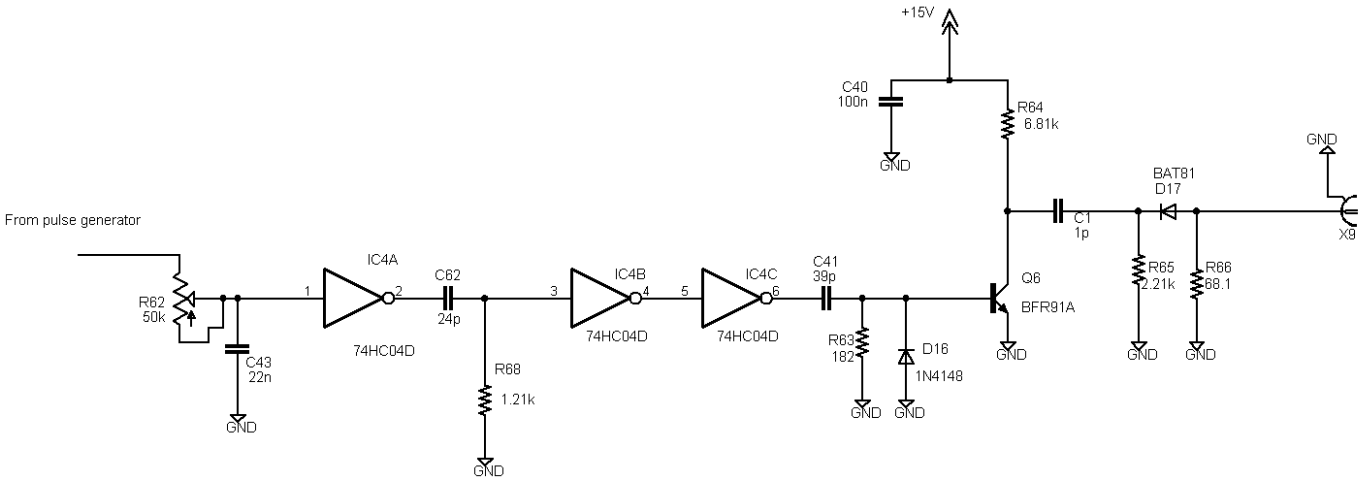

Figure 4.8: Transmitter circuit

Figure 4.7: Agilent 3320A 20MHZ Arbitrary Waveform Generator

The first element in the transmitter array is a manually adjustable variable RC (R62 and C43) delay. This variable delay allows the user to control when the transmitted pulse is released relative to the sampler (since they are both triggered from the same clock). Thus, if we want to sample objects at varying distances (further away than the range of the swept gate described in Section 4.5.2), we can do so by adjusting R62.

The next element in the transmitter chain consists of a pulse shaper, formed from a cascade of lead circuits. The effect of this element is to apply short, roughly 120ns-wide pulses to the base of the BFR91A transistor, see Figure 4.9.

These pulses trigger the transistor to turn on, which almost instantaneously discharges (via the shorted emitter to ground) the left hand plate (LHP) of capacitor, C1 (initially charged to +15V). When the transistor turns off, the left hand plate (LHP) of the capacitor charges up to +15V again (through R64). Conversely, when the LHP discharges to zero, the right hand plate (RHP) of the capacitor (initially at 0V) tries to drop instantaneously to -15V (although rise/fall times are in reality finite). When the transistor turns off, the RHP charges up (to 0V) much faster than the LHP due to the smaller resistance offered to the circuit through the parallel combination of R65 and R66. The result is that a negative going pulse in the order of 2V with a pulse width of 1ns is fed to the transmitting antenna. This forms a transmitted pulse with an ultra-wide bandwidth ($B = \frac{1}{\tau} = 1GHz$). See Figure 4.10.

The oscillations trailing the negative pulse are most likely due to antenna ringing. Ap-

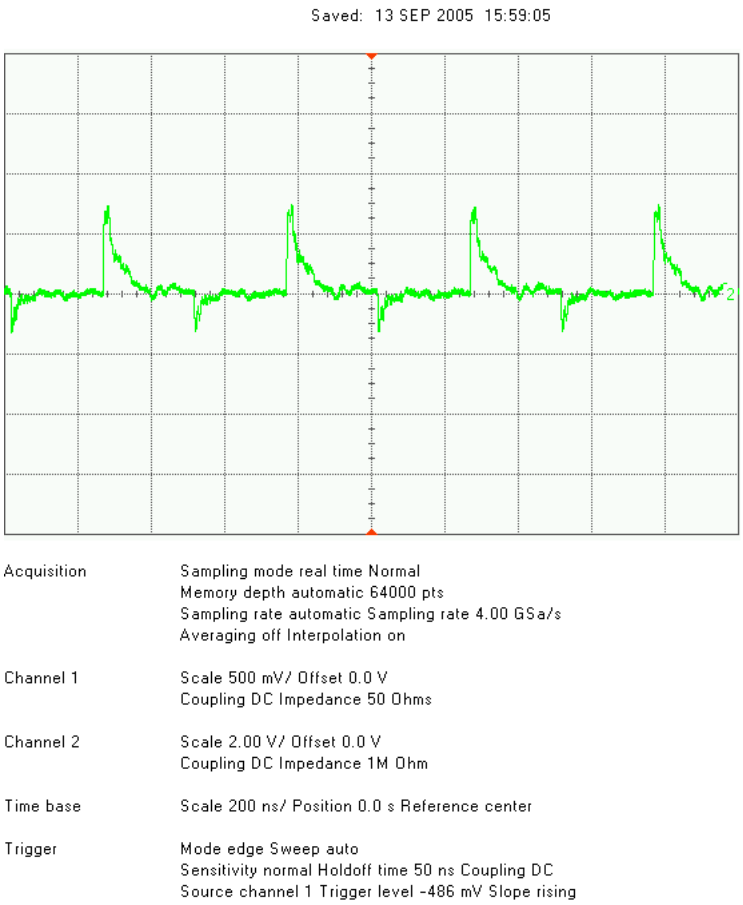

Figure 4.9: Pulses triggering transistor

plying a pulse to a resonating element such as a dipole antenna causes a wave of pulses (in addition to the main pulse) to be emitted, which eventually die out in a damped fashion [**?**].

4.5 The Receiver

The receiver chain consists of various modules, each of which will be dealt with systematically and separately. Figure 4.11 shows a circuit diagram of the receiver setup (bar the front-end RF amplifier, which is a separate unit).

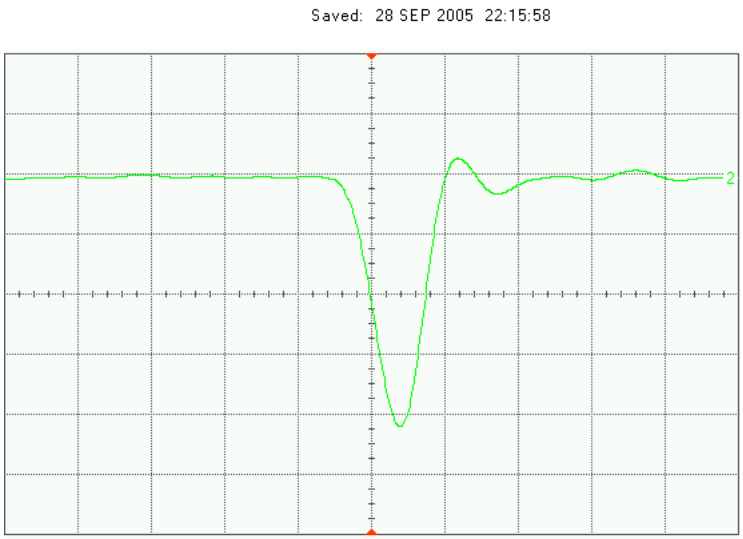

Acquisition	Sampling mode real time Normal Memory depth automatic 64000 pts Sampling rate automatic Sampling rate 4.00 GSa/s Averaging off Interpolation on
Channel 2	Scale 500 mV/ Offset -969 mV Coupling DC Impedance 50 Ohms
Time base	Scale 1.00 ns/ Position 0.0 s Reference center
Trigger	Mode edge Sweep auto Sensitivity normal Holdoff time 50 ns Coupling DC Source channel 2 Trigger level -969 mV Slope falling

Figure 4.10: Transmitted signal

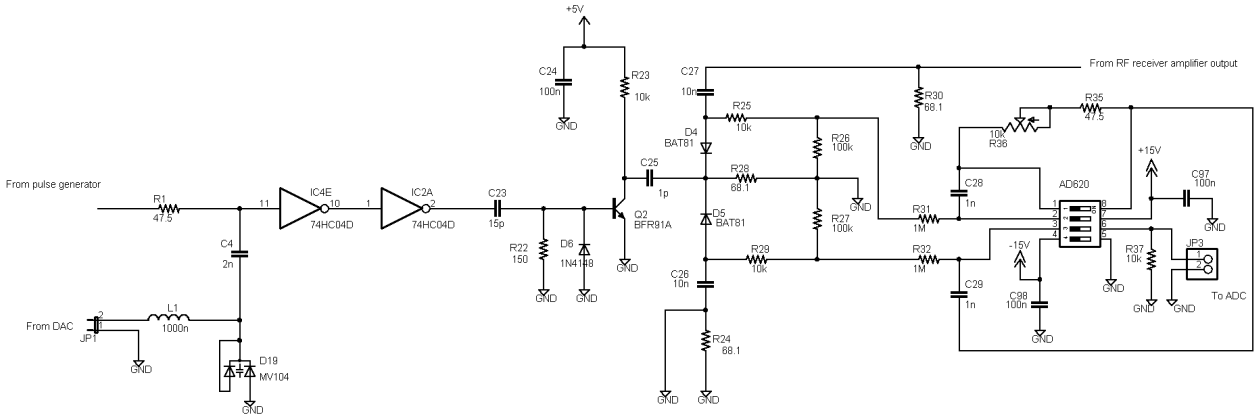

Figure 4.11: Receiver circuit

4.5.1 The RF Amplifier

The RF amplifier (developed by [22]) is a separate module into which the receive antenna is plugged in the receiver front-end. It consists of two MAR8 RF amplifiers in cascade, as shown in Figure 4.12. These amplifiers are quoted in [6] as having a gain of $25dB$ at 1.5GHz, and a noise temperature $T_a = 400K$ (corresponding to a noise figure, $F = 2.38$). These low noise, high gain amplifiers are needed to boost the weak radar return signals.

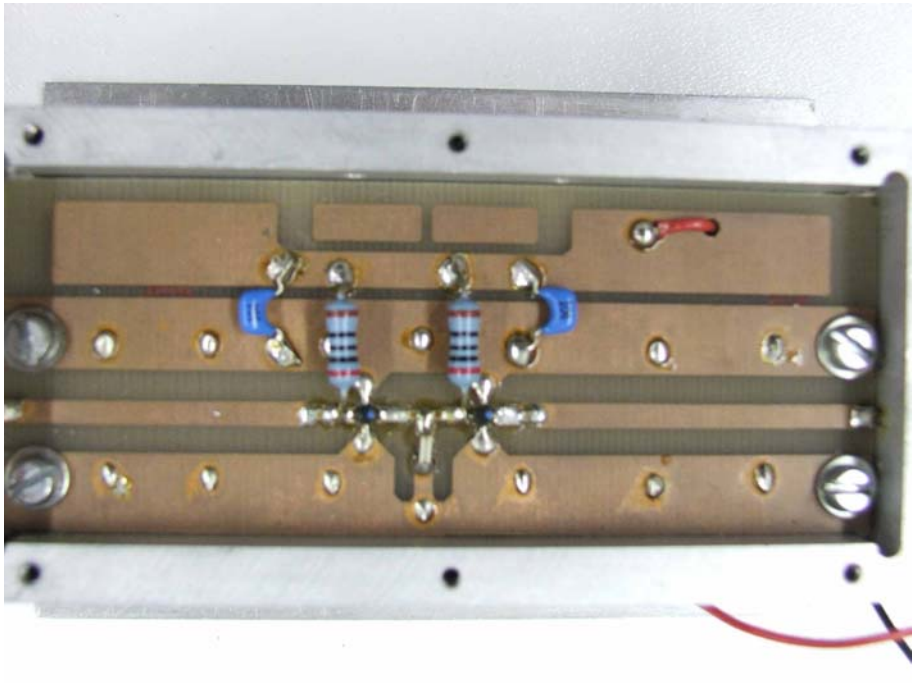

Figure 4.12: Photograph of the plug-in RF amplifier module

4.5.2 The Delay-line

The function of the nanosecond variable delay-line (in Figure 4.13) is to act as a sliding range gate in order to be able to sweep the sampler over a predefined range.

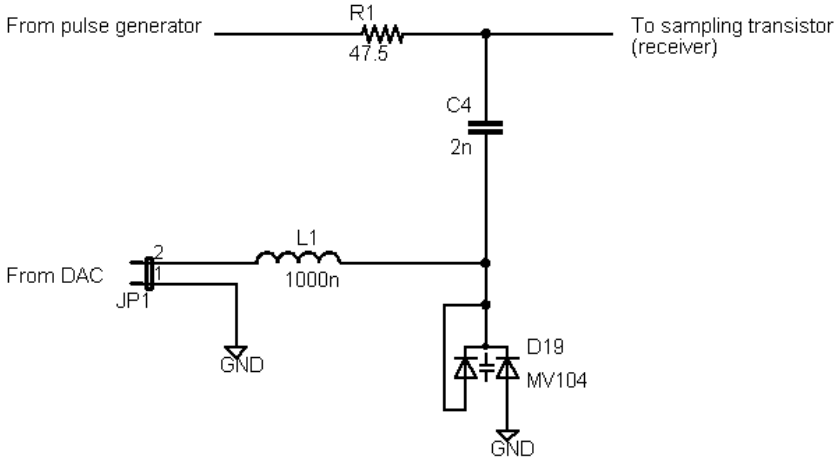

Figure 4.13: Voltage-controlled, nanosecond variable delay-line

This is also known as a sample-and-hold procedure, and the advantage of adopting this method is that we can sample at a much lower frequency than if we had to continuously sample the receiver between transmitted pulses.

The operation of the sample-and-hold circuit can be described as follows: the transmitter continuously transmits pulses while the receiver waits a predefined time period before sampling. This predefined delay is voltage controlled and is stepped up in length via the DAC output of the NI-DAQ card (see Section 4.2) linked to a computer. These incremental delays thus correspond to the stepped ranges at which samples are being taken. The

delay is achieved by varying the reverse voltage across a dual variable-capacitance diode called the MV104 (D19 in Figure 4.13), which in turn varies the capacitance of the diode, creating a variable RC time delay (together with resistor R1).

The capacitance of the device can vary between 20pF (at 30V) and 110pF (at 0.3V). In the system, the voltage is varied from 10 to 0.3V to achieve a 0 to 60ns variable time delay (see Figure 4.14 for a plot of voltage versus resultant time delay). Since the radar range for a target echo is twice the actual range of the target (in mono-static mode), using $R_{target} = \frac{c \times T_{delay}}{2}$, a 0 to 60ns time variation corresponds to a maximum sweep range of 0 to 9m. The DAC output of the NI-DAQ card is connected to the varicap diode via an inductor which acts to choke any RF signal from feeding into the card and computer.

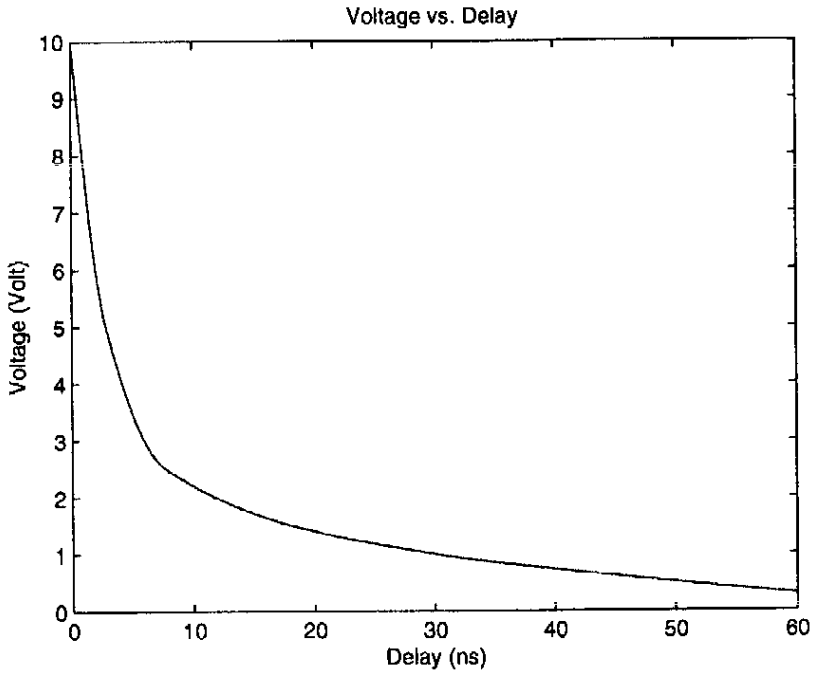

Figure 4.14: Graph of reverse voltage versus resultant time delay

4.5.3 Fast Sampler/Averager

The fast sampler/averager (depicted in Figure 4.15) has the same initial operation as the transmitter, up to the right hand plate (RHP) of capacitor C25, as it adopts the same architecture up to that point.

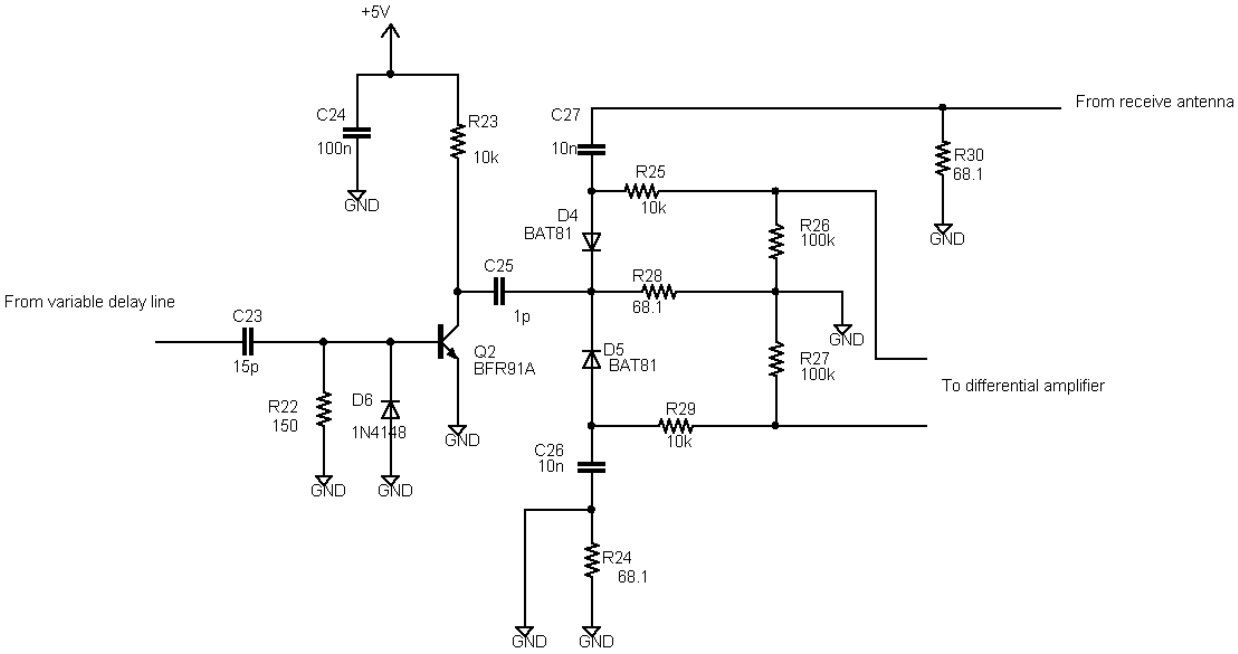

Figure 4.15: Fast sampler/averager

As the RHP of C25 is pulled negative (-5V in this case), the Schottky diodes (D4 and D5) are forced to conduct which means that C27 is charged up via the multiple received echoes (a type of averaging) received from the antenna during the conduction phase [**?**]. In this way, half-bridge rectification of the received AC signal is performed, and this low frequency (DC) signal is then sent to the differential amplifier in the next stage.

The branch from the receive antenna is matched with a mirrored branch to allow the differential amplifier to get rid of the common DC bias built up on C26 and C27 when the diodes conduct, as well as common mode distortion picked up by the circuitry from direct coupling and room reflections.

4.5.4 The Differential Amplifier

The signals from the fast sampler/averager are passed through RC low pass filters to get rid of any RF distortion. They are designed to cut out all frequencies above 160Hz. The low frequency signals are then fed into a differential amplifier (AD620), which helps to get rid of common mode distortion and to make the output single-ended [**?**]. The AD620 also helps to provide some gain to the low frequency signal, which is controlled via the potentiometer (R36). Figure 4.16 shows the configuration of the differential amplifier.

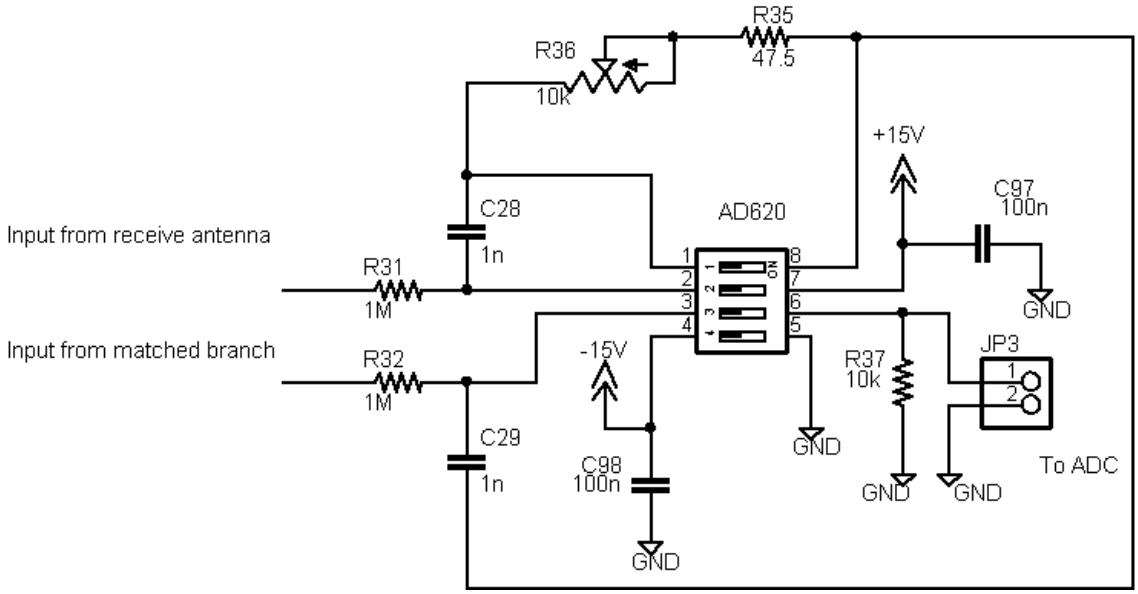

Figure 4.16: Differential amplifier configuration

4.6 Software Interface

A graphical user interface (GUI) was developed by [6] in Matlab using the GUIDE toolbox. The program is called *myRadar*. This GUI displays real-time, down-range profiles of targets, showing their distance relative to the antennas. In order to use the interface, the user must execute the following steps:

1. Choose the sweeping frequency, in sweeps per second (default is 0.5s per sweep)
2. Take a sequence of background snapshots for background removal, by clicking the background button
3. Perform point target calibration (to compensate for the differing filter effects of the antennas) by placing the antennas approximately 2m apart, facing each other and then executing the filter command
4. Click “Start” to activate a real-time display of the downrange profiles
5. Choose a frequency band of interest by adjusting the “Lower frequency” and “Higher frequency” fields
6. Choose a display mode. These include :

- *Raw* : showing real-time downrange profiles plus background clutter
- *Background* : displaying a still of the background clutter captured in Step 2
- *Difference* : displaying a downrange profile with the background removed

- *Filter* : displaying a snapshot of the downrange profile obtained during point target calibration, described in Step 3
- *Matched* : showing real-time downrange profiles (with the background removed) processed by a matched filter, with the option of applying a windowing function (Hanning, Hamming or Blackman) to the signal
- *Deconvolved* : showing real-time downrange profiles (with the background removed) processed by a deconvolution filter, with the option of applying a windowing function as above

Figure 4.17 shows a screen shot of the GUI.

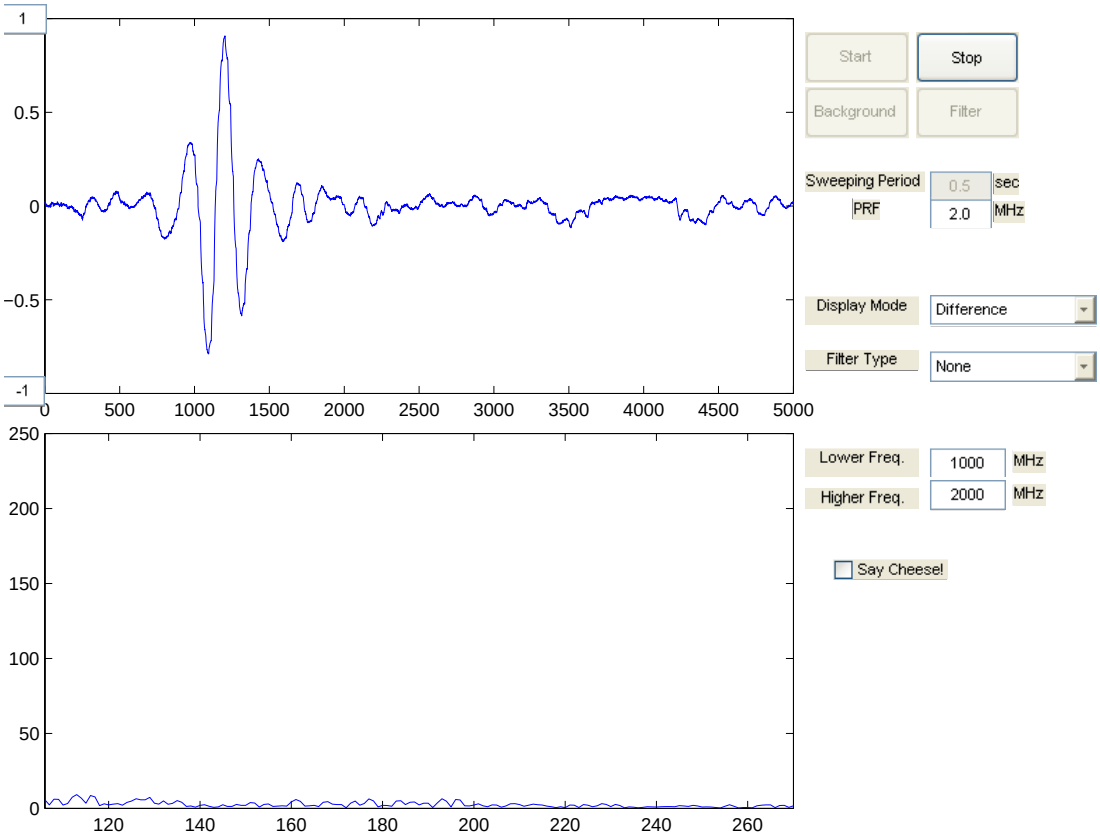

Figure 4.17: Screen-shot of the GUI *myRadar*

Chapter 5

Design and Implementation of an UWB Multi-Channel Radar System

The design of a multi-channel system with the following characteristics was proposed:

1. The system would comprise of multiple channels based on the single channel design in [6]
2. The entire system would be built on a single PCB using predominantly surface mount components
3. The PCB would be a two layer board, with a top signal layer, and a bottom ground plane also carrying the power tracks
4. An on-board oscillator would be designed and used instead of the signal generator shown in Figure 4.7
5. The RF amplifiers would be on-board instead of plug-in modules

Figure 5.1 shows a block diagram of the proposed system.

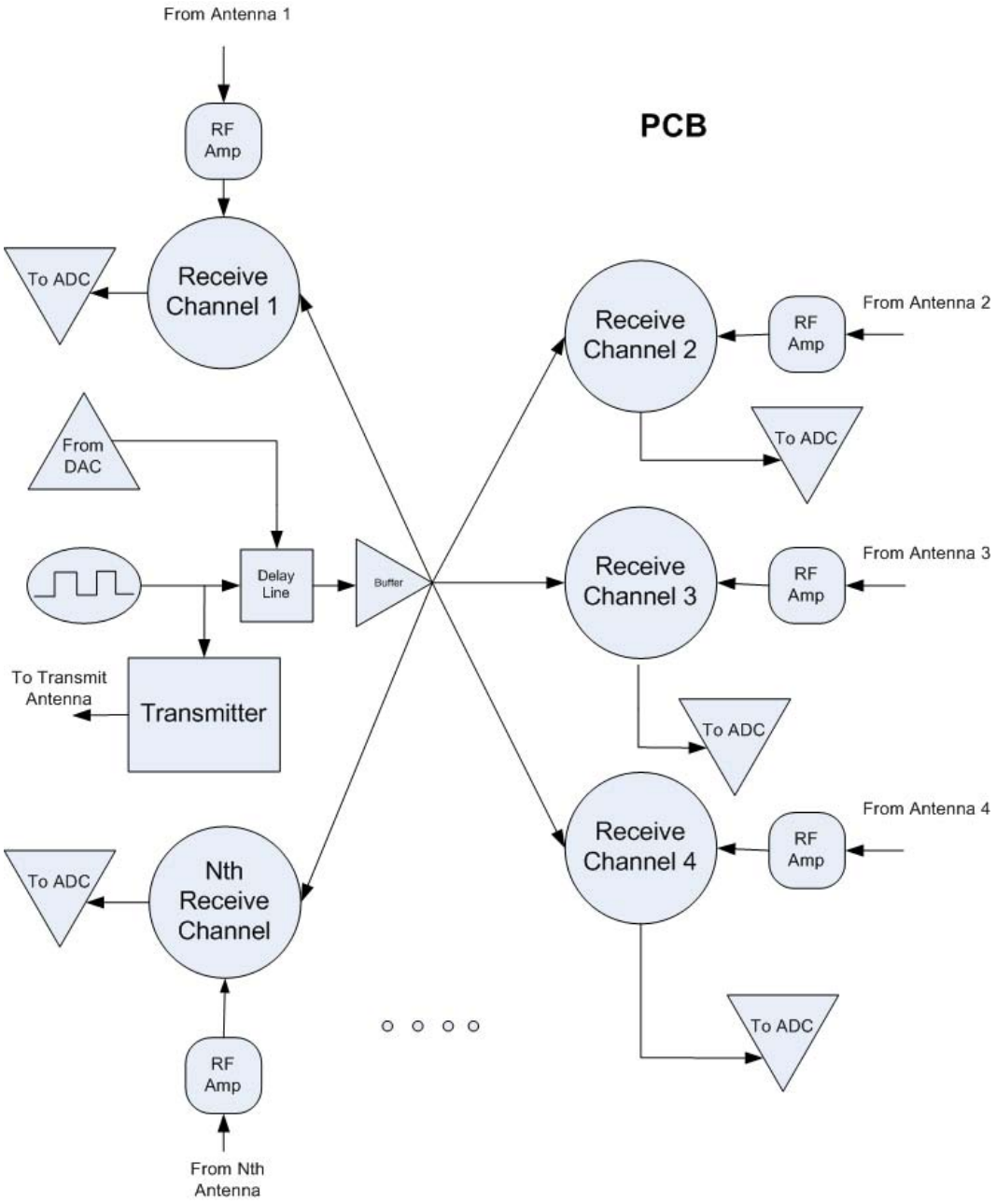

Figure 5.1: Block Diagram of Proposed Multi-Channel System

5.1 Design Criteria

5.1.1 Array Length

One of the system design criteria needed to be established when considering a multi-channel UWB system is indeed how many channels to include. What is clear from Section 3.1, is that grating lobes need to be avoided in order to prevent unwanted reflections and to preserve the directionality of the radar setup. The existing single channel system currently utilizes twin bow-tie antennas for transmitting and receiving. These antennas have an aperture dimension of roughly 0.2m each, and provide suitable gain over roughly a 1 GHz bandwidth, between 1-2GHz. Although the system is UWB (transmitted pulse), due

to the band-limiting nature of the antennas, the system operates at a centre frequency of around 1.5GHz. Thus the wavelength of the received pulses is $\lambda = 0.2m$, and we should have $N > 5$, or have greater than five receiver elements in our array to avoid grating lobes.

Five antennas each with an aperture of 0.2m placed next to each other results in an effective antenna aperture of 1m (as in the simulations). With a little bit of thought however, we can see that we could possibly get away with exactly five elements if we have a look at each antenna element's 3dB beamwidth. Each antenna has an aperture dimension, $d = 0.2m$. This means that each antenna has an effective 3dB beamwidth $\theta_{3dB} = \frac{\lambda}{d} = \frac{0.2}{0.2} = 1rad$ or 57^o.

If we look at the beam pattern for a multichannel receiver array with $N = 5$, (see Figure 3.5, in Section 3.1) we see that the grating lobes fall well outside of a 60^o beamwidth, and only take effect at angles $\pm 60^o$, on either side of the array boresite. The assumption is that any reflections each antenna picks up outside of this 3dB beamwidth will be be low enough in magnitude not to interfere with the desired response. Thus, five channels will be used in the design and construction of the UWB radar system.

5.1.2 PCB Layout

The PCB for the multi-channel UWB radar system was laid out in Eagle CAD, using the notes in [9]. This process involved drawing the circuit diagram (called a schematic) in Eagle, choosing/creating the correct component footprints, routing the tracks on the board, and, finally, creating Gerber files (needed to manufacture the board) from the Eagle files (the latter process was conducted with the aid of Mr Samuel Ginsberg). Copies of the schematic, board and Gerber files can be found on the CD supplied with this thesis (see the inside back cover).

One of the criteria needed to be established when laying the board was what part of the receiver circuit was to be shared, and what part needed to be duplicated to accommodate multiple channels (i.e. up to what point could the circuit be shared by all five channels). There were only two options to be decided between: either sharing the single channel circuit up to the collector of the sampling transistor, Q2 (see Figure 4.11) or up to the output of the hex inverter, IC4F.

Sharing the circuit for each channel up to the collector of Q2 means that the transistor's collector current needs to be shared by five channels, and hence R20 needs to possibly be five times smaller (2kΩ instead of 10kΩ) to account for this increased current demand. The problem with adopting this approach is that the current deliverable by a transistor is finite, and to drive it too hard or close to maximum rating is undesirable (thermal effects etc). The other effect that this permutation could have is that by connecting multiple capacitors (effectively in parallel) to the collector of Q2, the total capacitance as 'seen' by the collector is increased five-fold. One could then argue that since the voltage (v)

across a capacitance (C) rises as $\frac{d_v}{d_t} = \frac{i}{C}$, where i is the current delivered to the capacitor, these two changes would then cancel each other out. However, to be sure of the effects, unwieldy voltage superposition equations would probably have to be derived.

Sharing the circuit up to the output of one of the gates of a hex inverter (74HC04) means having to use separate sampling transistors for each channel, but the advantage is that each channel can be buffered by a gate. Since the sampling transistors (BFR91A) were cheap and readily available and because of its inherent simplicity, it was decided that the best configuration would be the latter. The five channels were thus each replicated from an output of a hex inverter.

In terms of the layout of the tracks, for the RF sensitive parts of the circuit (mainly transmitter and RF amplifier stage of receiver), the use of straight, in-line tracks was advised, as any 90^o bends or sharp discontinuities could act as corner reflectors, causing radiation losses and interference. It was also advised that the length of any tracks be kept as short as possible, since unnecessarily long lines add extra inductances to the circuit.

5.1.3 On-board Oscillator

The current system of using a signal generator to produce the 2MHz clock (needed as the PRF for the transmitter, and to provide coherent detection) was considered bulky and inappropriate, and so an on-board oscillator was designed using a SOIC package CD4047 oscillator in astable mode (see Figure 5.2).

In the application notes for the device (derived from [14]), in order to achieve a 2MHz signal, the IC was quoted as having to run off 15V, but since it was driving a CMOS hex inverter, the oscillator output had to be voltage divided down to 5V. In astable mode, the oscillator produces a guaranteed 50% duty cycle square wave of frequency f on the Q output (pin 10). The formula for the frequency, f is:

$$f = \frac{1}{4.4RC} \tag{5.1}$$

The frequency would be fine-tuned with the 10kΩ potentiometer (R80) in series with the 100Ω resistor (R18).

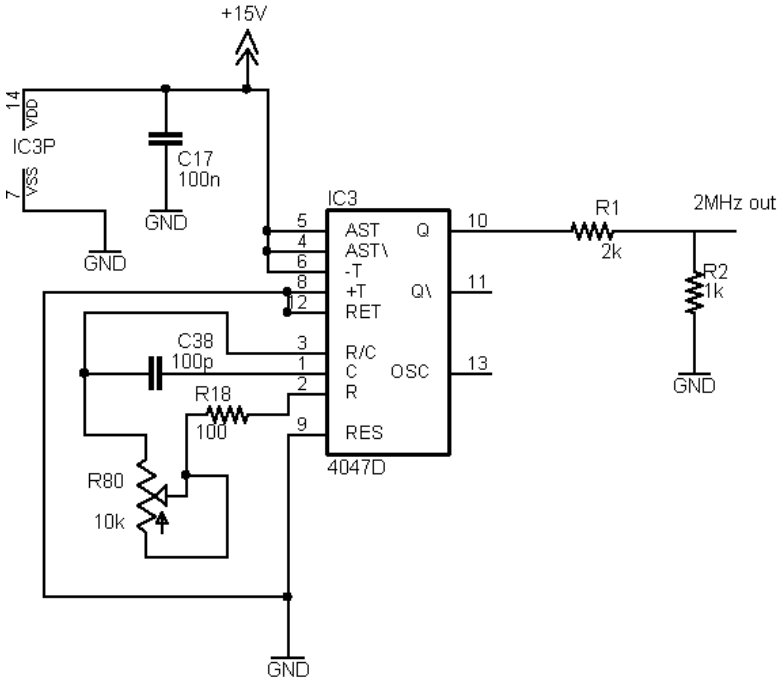

Figure 5.2: CD4047 oscillator

5.1.4 RF Amplifiers

In deciding on which RF amplifiers to use, a number of considerations had to be taken into account:

1. the required gain
2. tolerable noise figure
3. linearity of gain versus frequency
4. component lead time and availability
5. package type: drop-in, surface mount or plug-in

To provide a rough idea of the required gain, the following reasoning was adopted:

Assume an acceptable level of white, Gaussian noise (WGN) with no DC offset at the output of the RF amplification stage (before the sampler). For the purposes of this calculation, the magnitude of the standard deviation, σ of the noise (in volts RMS) was chosen as 5mV. This gives us an effective RMS voltage swing of $V_o = 10$mV, centred on 0V, at the output of the amplifier stage. The output noise power (across a matched, 50Ω load R) is thus $N_o = \frac{V_o^2}{R} = 0.5\mu$W.

Assume that the receive antenna is operating at standard noise temperature $T_a = T_o = 290K$. The input noise to the receiver system is thus simply $N_i = kT_aB$, where $B = 1$GHz (the bandwidth of the antenna), and k is Boltzmann's constant. Thus, $N_i = 4$pW. Hence, the overall system gain is $G_{sys} = \frac{N_o}{N_o} = 1.249 \times 10^5 = 50.967$dB. Note, this

calculation is a general one that does not take into account the noise added by the elements in the receiver chain (see Figure 5.3). Thus, a gain in the region of 50dB is a rough guide as to the amount required for the system.

The amplifiers used for the system were sourced from the chief suppliers of RF and microwave components, namely Minicircuits. Since the amplifiers were to be mounted on the PCB, it was decided to use the surface mount amplifiers, for which the ERA series matched this description. Table 5.1 shows a selection of medium power ERA-series amplifiers and a few of their typical characteristics.

Model number	Frequency (GHz)	Gain at 1 and 2GHz (dB)	IP3 pt (dBm)	Noise Figure (dB & linear)
ERA-6	DC-4	12.5 12.2	36	4.5 2.8
ERA-4	DC-4	14.0 3.4	34	4.2 2.6
ERA-5	DC-4	19.5 18.5	32.5	4.3 2.7
ERA-6SM	DC-4	12.5 2.2	36	4.5 2.8
ERA-4SM	DC-4	14.0 13.4	34	4.2 2.6
ERA-4XSM	DC-4	14.2 13.5	35	4.2 2.6
ERA-5XSM	DC-4	19.5 17.6	33	3.5 2.2
ERA-51SM	DC-4	17.4 16.1	33	4.1 2.6
ERA-5SM	DC-4	19.5 17.6	32.5	4.3 2.7
ERA-50SM	DC-1.5	19.4 18.3	32.5	3.5 2.2

Table 5.1: ERA medium power amplifier characteristics (typical)

From the table it is clear that in terms of providing wideband response, high gain and low noise figure, the ERA-5XSM should be the amplifier of choice. The ERA-5XSM possesses a fairly high $IP3$ point (to avoid intermodulation distortion caused by third order products [10]) and also has a gain that is relatively linear over a broad (4GHz) frequency band. Since the gain for the ERA-5XSM is approximately 20dB, and it was calculated that a gain of roughly 50dB was desirable, it was decided that using two amplifiers in cascade for each receiver channel would suffice. This would theoretically provide a gain of 40dB, which corresponds to an open circuit voltage gain of 100.

To get a feel for how sensitive our system would be, let us consider all the noise and gain contributing elements that compose the RF receiver amplifier stage and perform some calculations. Figure 5.3 depicts a diagram of the likely setup.

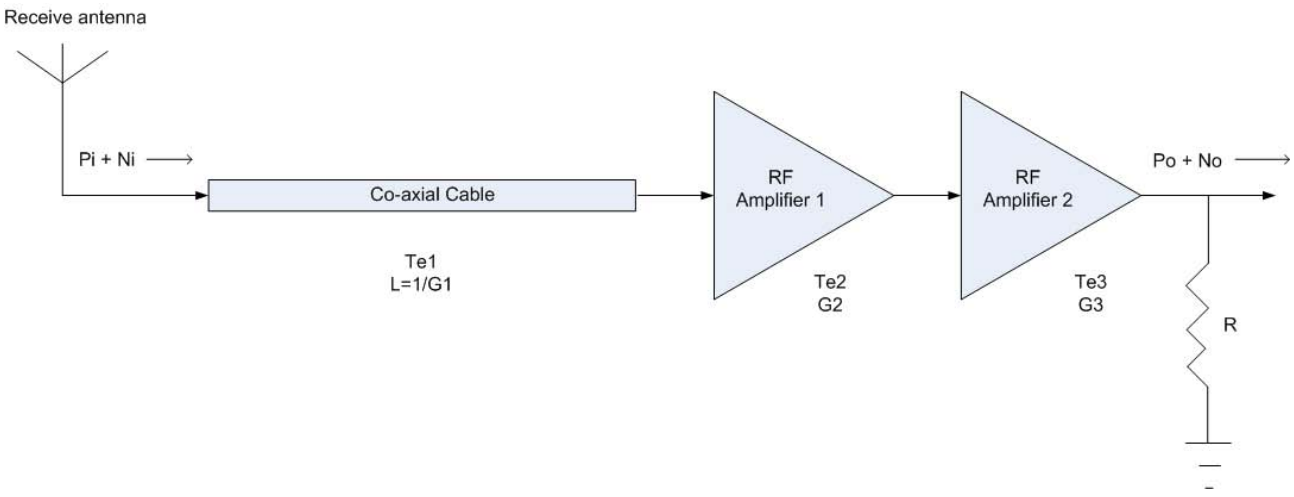

Figure 5.3: Receiver chain

Let us assume that ideally we would want a 1V (peak voltage) signal at the output of the amplification stage. Assume also, that the amplified received signal is of a sinusoidal nature, i.e. $V_o = A\sin(\omega t)$, where A is the amplitude of the sine wave, and ω is the angular frequency in rad/s. The average power at the amplifier's output (across a 50Ω load) is given by $P_o = \frac{0.5A^2}{R}$, where $A = 1$V (peak signal) and $R = 50\Omega$. Thus, $P_o = 10$mW.

The overall system gain is $G = G_1 \times G_2 \times G_3$, i.e. the product of the gains for the various elements in Figure 5.3.

The attenuation factor for typical RG58 (50Ω co-axial cable) at 1.5GHz is roughly 1dB/m [3]. Assume a two-metre length co-axial cable is used to connect the receive antenna to the receiver. Thus, the loss of the cable, in dB, is $L_{dB} = 2$dB. The loss, L, on a linear scale, is thus $L = 1.585$. The gain, G_1 due to the cable is $G_1 = \frac{1}{L} = 0.631$. $G_2 = G_3 = 20$dB. On a linear scale, $G_2 = G_3 = 100$. Thus, the overall gain, $G = 6.31 \times 10^3$, and the input power to the system is $P_i = \frac{P_o}{G} = 1.585\mu$W.

The peak input voltage (across a 50Ω load, R) is $V_{i_{peak}} = \sqrt{2P_oR} = 13$mV, and $V_{i_{RMS}} = 8.902$mV. Thus, if we received a roughly 13mV peak signal at our input, after amplification, we can expect a 1V peak at the output of the amplifier stage.

In order to gauge the effect of placing the RF amplifiers after the (lossy) co-axial cable instead of before, some noise calculations were performed. As can be seen from Figure 5.3, we have a three element (cable and two amplifiers) receiver chain. The noise power N_i at the input to the system is $N_i = 4$pW (as before). The overall equivalent noise temperature (in degrees Kelvin, K) of the system is [12]:

$$T_e = T_{e1} + \frac{T_{e2}}{G_1} + \frac{T_{e3}}{G_1G_2} \tag{5.2}$$

Since we assume that the line is at room temperature ($T_o = 290K$), the equivalent noise temperature of the lossy line is $T_{e1} = (L-1)T_o = 169.619K$. The noise figure for the amplifiers is $F = 2.239$ (from Table 5.1). This corresponds to an equivalent noise temperature $T_{e2} = (F-1)T_o = 259.229K = T_{e3}$. Hence, $T_e = 744.625K$.

The output noise, N_o for the equivalent three element cascade system can now be calculated as $N_o = kT_eBG = 6.484 \times 10^{-8}$W. This is the noise expected at the output of the second stage of the amplifier. This corresponds to noise with an RMS voltage (across 50Ω) of $V_{n_{RMS}} = \sqrt{N_oR} = 1.801$mV, which is equivalent to the RMS standard deviation of the noise. The signal to noise ratio (SNR) at the output of the amplifier (for the case where a 1V peak-to-peak signal was detected, i.e. $P_o = 10$mW), would then be $SNR = \frac{P_o}{N_o} = 1.542 \times 10^5 = 51.88$dB.

Let us determine the effect on system noise temperature T_e if we placed one of the amplifiers before the co-axial cable as opposed to having both of them succeeding the cable. In this case, $T_{e1} = T_{e3}$, $T_{e2} = T_1$ and T_{e3} would stay the same. Similarly, $G_1 = G_2$, $G_2 = G_1$ and G_3 would remain the same. Thus, $T_e = 366.619K$, and we would effectively halve the noise temperature. However, since the noise temperature is quite low in both instances, it was decided to proceed with positioning the RF amplifiers on-board.

The biasing configuration of the ERA-5XSM amplifiers was derived from the datasheet for the device, which can be found on the Minicircuits website (*www.minicircuits.com*) as well as on the CD supplied with this thesis (see the inside back cover) . Figure 5.4 shows a typical biasing configuration for the amplifiers.

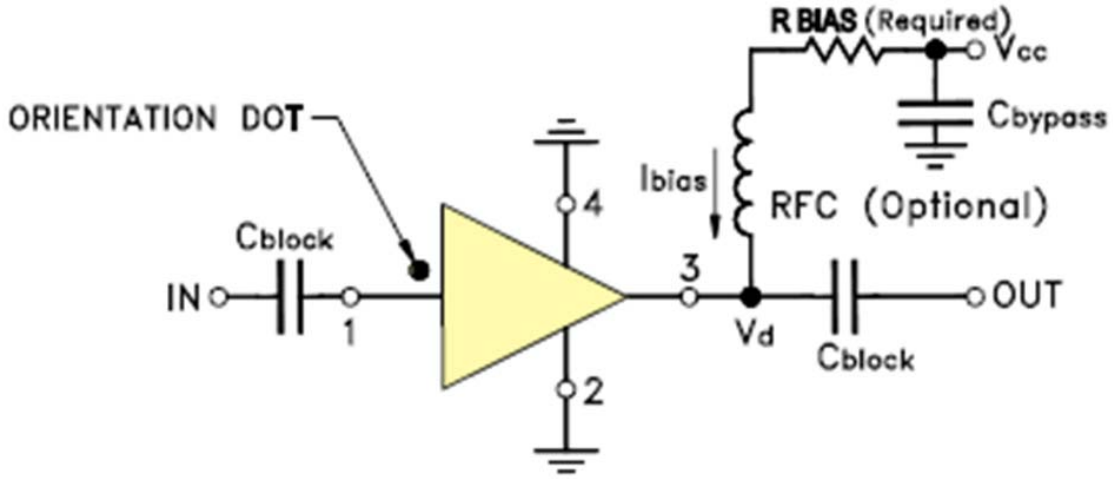

Figure 5.4: Typical biasing configuration for the ERA series amplifiers

For a 15V power supply, a 158Ω biasing resistor is recommended. Under normal biasing conditions, the output should lie halfway between the supplies. Thus, the output should be biased at approximately 7.5V, and hence the power dissipation through the resistor can be given by $P = \frac{V^2}{R} = 0.36$W, in which case a 0.5W resistor will be needed (instead of a chip resistor).

The use of an RF choke (inductor) at the output of the amplifier is optional, and can be used to increase the AC gain of the amplifier by presenting a large AC load in series with the 50Ω output impedance of the amplifier and the biasing resistor. DC blocking capacitors are present at the input and output of the amplifier.

5.1.5 Power Supplies and Decoupling

It was suggested that the power tracks be routed on the same side as the ground plane. This was reasoned according to the notion that to an AC signal, a DC power line looks like a fixed or unchanging voltage element. There were three power supplies needed: 15V, 5V and -15V (to be indicated by red, orange and green on-board light emitting diodes or LED's). Three main power lines were laid, and power was routed where necessary by tapping branches off these main lines.

The supplies to each transistor, amplifier or integrated circuit (IC) were to be decoupled with sufficiently large decoupling chip capacitors. The value chosen for the capacitors was 100nF, which presents an impedance to earth of Z<1Ω for signals greater or equal to approximately 1.6MHz. These decoupling capacitors were to be as close to the power pins as possible to short out unwanted signals effectively.

5.1.6 Impedance Matching

In order to match the 50Ω impedance of the antennas and co-axial cable, the width, w of the tracks for the RF sensitive parts of the circuit had to be calculated. In [5], equations to calculate the impedance of a microstrip line are given (referenced to have originally appeared in [13]). These equations are for approximation only, and were assumed for a PCB board of relative dielectric constant $E_r = 4.8$ and thickness $h = 1mm$ (values that appeared in [5]). These formulae are given below: (note, $Z_o = 50\Omega$)

$a = \frac{119.9}{\sqrt{2(E_r+1)}}$

$b = 0.5\left(\frac{E_r-1}{E_r+1}\right)\left[\ln\left(\frac{\pi}{2}\right) + \frac{\ln\left(\frac{4}{\pi}\right)}{E_r}\right]$

$d = \frac{59.95\pi}{\sqrt{E_r}}$

$w = h\left(\frac{2}{\pi}\right)\left\{\left[\frac{\pi d}{Z_o} - 1 - \ln\left(\frac{2\pi d}{Z_o} - 1\right)\right] + \left(\frac{E_r-1}{\pi E_r}\right)\left[\ln\left(\frac{\pi d}{Z_o} - 1\right) + 0.293 - \frac{0.517}{E_r}\right]\right\}$

Using these microstrip width synthesis formulae, a value for the width of $w = 1.6$mm for a 50Ω microstrip line was obtained. Thus, in Eagle, a track width of 66mil or 1.6764mm at the input/outputs of the RF stages was used.

5.1.7 Ground Vias for Possible Shielding

It was suggested that additional ground vias overlayed with non solder-masked tracks surrounding the transmitter as well as each receiver channel should be put in place in the event that cross coupling might occur between channels, and shielding would need to be erected.

5.1.8 Placement of Probe Pins

It was suggested that probe pins be placed at numerous points along the circuit in order to be able to easily measure the waveforms at those locations.

5.2 Hardware Implementation

5.2.1 Procurement and Choice of Components

Before the Eagle board files could be finalised and converted into Gerber files for PCB manufacture, all the components had to either be sourced or their dimensions had to be known in order to place the correct size footprint in Eagle. Most of the RF components were chosen to be surface mounts (SM), as their small size provides lower loss and better performance for RF signals. Since there was no tight constraint on board size (had to simply be less than A4 size), C1206 SM packages were chosen for the capacitor and resistor components.

All the chips (bar the differential amplifiers which operate at DC for our purposes) were chosen to be small outline IC (SOIC) packages. Most of these components were bought locally from Communica and Mantech, obtained from UCT's white lab, or salvaged from spares found in the Engineering department. The RF amplifiers (produced by Minicircuits) were ordered from ECS in Johannesburg as they are the sole distributors of Minicircuit components.

5.2.2 Manufacture of PCB

The Gerber files for the PCB were sent locally to WH Circuits for manufacturing. These files contain the drill plan, silkscreen, solder mask, pad and other vital information needed to construct a PCB.

5.2.3 Soldering of Board

Once the components arrived, they were soldered personally by hand. The entire board was populated except for the RF amplifiers which were left for last, to be soldered as each channel was tested/made active. The BNC connectors were also soldered piecewise. Vital equipment needed to carry out the task of soldering surface mount components included: inverse and normal tweezers, sharp-tipped soldering iron, magnifying glass, croc-clips stand, liquid flux, wire cutter and a pair of long nosed pliers.

Obstacles encountered when soldering the board included having to etch away bits of the tracks leading to the input and output pins of the RF amplifiers, as their pads were designed a bit too small in Eagle and having to file the leads of the board-mountable

BNC connectors (square leads instead of circular ones). Figure 5.5 shows a picture of the soldered board.

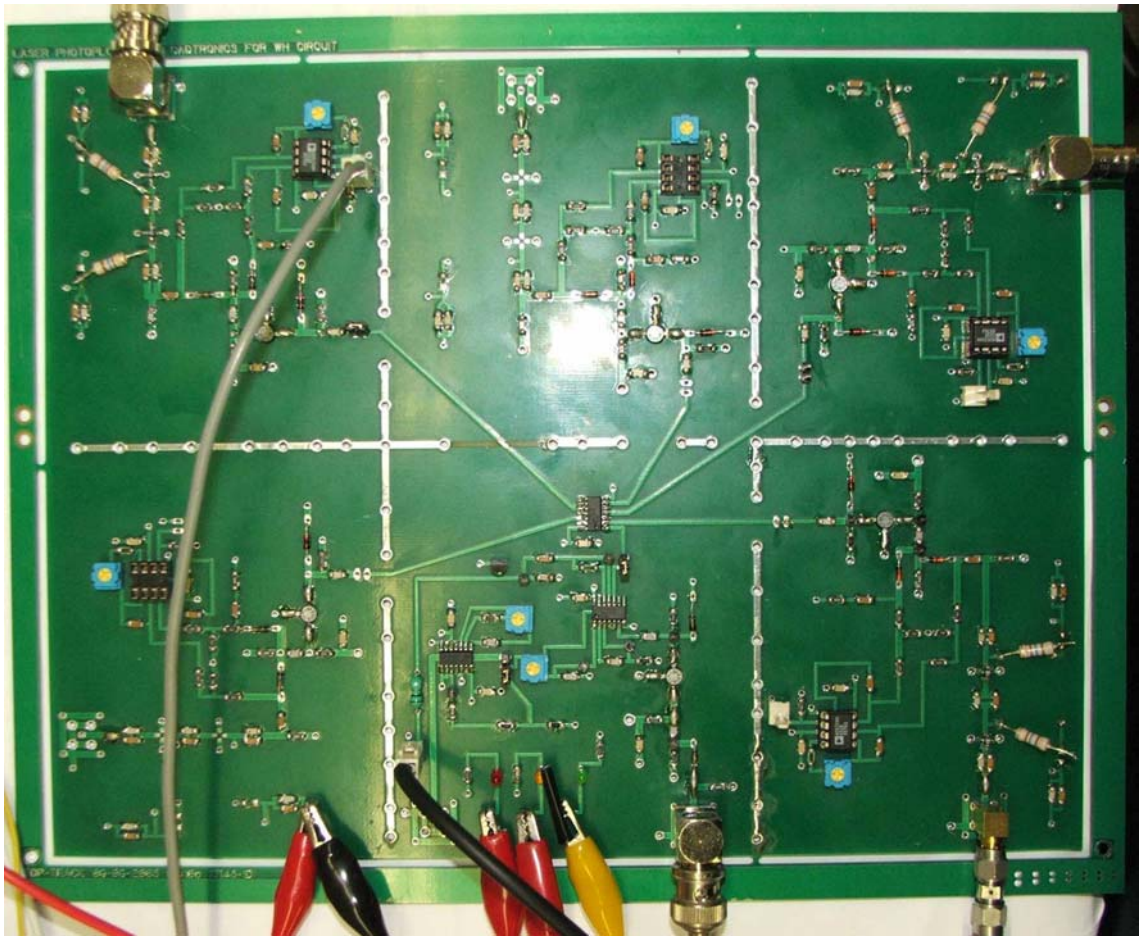

Figure 5.5: Soldered multi-channel UWB PCB

Chapter 6

Test and Results

6.1 Testing

Testing of the various modules of the board was carried out for system fidelity checks. Table 6.1 lists the equipment used in testing.

Equipment	Model
DC Power Supply	Escort EPS-3250
Digital Multimeter	Escort EDM 1111A
1GHz Oscilloscope	Agilent Infinium 54833A
Signal Generator	Agilent E4400B ESG
Data Acquisition Card&PC	NI-DAQ&Celeron 433MHz

Table 6.1: Bench equipment used for testing

6.1.1 Oscillator Testing

It was found that by adjusting the potentiometer (R80) in the oscillator circuit of Figure 5.2, a clean 2MHz, 15V square wave was produced at the output. However, once this square wave was voltage divided down to 5V, triangular distortion of the waveform was noticed. This was most likely due to the stray capacitance of the IC combining with the resistors to create edge rise-time. In order to reduce this effect, the value of the dividing resistors was dropped from 10kΩ to 1kΩ to reduce the RC time constant causing this sloping. This did not improve the shape of the waveform sufficiently, and so it was decided to test and see if the IC could produce a 2MHz signal off a 5V supply. The resistors were removed, the 15V supply line etched away, and a 5V line was routed to the IC supply pins. By adjusting the potentiometer, the oscillator was able to produce a 2MHz clock signal adequate for our use. Figure 6.1 depicts this generated clock waveform.

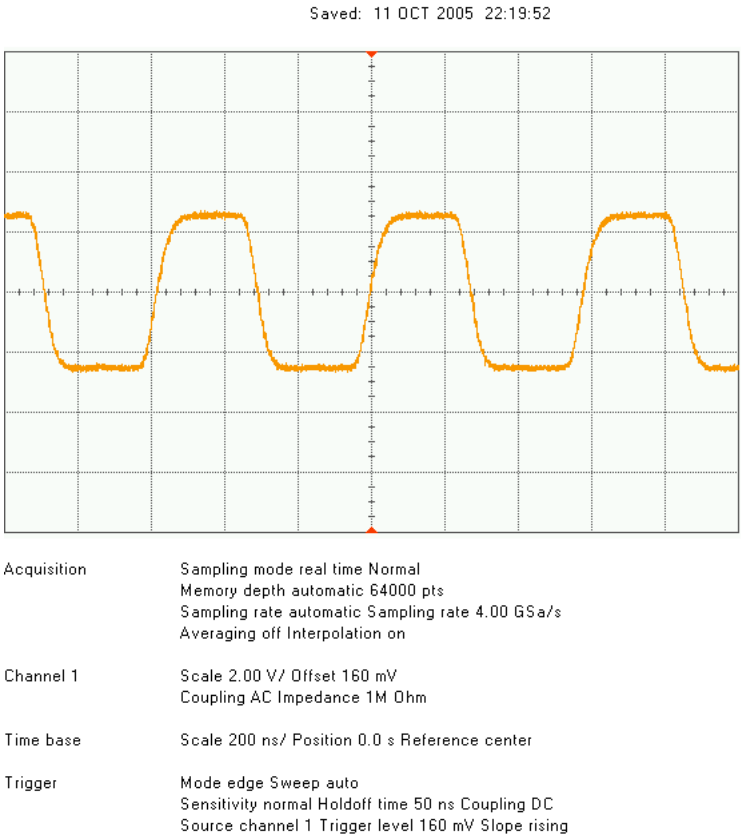

Figure 6.1: 2MHz clock waveform

6.1.2 Transmitter Testing

The transmitted signal was tested by connecting the transmitter to the oscilloscope via a length of co-axial cable. The resultant waveform (into 50Ω) is shown in Figure 6.2.

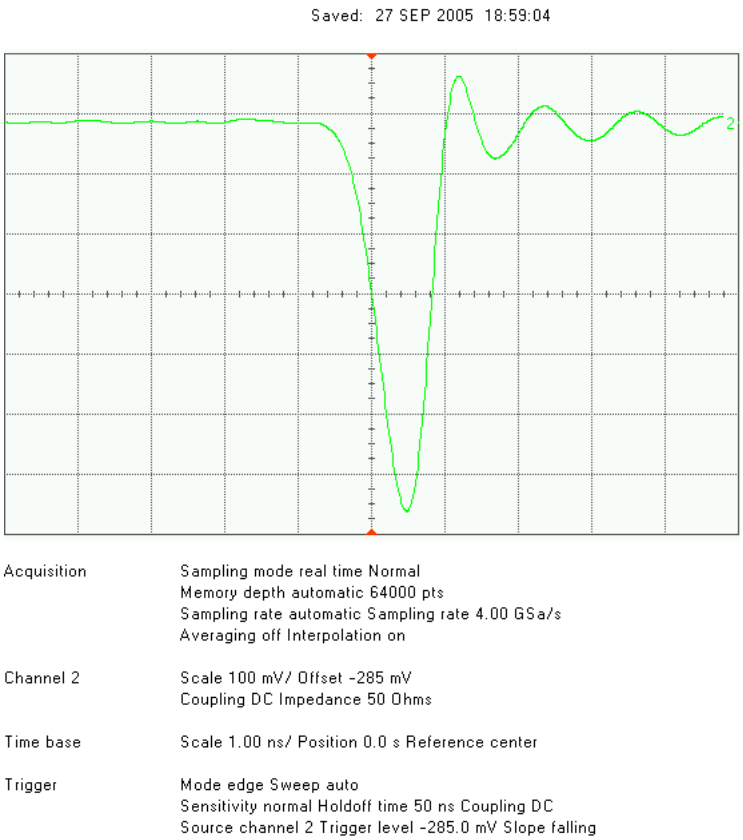

Figure 6.2: Transmitted pulse

It was noted that the pulse had a magnitude of around 650mV. This was over two times lower than expected from our analysis in Section 4.4. Since the the instantaneous peak transmitted power is proportional to the square of the transmitted voltage ($P = \frac{V^2}{R}$), in order to radiate sufficient power, this voltage magnitude had to be increased. After scrutinising the bottom layer of the circuit, it was thought that the clearance between the ground plane and the pads of the through-board components was too small, possibly representing a small capacitor to ground for the RF signal. Through-board components in the transmitter section included several probe pins. These were removed, their pads drilled through, and the track rejoined with solder on the top layer. This did not seem to produce any visible improvement to the situation.

It was also noticed that a few power lines routed on the bottom layer ran across what would be the RF signal path on the top layer. Since electromagnetic (EM) waves are actually guided between the signal and ground path, it was thought that perhaps this disruption in the continuity of the ground plane below the signal track would act by lengthening the RF transmission line, causing the addition of extra inductances and capacitances to the circuit. It was decided to bridge the two ground areas temporarily split by the power line with little wire jumpers. No noticeable improvement occurred however. To make this bridge more solid, it was decided to etch away the power line "crossing" the signal path, and connect the earth areas with a more direct connection by physically soldering the sections together. Once again no perceptible improvement was observed.

It was decided the only way to increase the signal strength was to adjust transmitter component values. From the description of the transmitter in Section 4.4, the transmitted signal is generated when the right hand plate of capacitor C1 (see Figure 4.8) charges up from some negative value to 0V. Since $\frac{dv}{dt} = \frac{i}{C}$, by increasing the capacitance of C1, we limit the rate at which the the voltage across the capacitor can increase (a disadvantage), but since the capacitor has a longer time to charge up (and a larger capacitance), it can hold more charge and hence develop a greater voltage across its terminals over time. There is thus a trade-off between pulse width and pulse magnitude.

The effect on the amplitude of the transmitted signal after adding one and two additional 1pF capacitors is shown in Figure 6.3 and Figure 6.4 respectively. Note how the magnitude changes from about 1.4 to 1.7V, and how the addition of the extra capacitance increases the pulse width.

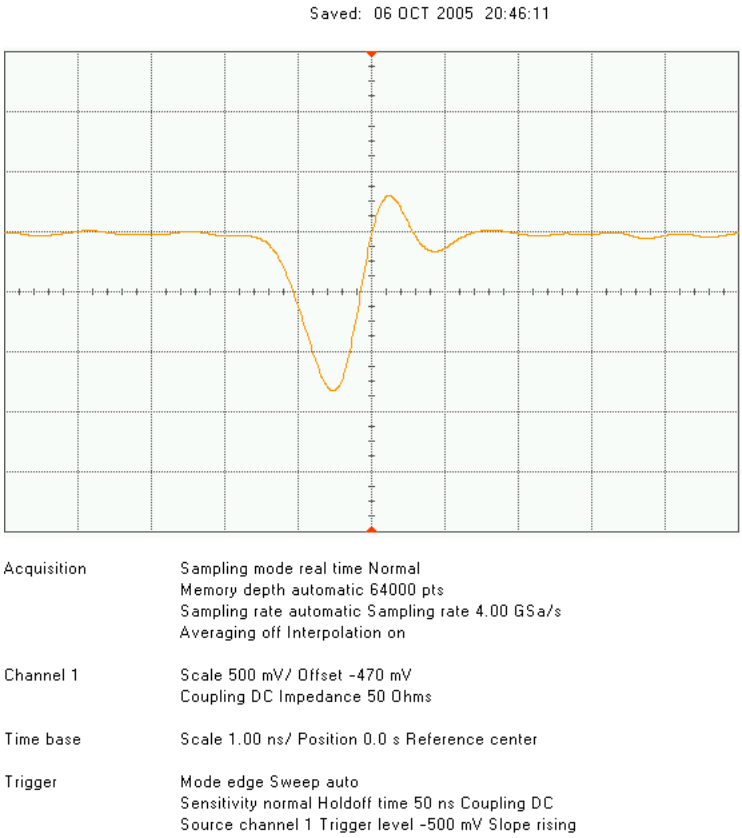

Figure 6.3: Transmitted signal after the addition of one capacitor

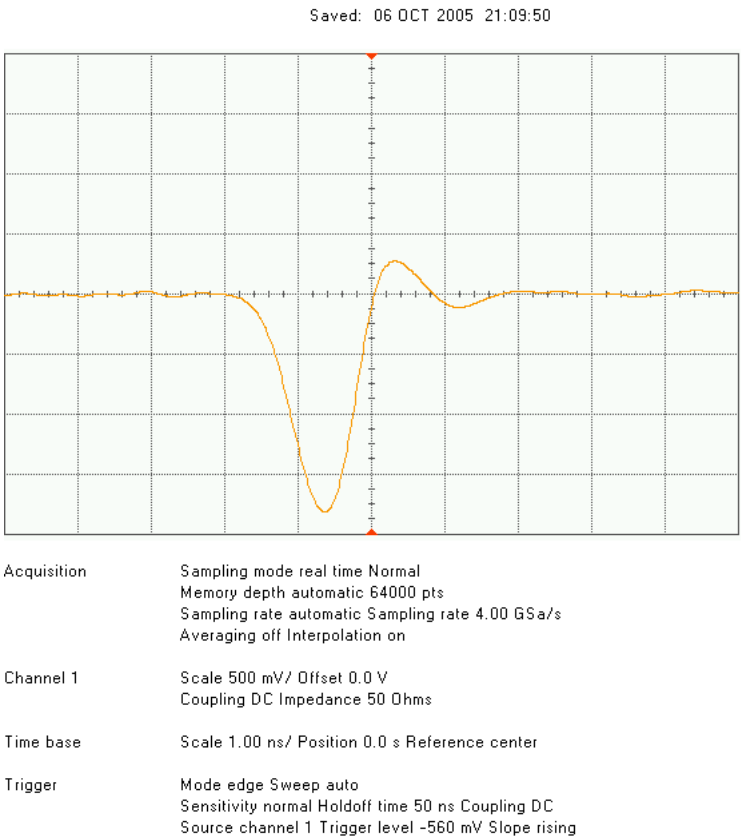

Figure 6.4: Transmitted signal after the addition of two capacitors

It was decided to adopt the latter configuration and use two additional capacitors to boost the strength of the signal. The transmitted signal now has amplitude 1.7V, with the drawback that the signal is now 2ns wide. This means that the effective bandwidth of the signal is $B = \frac{1}{\tau} = 500$MHz instead of 1GHz which decreases the radar's resolution as well as SNR (since the bow-tie antennas are effectively 1GHz bandpass filters). Fourier transforming the transmitted signal shows it has a 20dB bandwidth over 1GHz, i.e.the effective power of the signal drops by 20dB over a 1GHz band, which is equivalent to the effective output voltage dropping by a factor 10. See Figure 6.5.

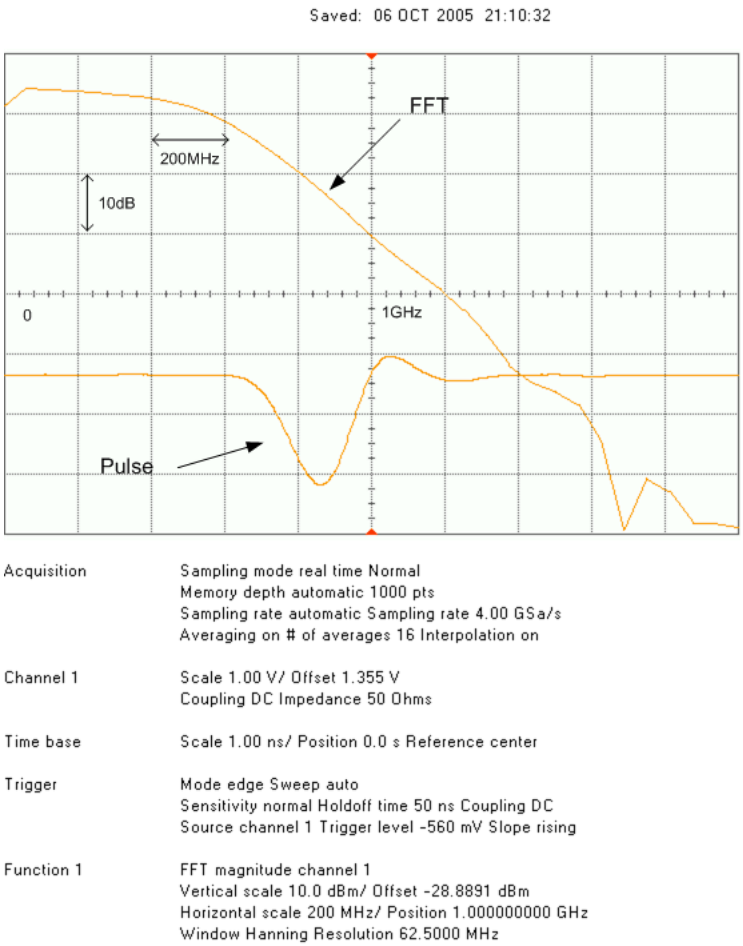

Figure 6.5: Fast Fourier Transform (FFT) of transmitted signal

The instantaneous power of the transmitted signal is roughly 35mW, as can be seen from Figure 6.6.

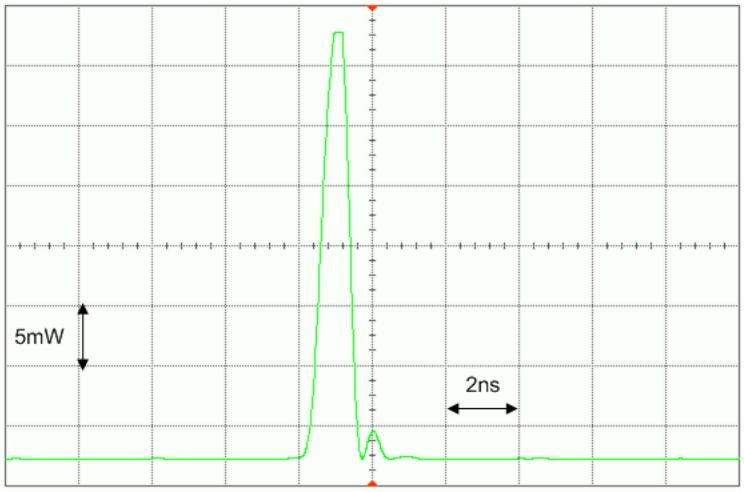

Figure 6.6: Waveform showing instantaneous transmitted power

6.1.3 RF Amplifier Testing

Once the RF amplifiers (ERA5XSM's) for a single channel were soldered, simple hand-wound RF chokes (seven turns) made from ordinary insulated copper wire were placed at the output of both amplifier stages. These were indicated as optional in the data sheets, and were inserted so as to increase their gain. Once they were in place, the RF amplifiers were tested to see if they were correctly biased. Under optimal biasing conditions, the amplifier outputs should lie roughly half-way between the supplies for maximum voltage swing. Testing indicated that their DC biasing was around 6V (slightly out for a 15V supply, but acceptable), although it was also noticed that oscillations were present, superimposed on the DC waveforms at both amplifier outputs. Initially it was thought that these oscillations were caused by cross coupling between the inductors. It was decided to remove these inductors, and to use only the biasing resistors. The oscillations were however still present, and in an effort to make the amplifiers stable, similar changes to those performed on the transmitter (see Section 6.1.2) were conducted (removing probe pins and bridging ground sections interrupted by power lines). These modifications seemed to stem the oscillations (since the inductors were optional, they were not replaced, to ensure that the system remained maximally stable).

It was also noticed that when the transmitter was on, the transmitted signal managed to couple (radiated from the board or fed along the tracks) to the amplifiers and was visible at fixed intervals at the output of the amplifiers. Since the software for the system includes a background removal algorithm, it was thought that these pulses would not appear in the downrange profiles. If not, it was envisioned that a grounded housing might be necessary.

To test the gain of the amplifiers, a sinusoidal signal was injected at the input to one of the receivers and the output stage of the amplifiers was monitored. A 40mV peak-to-peak, 500MHz sinusoidal signal was injected at the input to the first amplifier, and the voltage was measured at the first and second amplifier outputs. The oscilloscope measured a 100mV peak-to-peak signal at the output of the first stage (a voltage gain of 2.5), and a 400mV signal at the output of the second stage (a voltage gain of 4). This resulted in a two stage voltage gain of 10, which is much lower than and far from the expected gain of 100 (see Section 5.1.4).

Since the signal from the generator started to become severely attenuated by the oscilloscope for frequencies approaching 1GHz (the oscilloscope's limit), the amplifiers broadband gain could not be properly tested. It was decided that the best way to test the amplifiers would be to connect them directly to the transmitter, via a 10dB attenuator, and to observe how much the signal would be amplified by. A 10dB attenuation corresponds to decreasing the voltage of a signal by a factor of 3. Figure 6.7 shows the attenuated signal. It has a magnitude of roughly 600mV (across 50Ω), indeed close to a third of 1.7V (across 50Ω).

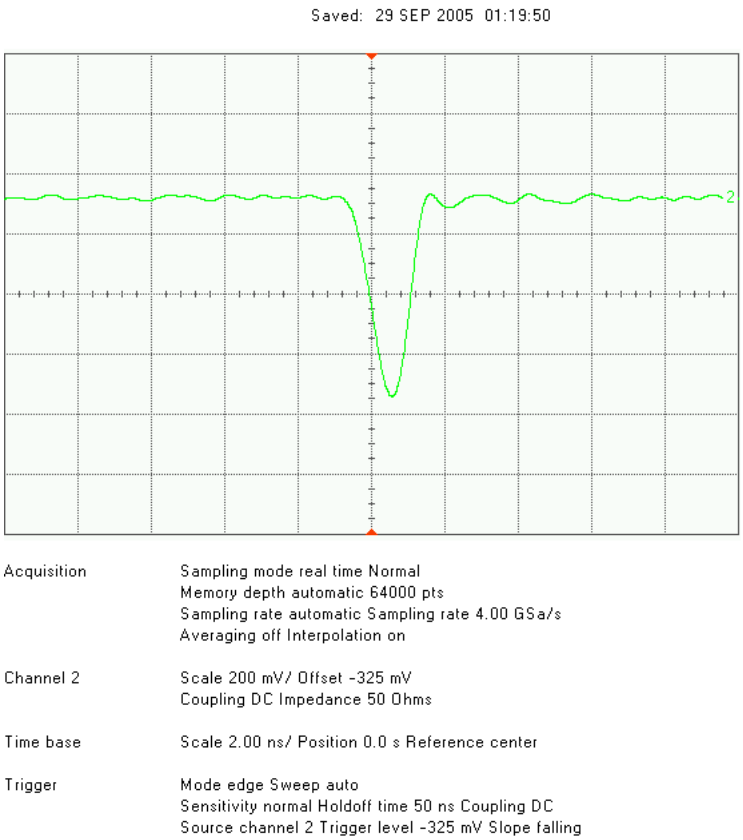

Figure 6.7: Transmitted signal attenuated by 10dB

The transmitted signal at the output of the second amplifier stage (see Figure 6.8) had an amplitude of roughly 2V across (1MΩ), which means that the effective value should be halved to find out the 50Ω gain (1MΩ corresponds to an open circuit, which means the voltage is doubled). Thus, the magnitude of the amplified signal is 1V. This indicates a gain of $G = \frac{1}{0.6} = 1.67$ which is extremely low. It was then decided to test and observe how the gain of an external amplifier (used in the existing system) would perform in amplifying the transmitted signal. With this amplifier (2XMAR8's), the voltage (across 1MΩ) was 6V, corresponding to 3V (for a 50Ω impedance) and a gain $G = \frac{3}{0.6} = 5$, about three times that of the on-board amplifiers (see Figure 6.9).

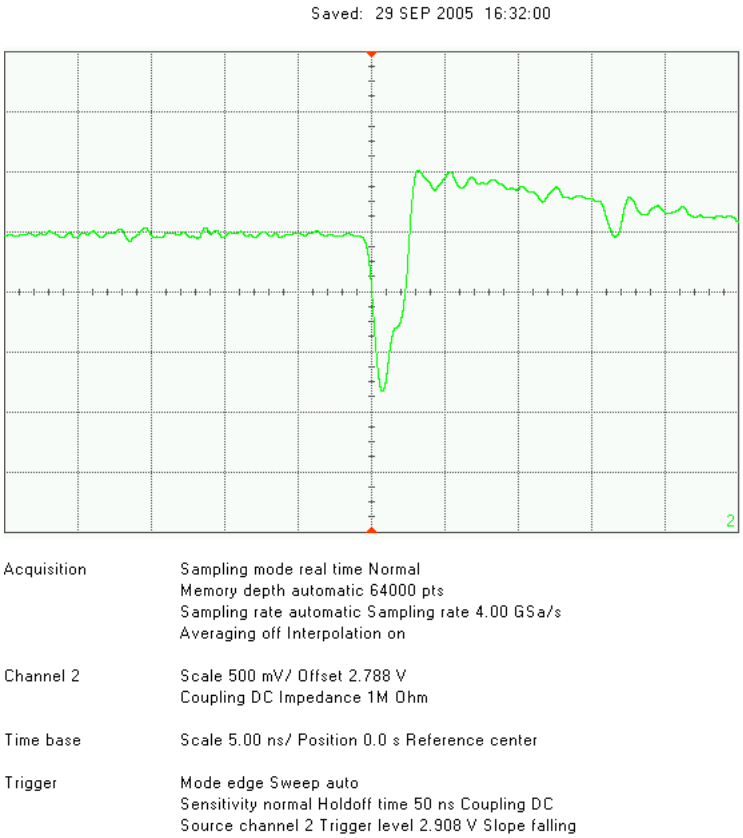

Figure 6.8: Transmitted signal first attenuated and then amplified by on-board ERA amplifiers

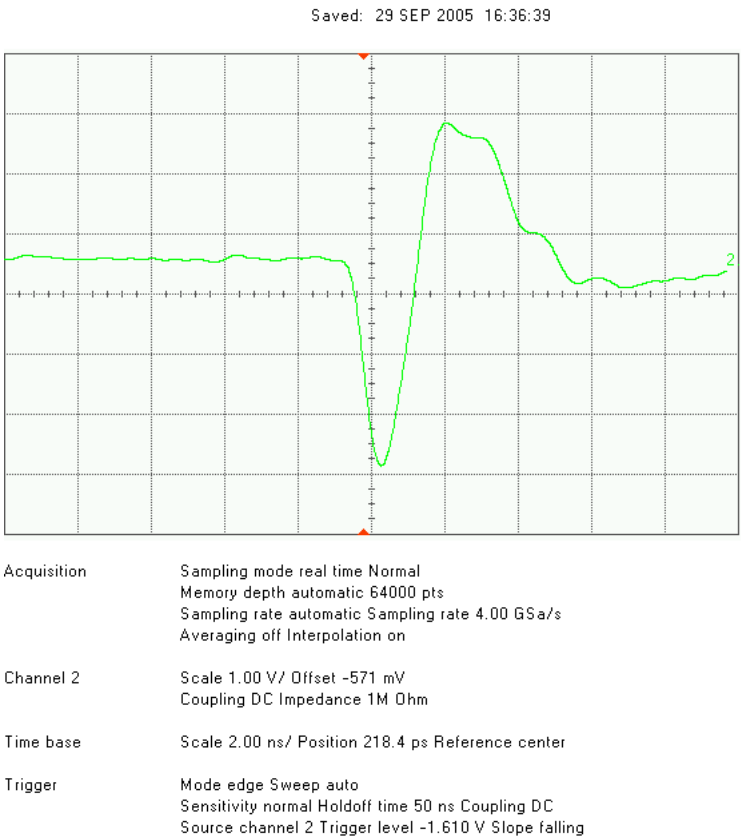

Figure 6.9: Transmitted signal first attenuated and then amplified by plug-in amplifier

Possible reasons for the poor RF performance of the on-board amplifiers could include the following:

- lack of a large, solid ground plane directly under entire RF signal path to act as an effective wave guide
- use of non RF specialised capacitors in the amplifier stages
- track lengths to the RF amplifier leads (especially between the output leads and ground) were possibly not kept short enough, resulting in extra inductance being created [7]
- ground vias were not placed directly under or as close to the ground pins of the RF amplifiers as possible to reduce the above effects
- the surface mount amplifiers were not drop-in modules but had leads bent at right-angles possibly creating extra inductance
- the calculation of the track width necessary to achieve a 50Ω impedance (conducted early on in the design phase) was based on a 1mm thick board (as opposed to 1.5mm, the actual PCB thickness), with an assumed relative dielectric constant of $E_r = 4.8$ (whereas this value could have been marginally off and vary from PCB to PCB)

The width of the track was recalculated with the correct board thickness (1.5mm) using the same approximation formula used in Section 5.1.6. The correct track width was found to be w = 2.424mm. To verify this, another approximation formula found in [11] was used, and this resulted in a calculated width of w = 2.681mm. Using these formulae, the existing track width ($w = 1.6764$mm) actually corresponds to a microstrip with a characteristic impedance of $Z_o = 63\Omega$. Although the relative dielectric constant could also change these values, one can see that a small change in board thickness can cause a fairly substantial change in 50Ω track width. These impedance mismatches (between the antennas and the tracks) could lead to power being reflected, thus minimizing the realizable gain of the on-board amplifiers.

In order to gauge what effect additional track lengths (effectively transmission line sections) between the amplifier output leads and ground might have on the amplifier stage of the circuit, the approximate equivalent series inductance for a short transmission line was calculated. For this scenario, (short transmission line, $l = 4mm$ and a large characteristic impedance, $Z_o = 62\Omega$) $Bl < \frac{\pi}{4}$, where $l = 4mm$ = the extra length of track to ground, and $B = \frac{2\pi}{\lambda} = 31.42$ = phase constant in rad/m. For a 1.5GHz signal, $\lambda = 0.2m$. Thus, for a transmission line section with characteristic impedance $Z_o = 63\Omega$, the equivalent series inductance of the line was calculated, using the following formula [12]:

$$X = Z_o Bl \tag{6.1}$$

where X = equivalent series inductance (in Ω) of the transmission line.

The extra length of transmission line thus potentially looks like an inductor with reactance $X = 7.79\Omega$ in series with the RF amplifier load. This could result in the gain of the amplifier being lowered due to the voltage division at its output.

6.1.4 Delay-line Testing

The next step was to test the delay-line. The procedure for testing this module was to compare the expected waveforms (recorded when analysing the existing system) with the measured waveforms on the multi-channel PCB version (each waveform at a particular point in the circuit was given a particular reference number). For the digital delay-line, it was discovered that a capacitor to ground (indicated in the original circuit diagram in [6]) was in fact an error. Once this was removed, the correct controlling waveform (a logarithmic function) needed to sweep the sliding range gate (see Section 4.5.2) was observed at the output of the digital delay-line.

6.1.5 Receiver Testing

The receivers were tested in a similar way to the delay-line. The waveforms at critical stages in the circuit were measured and compared to those expected/recorded from the

existing system. There is a subtlety involved however, in that the performance of the receiver at the front-end (RF amplifier) could not be accurately ascertained as the amplifiers were not delivering the expected gain. It was decided that the best way to test a receiver channel would be to connect the channel to the computer and to run the radar software interface *myRadar.m* in an attempt to obtain down-range profiles.

Initially no response could be obtained from the receiver channels. The on-board RF amplifiers were changed, and the gain of the differential amplifiers was adjusted, producing no visible effect. Once the the changes described in Section 6.1.4 were made to the delay-line however, the software was successfully made to interface with the circuitry.

Due to the poor gain of the on-board amplifiers, it was decided to test the single channel operation of the radar using the separate plug-in amplifier (described in Section 4.5.1). By bypassing the on-board amplifiers on one of the channels, and using the twin bow-tie antennas (described in Section 4.1), downrange profiles of a scene were obtained (see Section 6.2.1 for these results).

One of the problems encountered when running the radar software was that the origin of the sampler (usually sample number 0) was shifted about 3000 samples to the right (in the system, 1000 samples corresponds to a range of roughly 1m, and the screen shows a maximum range of 5m). This was due to the fact that the delay settings (potentiometer positions in RC delays, and length of cables) for the existing system did not match those of the new system. Since the origin of the sampler was designed to be hardware triggered, the software could not be modified to change this setting without reprogramming the sampling code. In order to try and shift the origin of the sampler to the left (earlier) using hardware, either the delay to transmit the pulse had to be shortened, the receive cable length shortened to reduce echo time, or the sampler had to be delayed. Since there was a limit as to how short the length of the cables could be made (for practical reasons), it was decided to add a variable RC time delay to the pulse sent to each sampling transistor (before the hex inverter buffer to each receiver channel, after pin 10 of IC4E in Figure 5.3). Adjusting these delays, the origin of the sampler was able to be moved more to the middle of the screen, but due to the set delays of the cables, was not able to be configured to start at sample number 0.

Once one channel was working, in order to be able to demonstrate multichannel operation, it was necessary to activate another channel. Due to the lack of UWB antennas (there were only two), Ellies TV Grid antennas (of which there were four) had to be utilized instead. See Figure 6.10 for a photograph of one of these antennas.

The advantage of using grid antennas is that they have larger apertures and hence higher directivity/gain (between 10-13 dB), but the drawback is that they have a bandwidth of only 288 MHz (frequency of operation roughly between 512-800 MHz), thus reducing the achievable range resolution to $\Delta R = \frac{c}{2B}$ =0.52m or 52cm (as opposed to the twin-bow tie antennas' resolution of 15cm).

The centre frequency of operation is 656MHz, which corresponds to a wavelength of

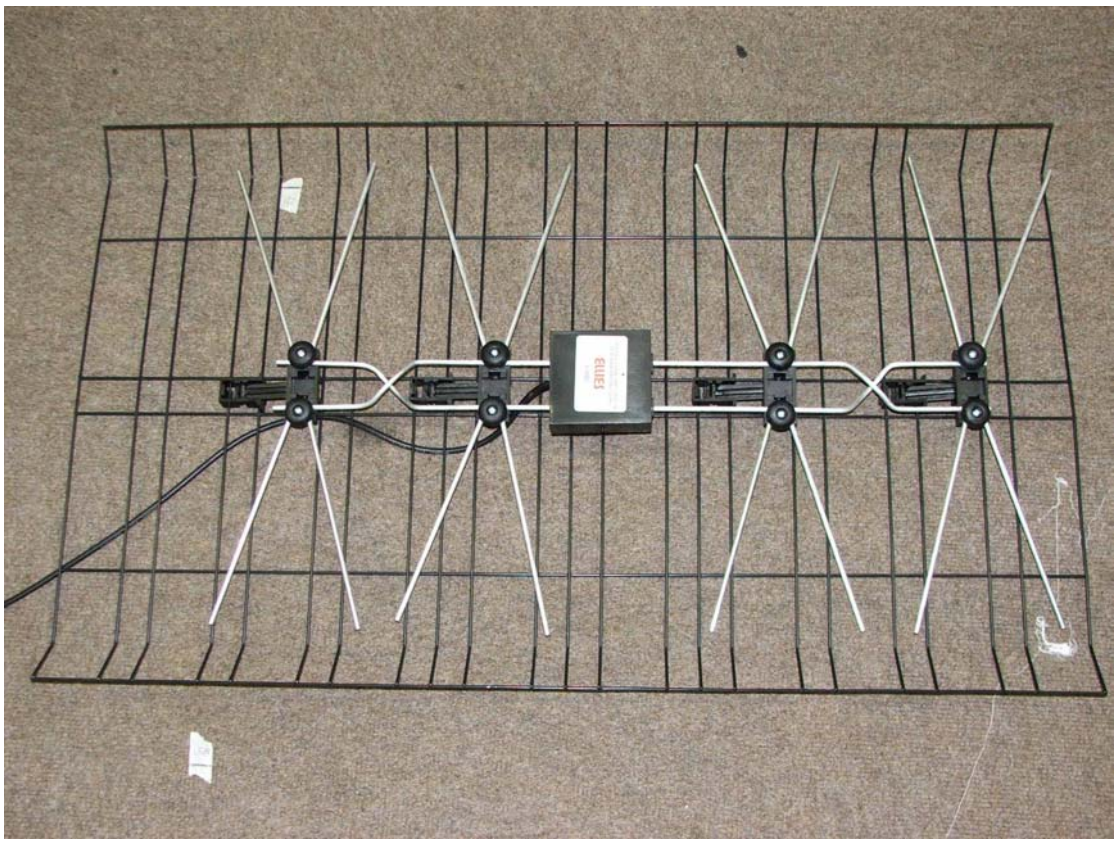

Figure 6.10: Ellies TV grid antenna

$\lambda = 0.46$m or 46cm. The antennas (including their mounting grids) have dimensions 830X590mm, and due to their large size, in order to place them side by side to form an array, it was decided to it use the antennas in their upright position (horizontal polarization). In an upright position, their effective aperture length (length of radiating element) is $d_{ant} = 0.4$m or 40cm. Their horizontal 3dB beamwidth can be calculated by $\theta_{3dB} = \frac{\lambda}{d_{ant}} = \frac{0.46}{0.40} = 65.89^o$.

Due to the fact there were only four Ellies antennas available, it was decided to test and see if a maximum of three channels could be activated (one antenna for transmit, the other three for receive, placed side-by-side to form an array). Since the last goal of this thesis was to test to see if multichannel (i.e. more than one channel) operation was possible, it was decided that three channels would sufficiently demonstrate this concept. In order to avoid grating lobes, as was mentioned in Section 3.1, the spacing d between the radiating elements must be less than or equal to the wavelength. The antenna's width (including its mounting grid) is 59cm, but the radiating element is 40cm wide, so the separation distance d between the receiver elements (considering they are placed next to one another) is $d = (0.59 - 0.4) \times 2 = 0.38$m. The wavelength of the radiated signal, as calculated above is $\lambda = 0.46$m. Thus, placing these antenna side by side we should be able to avoid grating lobes ($d < \lambda$). Section 6.2.2 shows the results obtained for multichannel operation.

6.2 Results

The experiments were conducted in a UCT laboratory, with the antennas facing an open space. At approximately five metres from the antennas there exists a back wall. Unnecessary background clutter in the vicinity of the scene was removed as best as possible. Unfortunately an anechoic chamber was not available so as to optimise the experimental conditions by removing room reflections, although these should be eliminated by the background removal step in the *myRadar* software (see Section 4.6).

A few points to consider: in the single channel experiments, the origin of the sampler is around 1000 samples (due to different length cabling and system parameters compared to the original system, thus introducing extra delays). Since the sampler is hardware triggered, the origin could not be easily changed (e.g. by changing the existing software). In the software programme for the single channel, 1000 samples corresponds roughly (but not exactly) to a 1m range, but what is important to notice in the downrange profiles is the relative phase and magnitude of the various plots.

For the multichannel plots, the software had to be modified (with the assistance of UCT *Msc* student Alvin Chiang) to sample multiple channels. Increasing the sampling rate rescales the time axis, and so 10000 points instead of 5000 points is shown for the multichannel plots. The purpose of these plots are mainly demonstrative, to show that a working multi-channel UWB system can be built on a PCB, rather than for conducting any post processing on the data (requiring accurately scaled plots).

In the downrange profiles, there exist some pulses at around 4200 samples (in the single channel version of *myRadar*) and around 8000 samples in the multichannel version. Note that this these pulses are not due to noise, but are in fact reflections from the back-wall. When a target is present, it blocks certain transmitted pulses from reaching the back-wall (part of the background), thus, when the background (containing the back-wall) is subtracted from nothing, it in fact reappears.

6.2.1 Results for Single Channel Operation

As described in Section 6.1.5 the external plug-in amplifier was used to test the radar's single channel mode of operation. The UWB, twin bow-tie antennas of Section 4.1 were also used in this experiment. Figure 6.11 shows a photograph of their configuration, perched atop a box facing a scene or small open space in a UCT laboratory.

Figure 6.11: Twin bow-tie antenna configuration for single channel testing

Various metallic reflectors were used in the experiments. They included: a metal pole (Figure 6.12) of length 2m, metal grid (Figure 6.13) 550X390mm and a pyramidal corner reflector (Figure 6.14) with sides 500mm long. The metal grid acted as the best reflector, and so was used for the majority of the experiments (unless otherwise stated).

Figure 6.12: Metal pole used as reflector/target

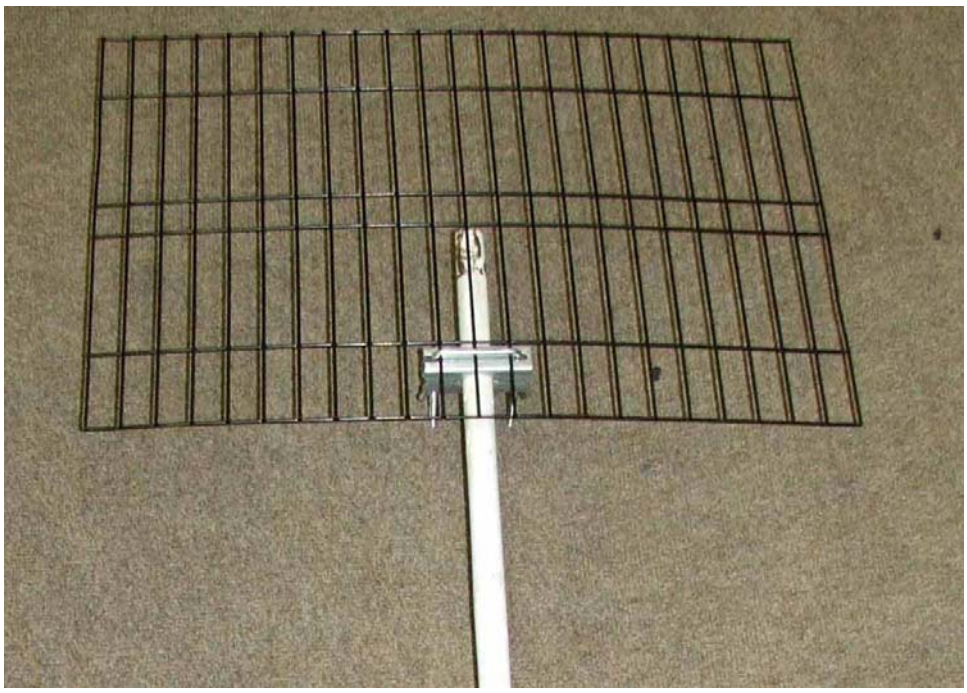

Figure 6.13: Metal grid used as target/reflector

Figure 6.14: Pyramidal corner reflector used as target/reflector

The target was propped in a stand and its position or range from the antennas was varied. The software *myRadar* was then run, with the steps taken to derive downrange profiles described in Section 4.6.

Figure 6.15 shows the background snapshot of the scene.

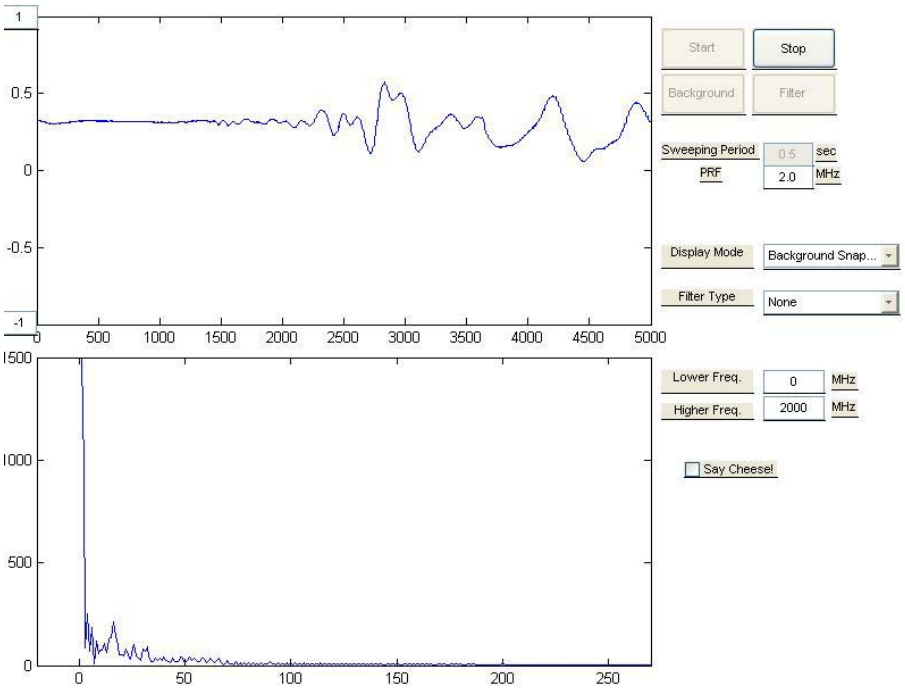

Figure 6.15: Background snapshot

Figure 6.16 shows a target at 1m using the difference display mode (downrange profile minus the background clutter). The pulses trailing the main pulse are confirmed to have been caused by antenna ringing (as they disappear once the target is removed). This is because an antenna is a resonating element, and when excited by a pulse, will result in additional oscillations forming (which eventually become dampened and die out). Notice how the received pulse is not just a scaled and shifted version of the transmitted pulse (as in the idealized case for the simulation in Section 3.2), but has in fact been reshaped due to both system propagation and antenna filtering and resonance effects.

Figure 6.17 shows a target at 1m, match filtered.

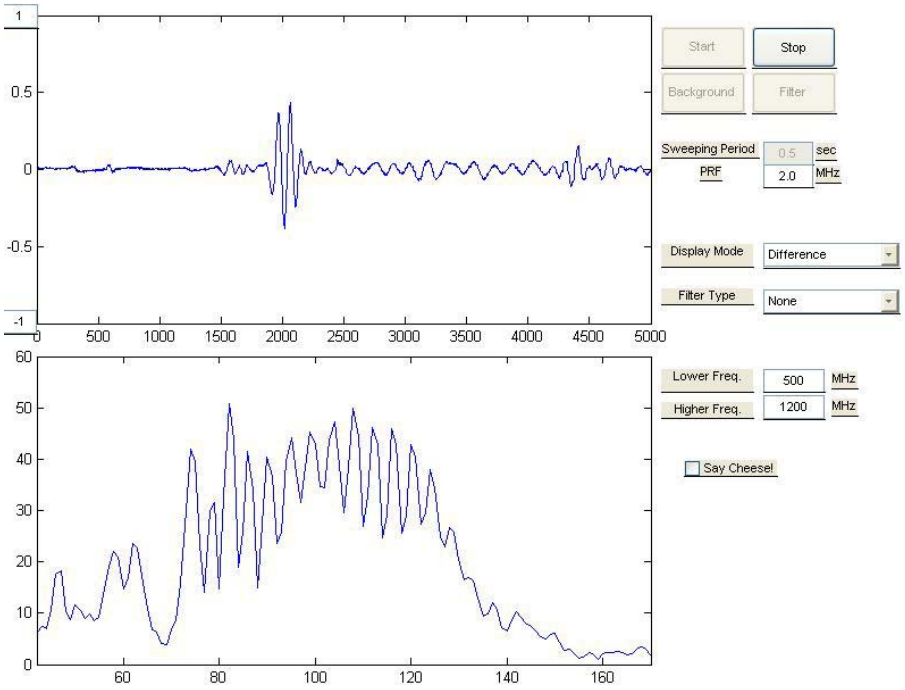

Figure 6.16: Target at 1m

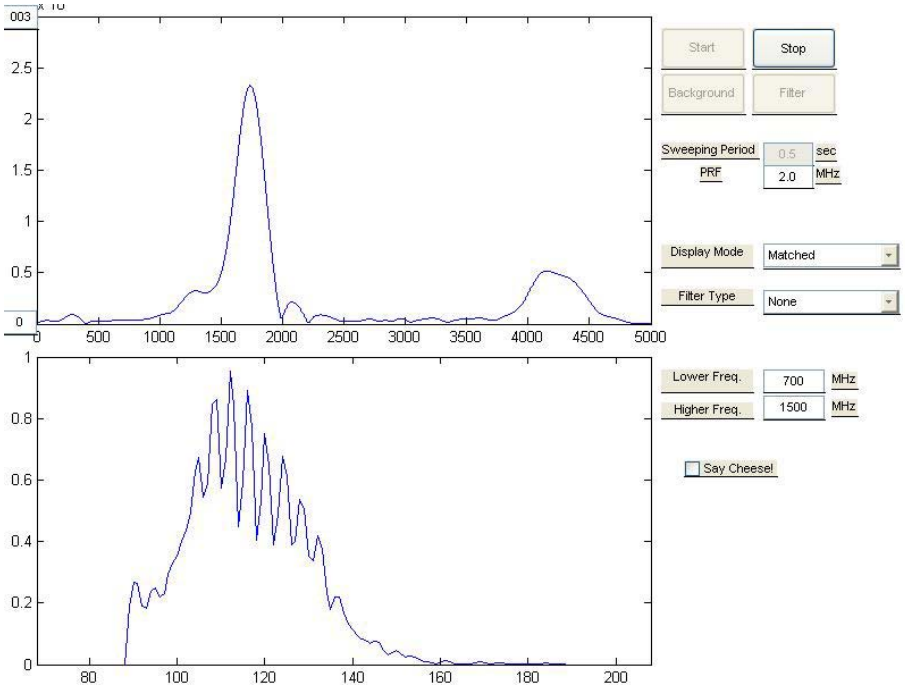

Figure 6.17: Target at 1m (match filtered)

Figure 6.18 shows a target (corner reflector) at 1.5m, match filtered and hanning windowed.

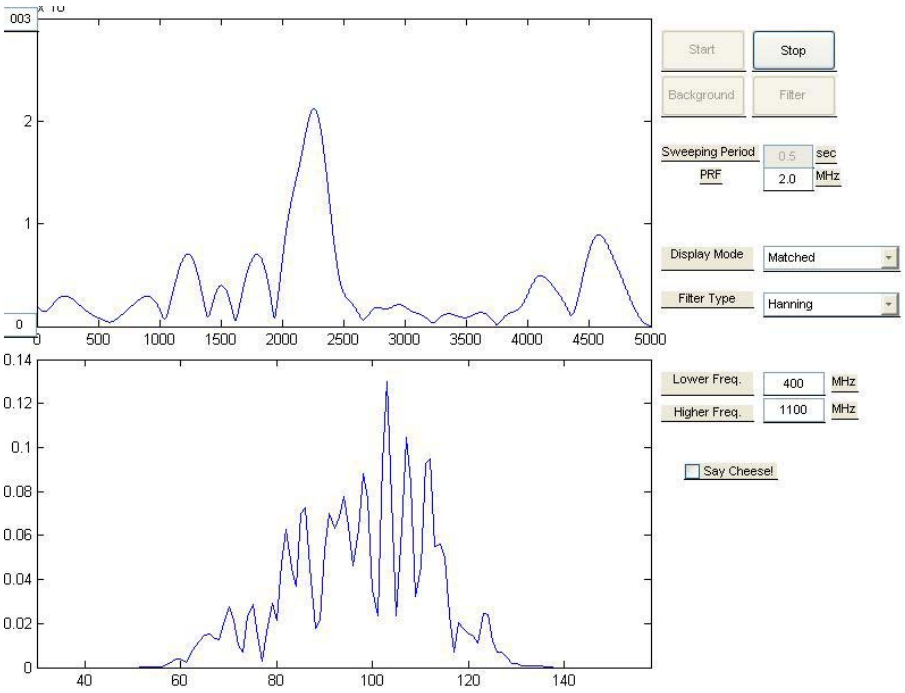

Figure 6.18: Target (corner reflector) at 1.5m

Figure 6.19 shows a target at 2m, match filtered and hanning windowed.

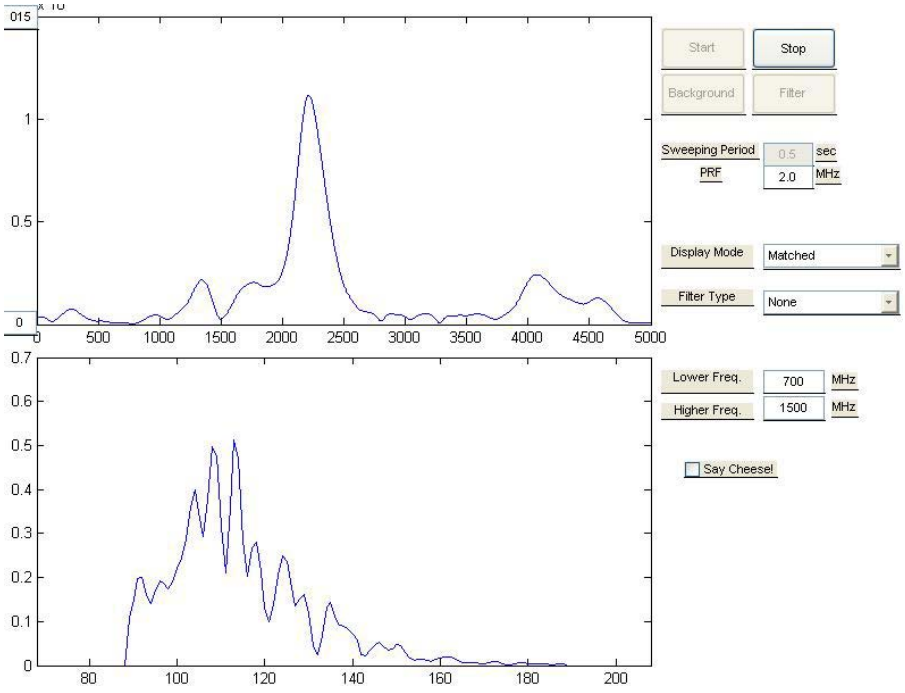

Figure 6.19: Target at 2m

Figure 6.20 shows a target at 2.5m, deconvolved and hanning windowed.

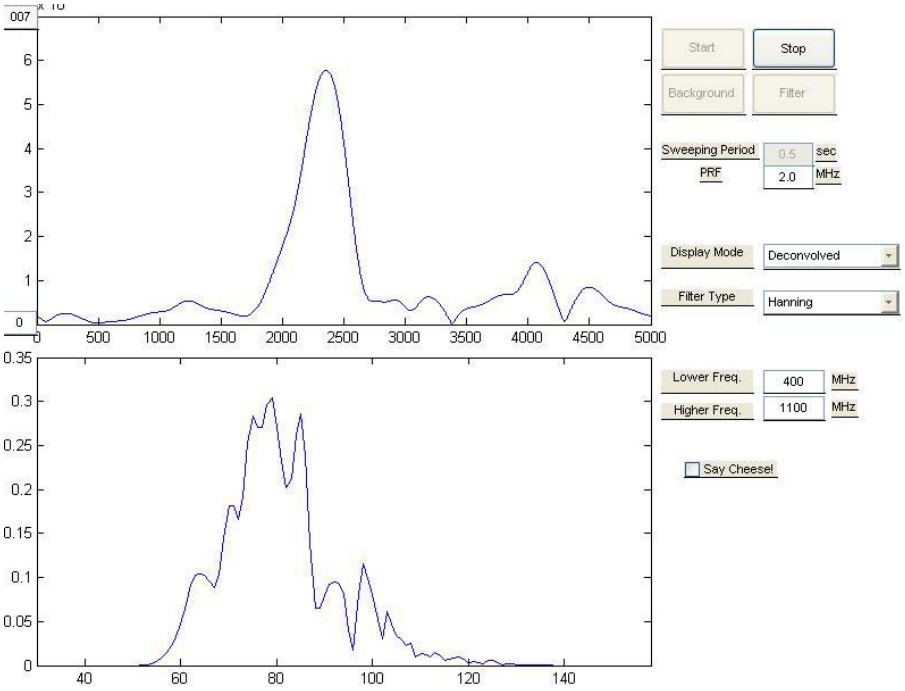

Figure 6.20: Target at 2.5m

Figure 6.21 shows a target at 3m, match filtered and hanning windowed.

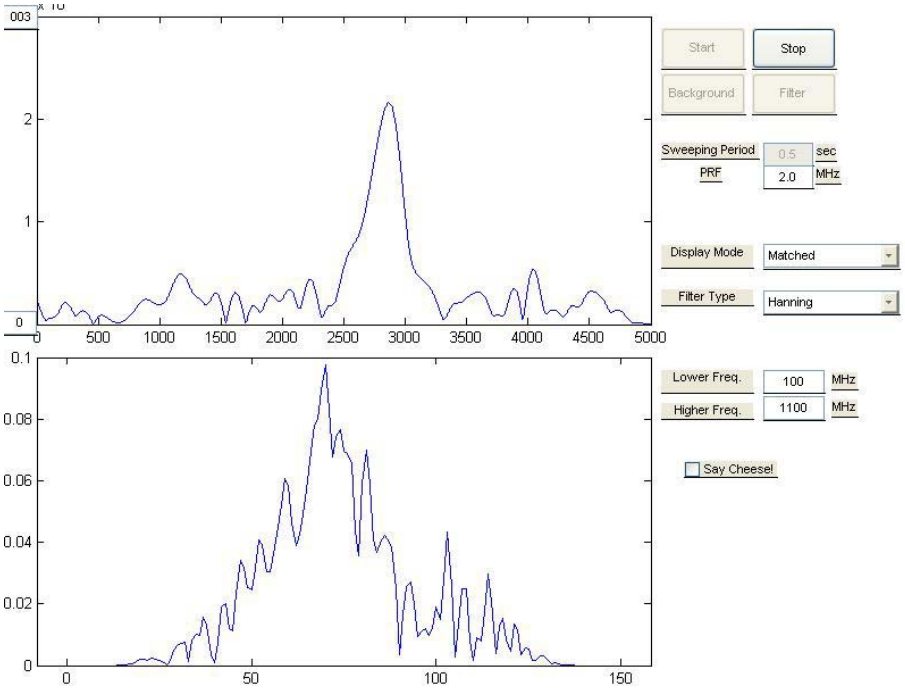

Figure 6.21: Target at 3m

6.2.2 Results for Multiple Channel Operation

As was described in Section 6.2, the software was then modified to display simultaneous downrange profiles for multiple channels. Since multiple channels were needed, the on-board amplifiers had to be used, despite their substandard gain. To combat this lack

in gain, the gain of the differential amplifiers for the multiple channels was increased, thereby increasing the signals fed to the NI-DAQ, and unfortunately the systems sensitivity to noise as well. For this reason, the multiple channel operation could not be demonstrated for distances much greater than 1m.

As was described in Section 6.1.5, Ellies grid antennas were used to form the receive antenna array.

It was endeavoured to keep the length of the cables as similar as possible, in order to sample the returns at the same point for each receiver. Figure 6.22 shows the configuration of the grid antennas, as they were arranged in the three channel setup.

Figure 6.22: Ellies grid antenna configuration for the three channel setup

The target used was a large grid with dimensions 850X390mm, propped up against a plastic structure (smaller in size).

This target was positioned 1m (vertically) in front of the antenna array, while its horizontal position was moved, from left to right i.e. from in line with the first receiver, to in line with the last receiver. Since the gain for each receiver channel was slightly different (component tolerances, subtle PCB layout changes, different cabling etc), the main objective was to see if the peaks of the received pulses shifted to the right in time as the distance to the receivers was increased, and that the relative magnitude of the pulses decreased as well.

Two Channels

For the two channel system, the transmitter antenna was placed in between the two receiver elements. Returns from the first receiver element (to the left of the transmitter,

looking towards the transmitter) are plotted in blue, while returns from the second receive antenna are plotted in green.

Figure 6.23 shows the background snapshot.

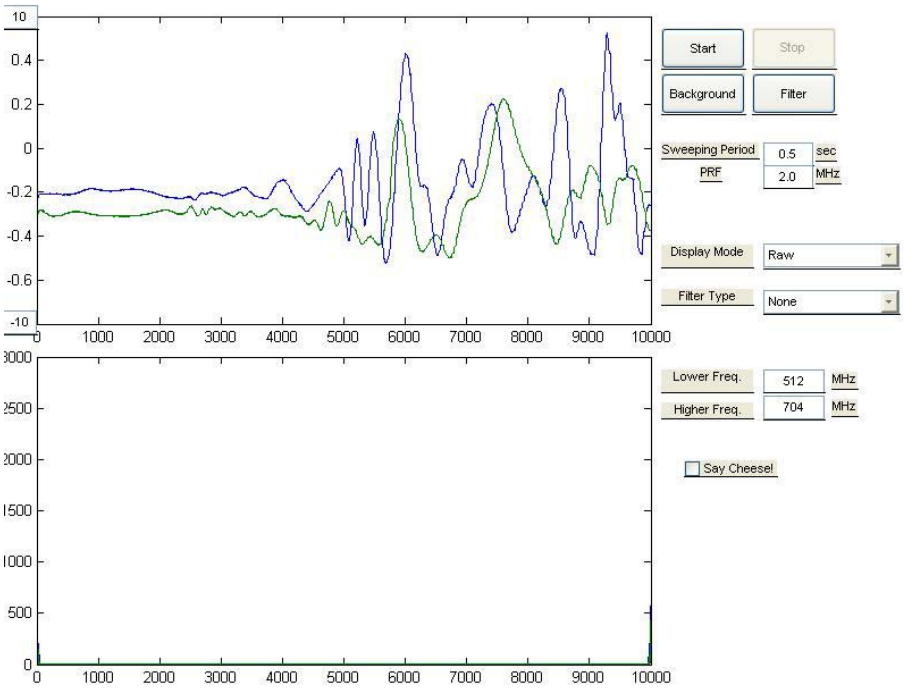

Figure 6.23: Background snapshot for two channels

Figure 6.24 shows the target in front of the first receive antenna, using the difference display mode.

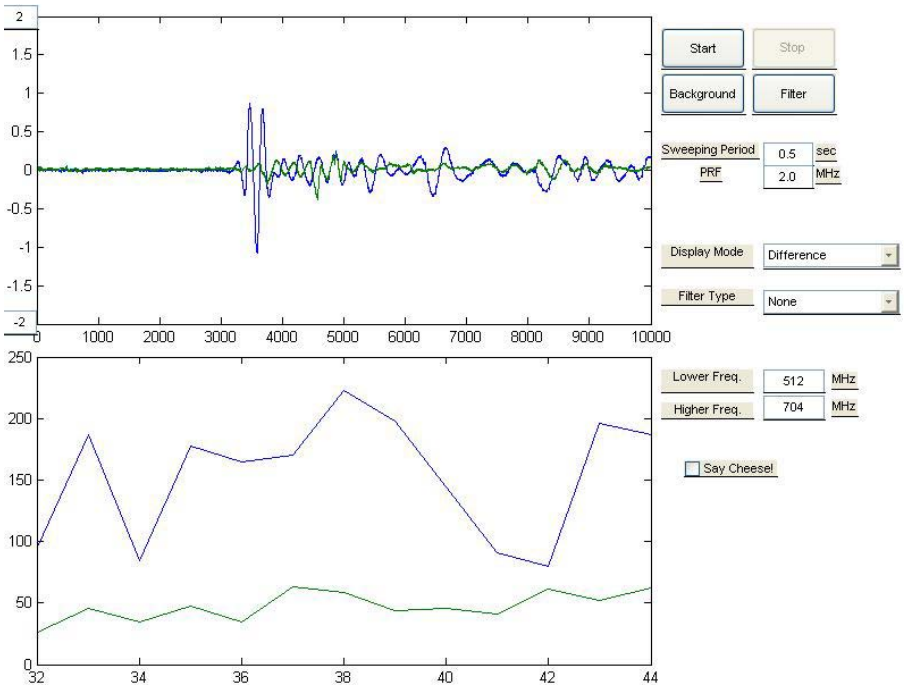

Figure 6.24: Target in front of first (blue) receive antenna

Figure 6.25 shows the target directly in front of the transmitter. The peaks of the two

returns are aligned, as the time delay to each element is roughly the same.

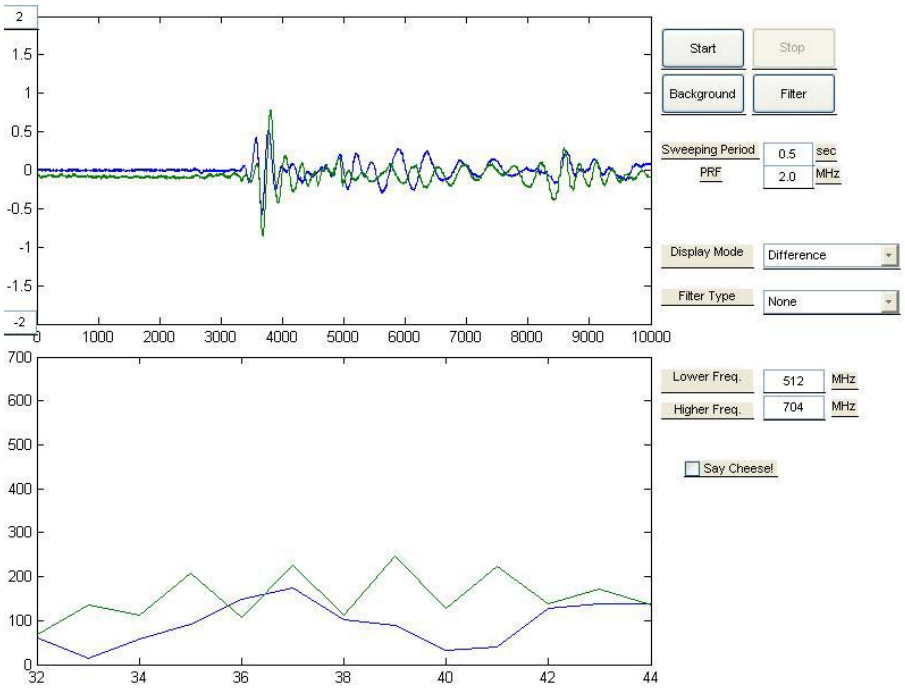

Figure 6.25: Target directly in front of transmitter

Figure 6.26 shows the target in front of the second receive antenna.

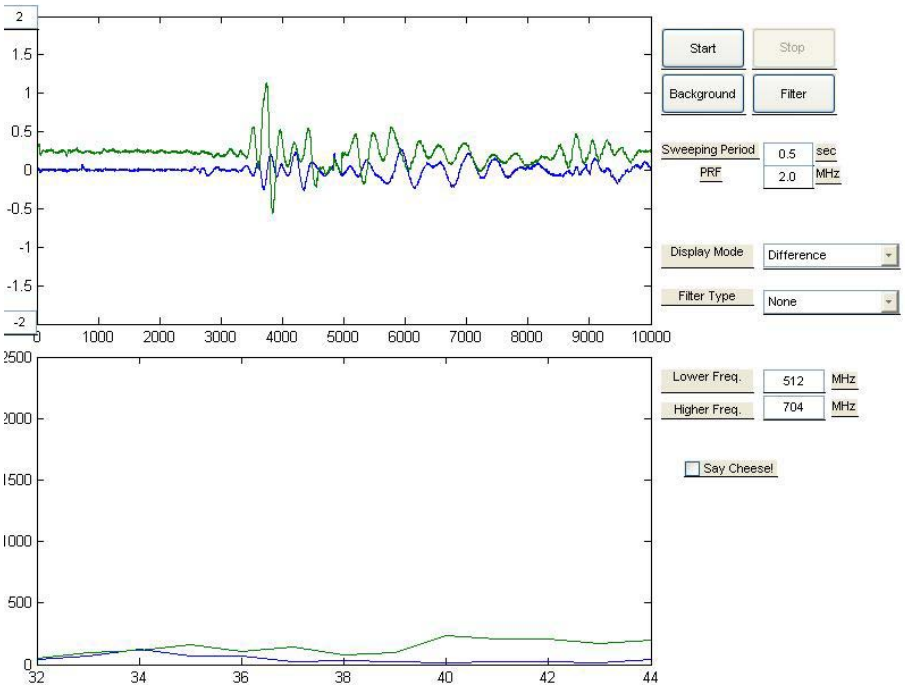

Figure 6.26: Target in front of second (green) receive antenna

Figure 6.27 shows the target snapshot for two channels.

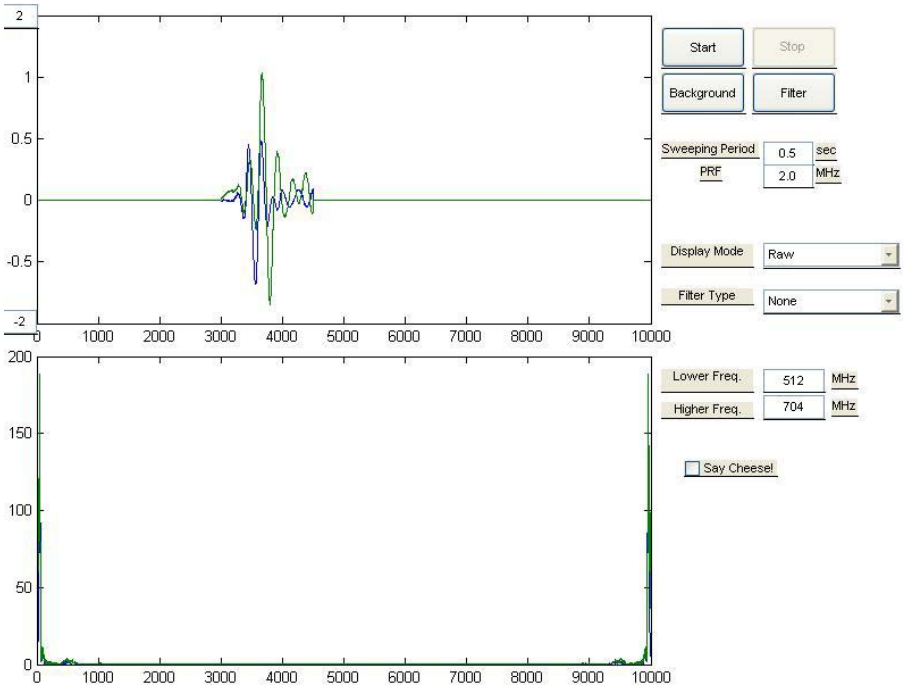

Figure 6.27: Filter snapshot for two channels

Figure 6.28 shows the target in front of the first antenna, match filtered.

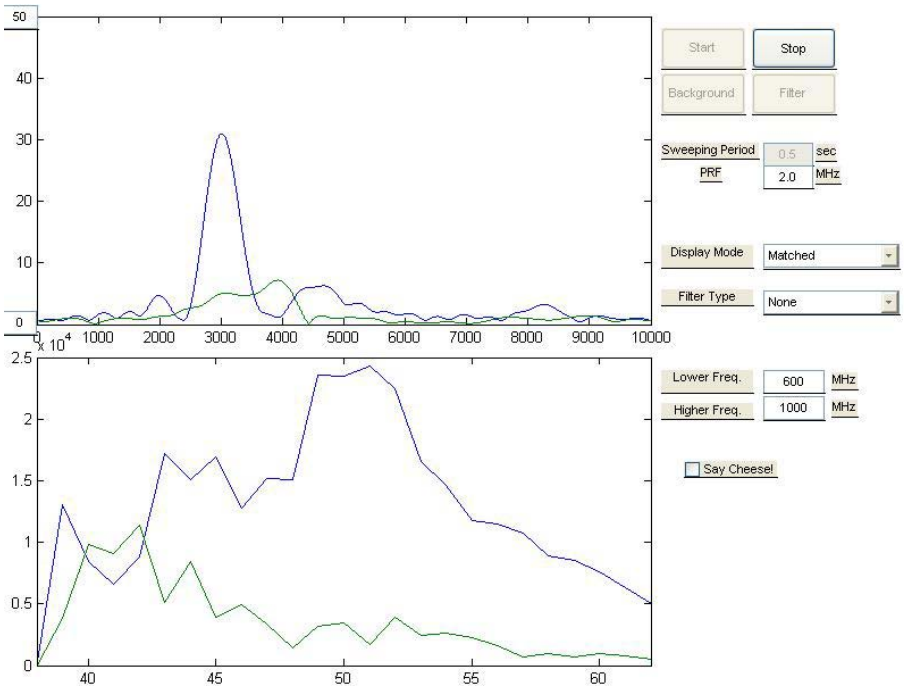

Figure 6.28: Target in front of first (blue) receive antenna, match filtered

Figure 6.29 shows the target in front of the transmitter, match filtered.

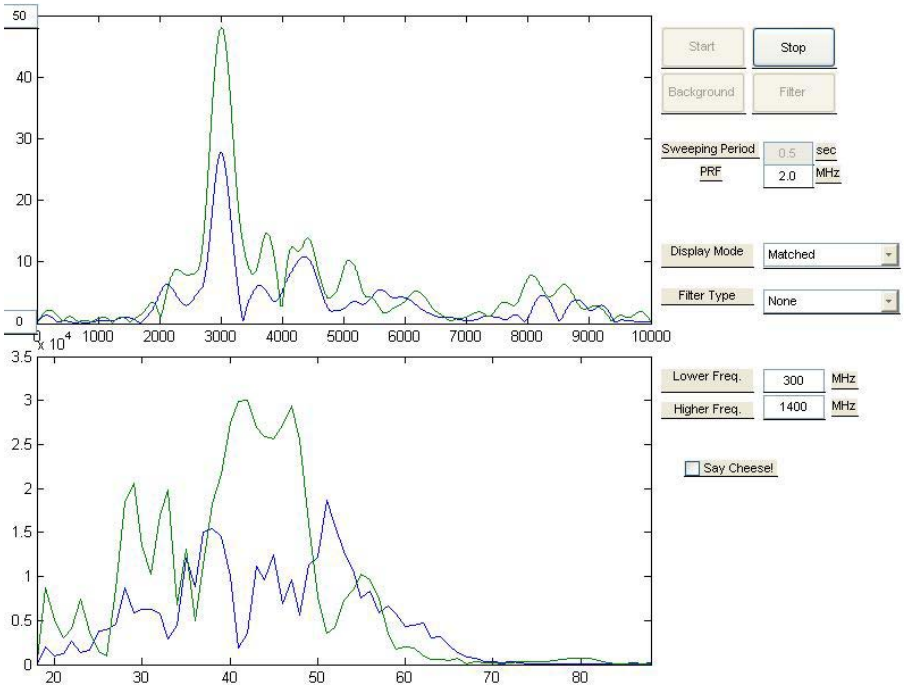

Figure 6.29: Target in front of transmitter

Figure 6.30 shows the target in front of the second antenna, match filtered. The relative movement of the peaks is not easily seen, due to the relatively low target range resolution,and small range over which the target is moved.

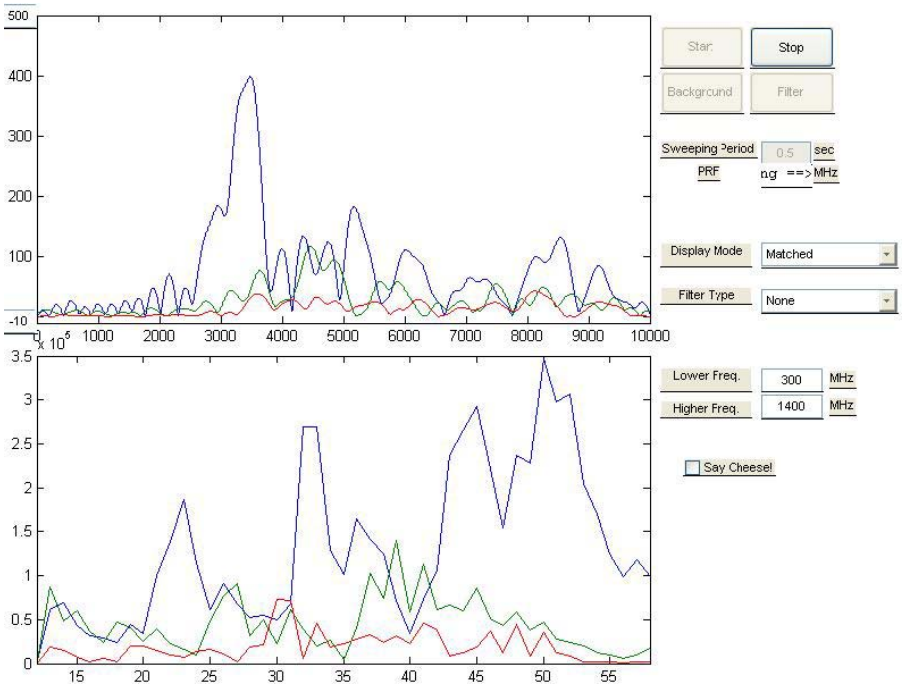

Figure 6.30: Target in front of second (green) receive antenna, match filtered

Three Channels

For the three channel system, the antennas were arranged in the following order, from left to right (looking towards the antennas): first receiver, transmitter, second receiver, third

receiver. In the downrange profiles, returns from the first receiver are plotted in blue, the second in green, and the third in red.

Figure 6.31 shows the background snapshot for the three channels.

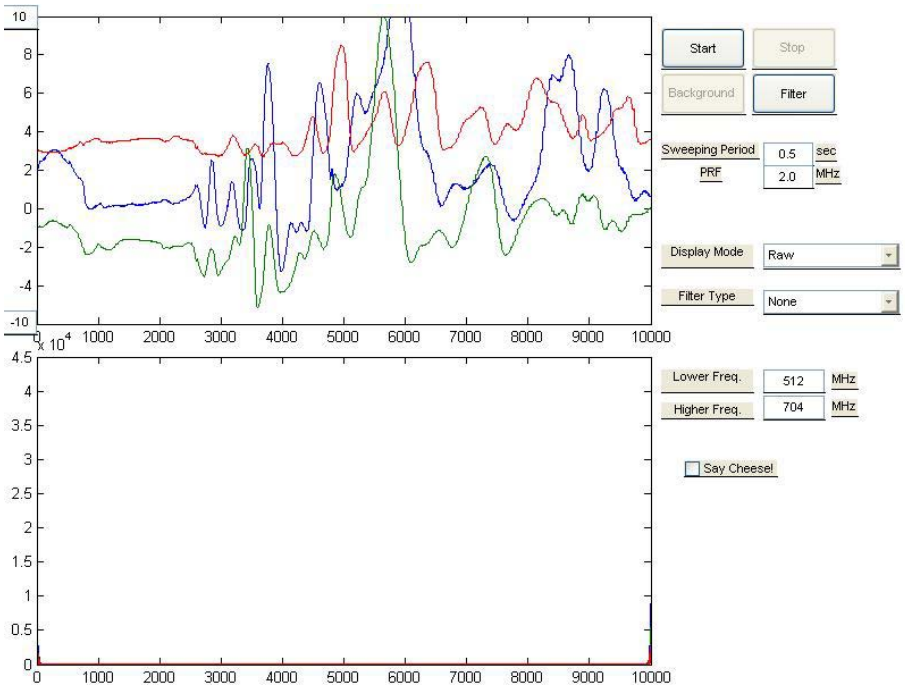

Figure 6.31: Background snapshot for three channels

Figure 6.32 shows the target in front of the first antenna, in difference mode.

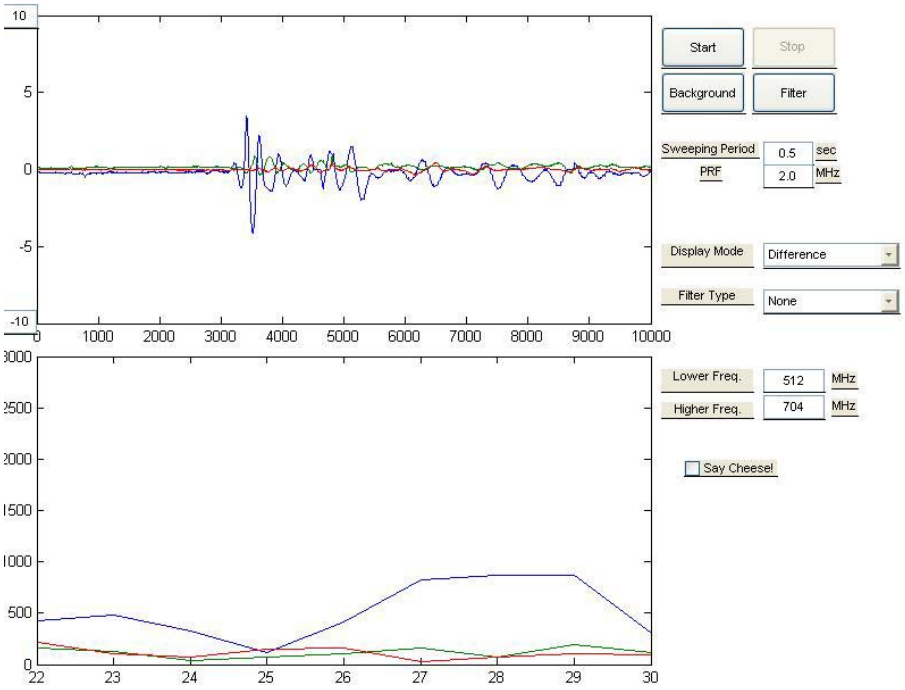

Figure 6.32: Target in front of first (blue) receive antenna, difference mode

Figure 6.33 shows the target in front of the second antenna, in difference mode. Note the shift and lowered magnitude of the red pulse, as this is the return from the third antenna

(next to the second antenna, green pulse, hence further away).

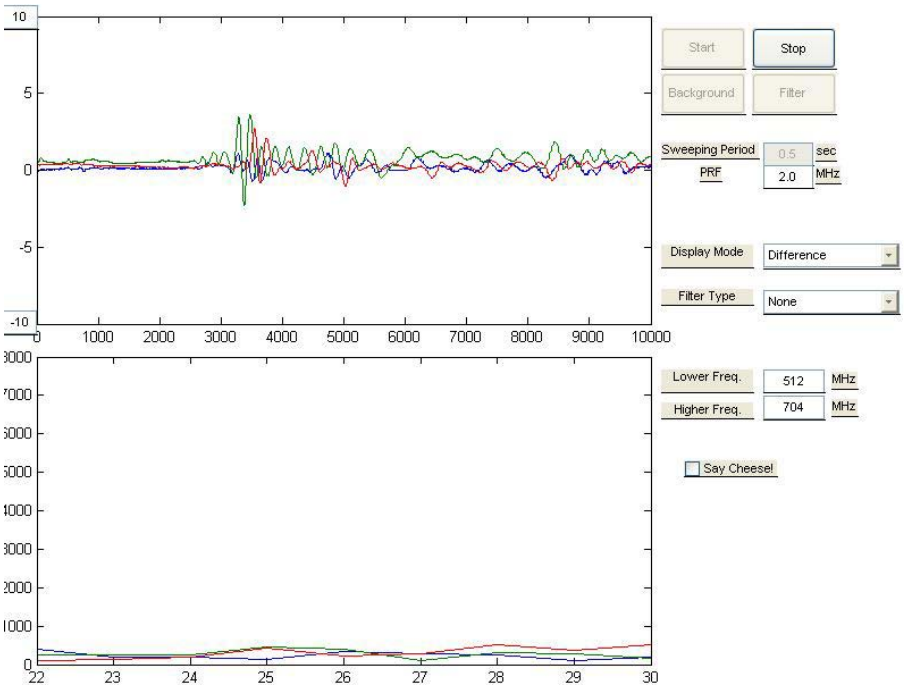

Figure 6.33: Target in front of second (green) antenna, difference mode

Figure 6.34 shows the target in front of the third antenna, in difference mode.

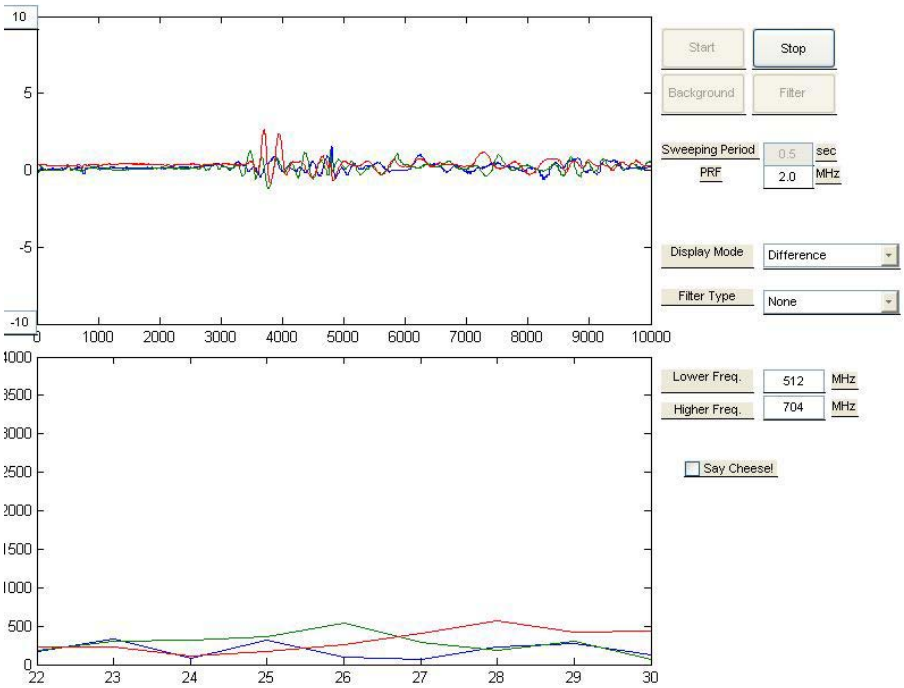

Figure 6.34: Target in front of third (red) antenna, difference mode

Figure 6.35 shows the filter snapshot for the three channel configuration.

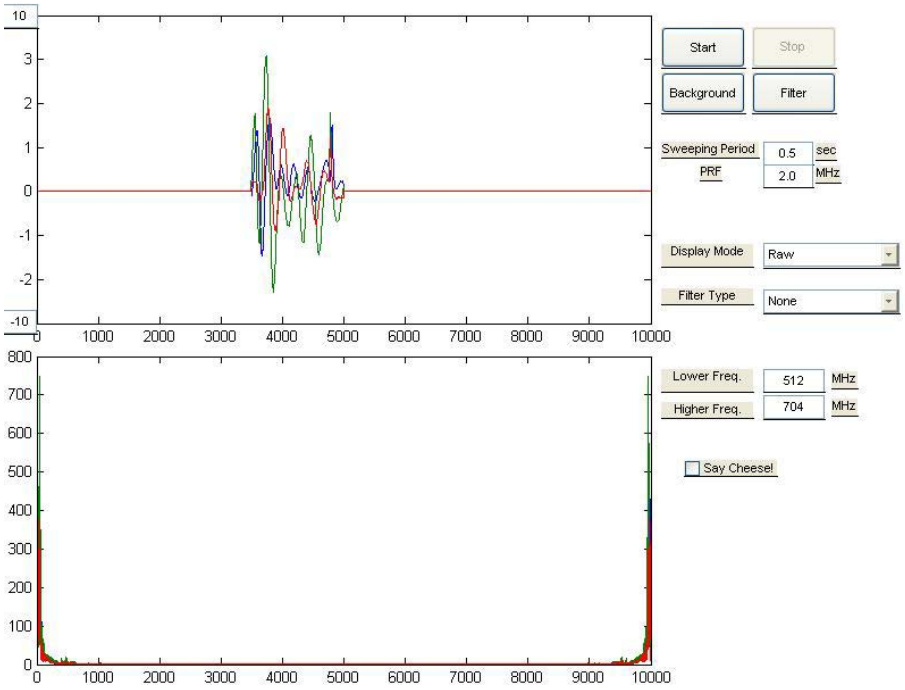

Figure 6.35: Filter snapshot for three channels

Figure 6.36 shows the target in front of the first antenna, match filtered.

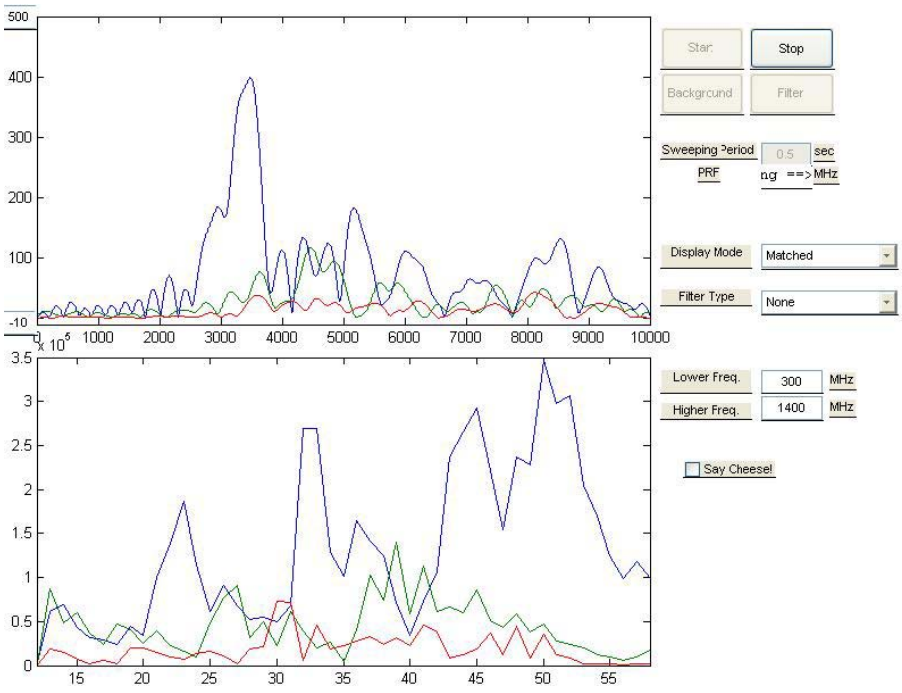

Figure 6.36: Target in front of first (blue) receive antenna, match filtered

Figure 6.37 shows the target roughly in the middle of the scene (between transmitter and second, green, receive antenna). The target reflection from the second antenna (green) is stronger in magnitude and its peak should be slightly advanced from the other returns.

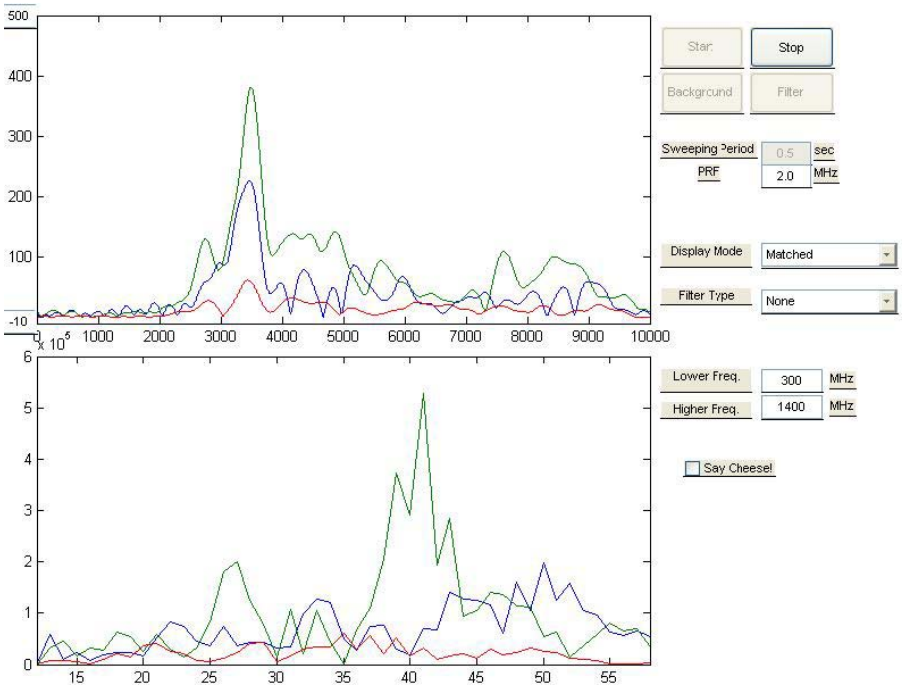

Figure 6.37: Target in middle of scene, match filtered

Figure 6.38 shows the target in front of the third (red) antenna, match filtered (note how the green pulse is lower in magnitude, and delayed in time, and the blue pulse has died out).

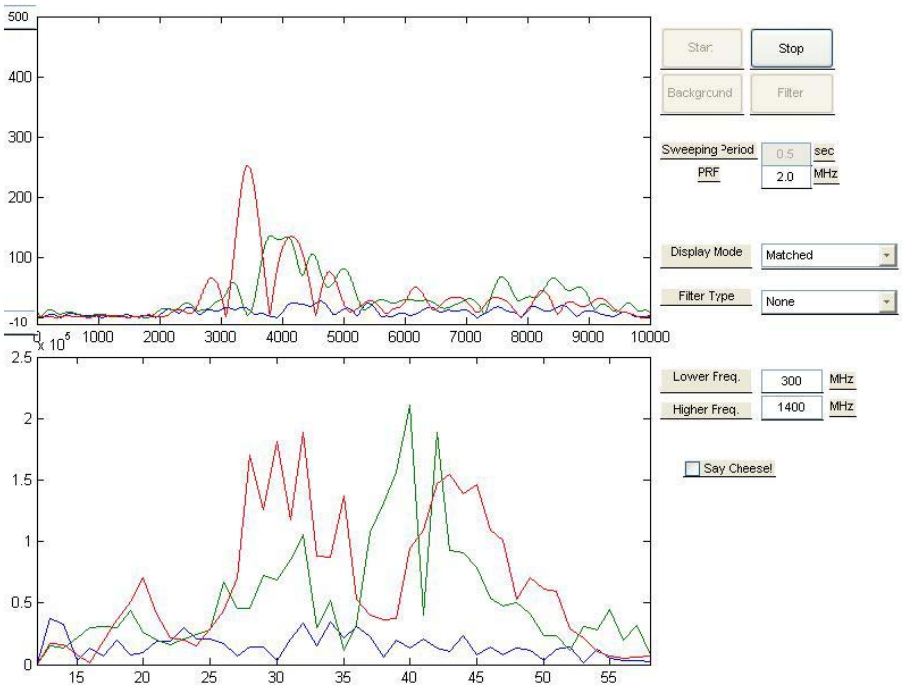

Figure 6.38: Target in front of third (red) receive antenna, match filtered

Chapter 7

Conclusions and Recommendations

This document detailed the research, simulation, design and implementation of a multi-channel, ultra-wideband (UWB) radar system. The results indicate the potential for UWB impulse radar to be used for short range target detection/positioning applications. A number of conclusions have been drawn based upon the findings of this thesis. They are listed in this chapter, along with recommendations for improvements and future work.

7.1 Conclusions

- The software simulations were successful and demonstrated important concepts in antenna array theory, UWB impulse radar downrange profiles and beam focussing.
- The UWB transmitter produced a pulse that enabled downrange profiles to be displayed real-time using a software interface. The pulse was however broader than 1ns (due to the trade-off between pulse width and pulse magnitude), having implications for the radar's range resolution.
- The on-board RF amplifiers, although operational, did not deliver the expected gain of 40dB. Lack of a continuously solid ground plane, the dielectric constant of the PCB, impedance mismatches and inductance caused by extra track/lead lengths is held responsible for this. Results obtained with the plug-in amplifier allowed the capture of downrange profiles at larger ranges (>1m).
- The receivers successfully performed their task of sampling the radar return echoes, and three channels were activated to demonstrate multichannel operation. The performance of the system during multichannel operation was however not of the same standard as that attained for a single channel. Use of the on-board amplifiers (as opposed to the higher gain plug-in amplifier), Ellies grid antennas (as opposed to the high bandwidth twin bow tie antennas) and low quality cabling are cited as possible reasons for this deviation.

- The modified version of the radar software interface *myRadar* managed to produce real-time downrange profiles for multiple receiver channels.

7.2 Recommendations

- For future designs, the schematic of the multi-channel system could be modified to: include a separate supply layer to accommodate a larger, independent ground plane for improved RF performance (improved waveguide) and to include shorter track lengths.
- The track widths should be corrected for accurate impedance matching.
- The board should be manufactured on high quality, low loss (low relative dielectric constant) microstrip for improved RF performance.
- Drop-in RF amplifier modules instead of surface mounts should be used to reduce extra inductance caused by longer, bent leads. Any vias to the amplifier leads should be placed as close to the component package as possible.
- High quality, low loss SMA coaxial cable should be used to connect the antennas to the radar system for enhanced performance.
- Higher quality, smaller package, RF specific surface mount components should be used for improved RF performance.
- The transmitter should be modified (improved components and fine-tuned values) to produce sub-nanosecond pulses in order to achieve finer range resolution thus providing more detailed scene impulse responses.
- Additional UWB antennas with larger bandwidths should be designed and constructed for use with an improved version of the multi-channel system.
- Higher gain RF amplifiers and/or a higher power transmit signal should be employed to improve the range capabilities of the multi-channel design.
- The existing software interface should be modified to incorporate the beam focusing algorithm developed in this thesis, to achieve real-time target positioning capabilities.

Appendix A

Software Source Code

A.1 Antenna Beam Pattern Simulation Code

```
fo = 1.5e9;
c = 3e8;
lamda = c/fo;
theta_min = -pi;
theta_max = pi;
d_theta = 2*pi/200;
N = 60; % if we make the distance between receiver ele's too large,
%ie poor resolution,we get grating lobes we start to see grating
%lobes when n = 6. When n = 5, large grating lobes are observed,
%of roughly equal magnitude to the main lobes but with a larger
%beamwidth. At n = 5, d = 0.2, i.e. the distance between
%ele's is equal to the wavelength. This phenomenon is similar to
%aliasing when sampling - to avoid grating lobes, we must have a
%receiver array with spatial resolution finer than the wavelength
%of the received wave, i.e. d<lambda, i.e. N = 6 elements at least
%for lamda = 0.2m . If we decrease our aperture length, we can
%decrease our element spacing, and avoid aliasing again. For N = 5,
%with D = 0.85, d = 0.17, and we start to see grating lobes.
%With D = 0.84, the grating lobes are the same size as the
%side-lobes.
D = 1;
d = D/N;
i = 0:N-1;
theta = theta_min:d_theta:theta_max;
for a = 1:length(theta)
delta_i = i.*d.*sin(theta(a));
delta_t = -delta_i./c;
```

```
mag = abs (sum(exp(-j*2*pi*fo.*delta_t)));
mag_v(a) = mag;
end
plot((theta/pi)*180, mag_v);
% figure %  % polar(theta,mag_v);
```

A.2 Multi-Channel UWB Radar Simulation Code

```
c = 3e8; % Speed of light
fo = 1.5e9; %centre frequency of pulse
pulse_length = 1e-9;
fs = 100e9; % This is the sample rate (15*Nyquist)
dt = 1/fs; % This is the sample spacing
PRF = 2e6;
Runambig = c/(2*PRF);
R_max = 15; td = 0.5e-9;
lambda = c/fo;
%G_ant =
%sigma =
%zeta = sqrt((G_ant^2*sigma*lambda^2)/((4*pi)^3*R^4));
T_max = 2*R_max/c;
%T_max = 5e-9;
t = 0:dt:T_max;
num_sa = length(t);
%v_tx = rect((t-td)/pulse_length); %1ns pulse extending from
%0 to 1ns
%plot(t,v_tx);
%v_tx = cos(2*pi*fo.*t).*rect((t - td)/pulse_length);
% pulsed sinusiod,from 0 to 1ns
%v_tx = exp(j*2*pi*fo.*t).*rect((t - td)/pulse_length);
%analytical representation of pulsed sinusoid
%figure;
%plot(t,abs(v_tx));
%V_TX = fft(v_tx);
%plot(abs(V_TX));
array_length = 1;
N_elements = 20; tar = [0.1 4 0.8 8];
figure;
N_targets = length(tar(:,1));
ele([(1:N_elements)],1) =
```

```
((0:N_elements-1)/(N_elements-1))*array_length;
ele([1:N_elements],2) = 0;
tx = [0.5 0];
for i = 1:N_elements
line( [ele(i,1)-0.1 ele(i,1)+0.1],[ele(i,2) ele(i,2)]);
end %
for l = 1:N_targets
line([tar(l,1) tar(l,1)+0.1], [tar(l,2) tar(l,2)] );
end
hold on;
for l = 1:N_targets plot(tar(l,1),tar(l,2),'*r'); end
axis([-1 2 -1 12])
v_rx_tot(1:N_elements,1:num_sa) = 0;
ele_weight = hanning(N_elements); %apply hamming window
%in space to receiver elements to reduce sidelobes
for n = 1:N_elements
v_rx_ele(1:num_sa) = 0;
for p = 1:N_targets
xpos = tar(p,1); ypos = tar(p,2);
R_x_tx_tar = tx(1,1) - xpos;
R_y_tx_tar = tx(1,2) - ypos;
R_tx_tar = ((R_x_tx_tar)^2 + (R_y_tx_tar)^2)^0.5;
R_x_ele_tar = ele(n,1) - xpos;
R_y_ele_tar = ele(n,2) - ypos;
R_ele_tar = ( (R_x_ele_tar)^2 + (R_y_ele_tar^2) )^0.5;
R_2way_tar = R_tx_tar + R_ele_tar;
Ti = R_2way_tar/c;
zeta = 1/(R_tx_tar)^2;
%v_rx = zeta*exp(j*2*pi*fo*(t-Ti)).*rect((t-Ti-td)/pulse_length);
%received signal, i.e. scaled, delayed version of v_tx %transfer
%down to baseband, by multiplying by %exp(-j*2*pi*fo*t)
v_rx = zeta*exp(-j*2*pi*fo*Ti).*rect((t-Ti-td)/pulse_length);
v_rx_ele = v_rx + v_rx_ele;
end
v_rx_tot(n,:) = ele_weight(n).*v_rx_ele;
%v_rx_tot(n,:) = v_rx_ele;
end
figure;
for p = 1:N_elements
subplot(N_elements,1,p), plot(t, abs(v_rx_tot(p,:))),
xlabel('time (s)'),
```

```
ylabel('Magnitude of Return'),title('Element');
end
figure;
plot(t,abs(v_rx_tot(1,:))),xlabel('time (s)'),
ylabel('Magnitude of Return Signal'),title('Element 1');
%show time plot for receiver element#1
figure;
r = (c*t)/2;
plot(r,abs(v_rx_tot(1,:))),xlabel('Range (m)'),
ylabel('Magnitude of Return Signal'),title('Element 1');
% show range plot for receiver element#1
figure;
imagesc(abs(v_rx_tot(1,:))), xlabel('Sample Number'),
ylabel('Magnitude of Fourier Response'),title('Element 1');
% show image plot for receiver element#1
% V_RX_TOT = fft(abs(v_rx_tot(1,:))); % figure;
 % plot(abs(V_RX_TOT));
```

A.3 Beam Focusing Algorithm

```
%focussing the image receieved by each receiver element for
%every point in a grid
c = 3e8; % Speed of light
fo = 1.5e9; %centre frequency of pulse pulse_length = 1e-9;
fs = 100e9; % This is the sample rate (15*Nyquist)
dt = 1/fs; % This is the sample spacing
R_max = 15;
td = 0.5e-9;
T_max = 2*R_max/c;
%T_max = 90e-9;
t = 0:dt:T_max;
%v_tx = exp(2*pi*fo.*t).*rect((t-td)/pulse_length);
xo = -1;
yo = 3;
dx = 0.1;
dy = 0.05;
x_width = 3;
y_width = 6; %range direction
Nx = round(x_width/dx)
```

```
Ny = round(y_width/dy)
N_elements = 20;
v_foc_tot = zeros(Nx,Ny);
ele([(1:N_elements)],1) =
((0:N_elements-1)/(N_elements-1))*array_length;
%x-co_ord of elements
ele([1:N_elements],2) = 0;  %y-co_ord of elements
tx = [0.5 0];
v_rx = zeros(1,length(t));
v_rx_ele = zeros(1,length(t));
for  iy = 1:Ny
for ix = 1:Nx
v_foc = 0;
xpos = ix*dx + xo;
ypos = iy*dy + yo;
for n = 1:N_elements
R_x_tx_tar = tx(1,1) - xpos;
R_y_tx_tar = tx(1,2) - ypos;
R_tx_tar =  ((R_x_tx_tar)^2 + (R_y_tx_tar)^2)^0.5;
R_x_ele_tar = ele(n,1) - xpos;
R_y_ele_tar = ele(n,2) - ypos;
R_ele_tar = ( (R_x_ele_tar)^2 + (R_y_ele_tar^2) )^0.5;
R_2way_tar = R_tx_tar + R_ele_tar;
Ti = R_2way_tar/c;
A = 1/zeta; %range compensation gain
%v_rx = zeta*exp(j*2*pi*fo.*(t - Ti)).*rect((t-Ti-td)/pulse_length)
%received signal is scaled shifted version of transmitted
ts = round(Ti/dt); %find sample number which represents the delay
%to a point in the grid
v_foc = A*v_rx_tot(n,ts).*exp(j*2*fo*pi*Ti) + v_foc; % focus that
%point for each receiver element by time shifting %it by the two
%way time delay to the point
end
v_foc_tot(ix,iy) = v_foc; %store the focused radar returns
%from each element for each point in the grid
end
end
figure;
imagesc(abs(v_foc_tot));
figure;
mesh(abs(v_foc_tot));
```

Bibliography

[1] *Research in Ultra Wideband Radar*. http://www.ittc.ku.edu/rvc/html/uwbresearch.html, August 2005.

[2] *Ultra Wideband (UWB) Frequently Asked Questions (FAQ)*. http://www.multispectral.com/UWBFAQ.html, August 2005.

[3] *RF Cables and Connectors*. www.wppltd.demon.co.uk/WPP/ConnectorsCablesTools/RfCablesConnectors/rfcablesconnectors.html, October, 2005.

[4] *Radarvision*. www.radarvision.com, September, 2005.

[5] T.-L. Chen. *Printed Circuit Board Antennas and Dipole Antenna Array Operating at 1.8GHz*. University of Cape Town, , pp. 12-14, 2003.

[6] A. Chiang and A. Wilkinson. Investigation of uwb-pulse technology for short range radar applications. Master's thesis, University of Cape Town, 2005.

[7] D. G. Coetzer. Design and implementation of a x-band transmitter and frequency distribution unit for a synthetic aperture radar. Master's thesis, University of Cape Town, May, 2004.

[8] R. Fontana. Recent system applications of short-pulse ultra-wideband (uwb) technology. *IEEE Microwave Theory and Tech.*, 52, No. 9, September 2004.

[9] S. Ginsberg. *MEC102W notes: Electrical Engineering CAD*. University of Cape Town, 2005.

[10] M. Inggs. *RF and Microwave Systems*. University of Cape Town, 2005.

[11] P. H. JR James. *Handbook of Microstrip Antennas*. Peter Peregrinus, , pp. 1014-1020, 1989.

[12] D. M. Pozar. *Microwave and RF Design of Wireless Systems*. John Wiley and Sons, Inc., 2001.

[13] D. Roddy. *Microwave Technology*. New Jersey: Prentice Hall, Inc., , pp. 148-150, 1986.

[14] S. Shrire. *EEE371W notes - Electronic components, circuits and modules*. University of Cape Town, 2004.

[15] L. Shuuya. *Design and Construction of a Twin Bowtie Antenna for the Frequency Range 1-2GHZ.* University of Cape Town, October 2004.

[16] M. I. Skolnik. *Introduction to Radar Systems*. McGraw-Hill Book Company, Inc., , pp.1-4, 1962.

[17] M. S. Smith. *Introduction to Antennas*. Macmillan Education Ltd, 1988.

[18] E. M. Staderini. *Everything you always wanted to know about UWB radar... : a practical introduction to the ultra wideband technology*. OSEE, December, 2001.

[19] J. Taylor. *Introduction to Ultra-Wideband Radar Systems*. CRC Press, , pp. 1-10, 2001.

[20] A. Wilkinson. *EEE358S notes - Fundamentals of Communcations Engineering*. University of Cape Town, 2005.

[21] A. Wilkinson. *EEE401F notes - Radar Signal Processing: Fundamentals*. University of Cape Town, 2005.

[22] A. Wilkinson. *Design, Construction and Performance of a Microwave Radiometer*. November, 1989.